NASA CASE FILE COPY

HIGH-LOADING LOW-SPEED FAN STUDY
I. DESIGN

by
N. T. Monsarrat, M. J. Keenan and P. C. Tramm

Pratt & Whitney Aircraft Division
United Aircraft Corporation

prepared for
National Aeronautics and Space Administration

HIGH-LOADING LOW-SPEED FAN STUDY

I. DESIGN

by

N. T. Monsarrat, M. J. Keenan and P. C. Tramm

prepared for
National Aeronautics and Space Administration

July 28, 1969

Contract NAS3-10483

FOREWORD

The work described herein was done by the Pratt & Whitney Division of United Aircraft Corporation under Contract NAS3-10483. Thomas F. Gelder, Fluid System Components Division, NASA – Lewis Research Center, was the NASA Project Manager.

TABLE OF CONTENTS

LIST OF FIGURES

LIST OF FIGURES (Cont'd)

LIST OF FIGURES (Cont'd)

LIST OF TABLES

LIST OF TABLES (Cont'd)

ABSTRACT

HIGH-LOADING LOW-SPEED FAN STUDY
I. DESIGN

A single-stage fan with a tip speed of 1000 ft/sec (304. 8 m/sec)
and a hub-tip ratio of 0. 392 was designed to deliver a 1. 5 pressure
ratio with an efficiency of 87. 3 percent at a flow rate of 185 lb/sec
(83. 92 kg/sec). Rotor tip speed, the axial spacing of the rotor
and stator, and the number of stator vanes were selected to mini-
mize compressor noise. Blade-loading D factor exceeded 0. 5 for
both rotor and stator. The rotor hub turned 39. 6 degrees (0. 691
radian) past axial.

I. SUMMARY

A low-tip-speed single-stage fan has been designed under NASA Contract NAS3-10483. This fan was designed to investigate the aerodynamics of a highly-loaded low-speed fan that would be applicable to a low-noise engine. The features of the design are that it has no inlet guide vanes, a rotor tip speed of 1000 feet per second (304.8 meters per second), and a stator whose axial location and number of vanes were determined from noise considerations.

The aerodynamic design was based on the approximate design parameters specified in the contract plus others typical of fans for high-bypass-ratio low-noise engines. The fan diameter was selected to fit existing test facilities. The design value of the flow per unit annulus area at the rotor leading edge is 42 lb/sec/ft^2 (205.07 kg/sec/m^2). The rotor was designed for a constant spanwise pressure ratio of 1.54 which, with stator losses, yields an overall stage pressure ratio of 1.50. Blade losses for both rotor and stator were estimated using a shock-profile loss model. The predicted rotor adiabatic efficiency is 93.3 percent, and the predicted overall stage average adiabatic efficiency is 87.3 percent.

The flow path has a constant outer diameter of 31.0 inches (0.7874 meter) and a rotor inlet hub-tip ratio of 0.392. The rotor and stator aspect ratios are 1.92 and 3.67 respectively, using root chord and average length.

There are 24 rotor blades and 64 stator vanes, a relationship determined by noise considerations. The ratio of rotor tip chord to root chord is 1.23 which, with a tip chord of 5.525 inches (0.1403 meter), yields a tip solidity of 1.358. The stator chord of 1.83 inches (0.0465 meter) is constant spanwise and provides a hub solidity of 2.169. The rotor-stator axial spacing is approximately two axially-projected rotor chords, a value that was also set from noise considerations.

Mechanical design included a structural and vibration analysis. A pin-root rotor attachment was designed to avoid resonance at two excitations per revolution. Rotor stress due to centrifugal loads, gas bending, and blade untwist were calculated and are well below the capabilities of the AMS 4928 titanium alloy being used for the blades. Stator stresses due to gas bending loads are well below the capabilities of the AMS 5613 stainless-steel stator material. Stator vibration frequencies were calculated for different stator end contraints from which it was decided that a cantilevered stator would probably flutter; therefore both ends were fixed to prevent flutter.

II. INTRODUCTION

Future aircraft power plants must provide increased thrust and performance but with substantially less noise than current engines. For the turbofan powerplant there are two major sources of noise. The first of these is the noise generated external to the engine in the turbulent shearing region downstream of the jet nozzle. This is low-frequency broadband noise, referred to as jet noise. The other source is the noise produced by the fan that radiates from the inlet and discharge ducts. This fan noise contains both broadband noise and discrete tones. Design trends in subsonic engines are towards very high bypass ratios. Such designs improve fuel consumption and reduce jet noise. However, the larger fans are creating fan noise problems.

Fan noise has been related to certain features of configuration, and to operating conditions. Effective ways of reducing fan noise are to: 1) eliminate inlet guide vanes, 2) use a single stage, and 3) increase the axial spacing between the rotor and stator. Also, in theory[1] at least, the ratio of the number of stator vanes to rotor blades can be selected to control the propagation of some discrete tone noise. In addition, rotor relative velocities and loadings are prime factors in noise generation. These factors are inversely related for a particular pressure ratio. Presently, it is not clear what is the best balance between blade speed and loading for lowest noise. One extreme is low speed with high loading which is the subject of the present study. A low-wheel-speed design with a useful single-stage pressure ratio also means large negative relative air angles at the rotor root exit (i.e., turning past axial direction), and high inlet Mach numbers at the stator inlet. These are unconventional aerodynamic design requirements.

Therefore, it is necessary to investigate experimentally the aerodynamic performance characteristics of such a fan designed specifically for low noise. A highly-loaded low-tip-speed fan was designed and fabricated, and will be tested under Contract NAS3-10483. The design approach and overall parameters are presented and discussed in the next sections, and details of the many inputs to the overall design system are presented in separate appendices to this report. Appendix 6 contains definitions of symbols.

---

[1]See Page 86 for numbered list of references

III. AERODYNAMIC DESIGN

A. Noise Considerations

Fan noise is the result of three separate phenomena. These are blade-vane interaction tone noise, broadband noise, and supersonic-fan noise. The blade-vane interaction noise is caused by the rotor blades chopping the wakes of upstream inlet guide vanes and the rotor wakes passing over the downstream stators. These interactions cause discrete tones to be generated at the fundamental blade-passing frequency and its higher harmonics. The blade-passage frequency is given by the number of blades multiplied by the rotor speed. For this design no inlet guide vane was used, thus eliminating any inlet-guide-vane effect. A large axial space between the rotor and stator permits the rotor wakes to decay, thus reducing the severity of disturbances experienced by the stator. Figure 1 shows the general trend of the fundamental blade-passing frequency noise level as a function of axial spacing. Although results from different investigators vary, the major noise reduction should be attained with a separation of about two axially-projected rotor chord lengths. Generally in this report, chord lengths are along the flow surface unless otherwise specified. Whether this interaction-generated noise propagates out of the inlet and fan ducts depends on the number of blades and

ROTOR-VANE SPACING IN PERCENT OF ROTOR-
BLADE AXIAL CHORD LENGTH
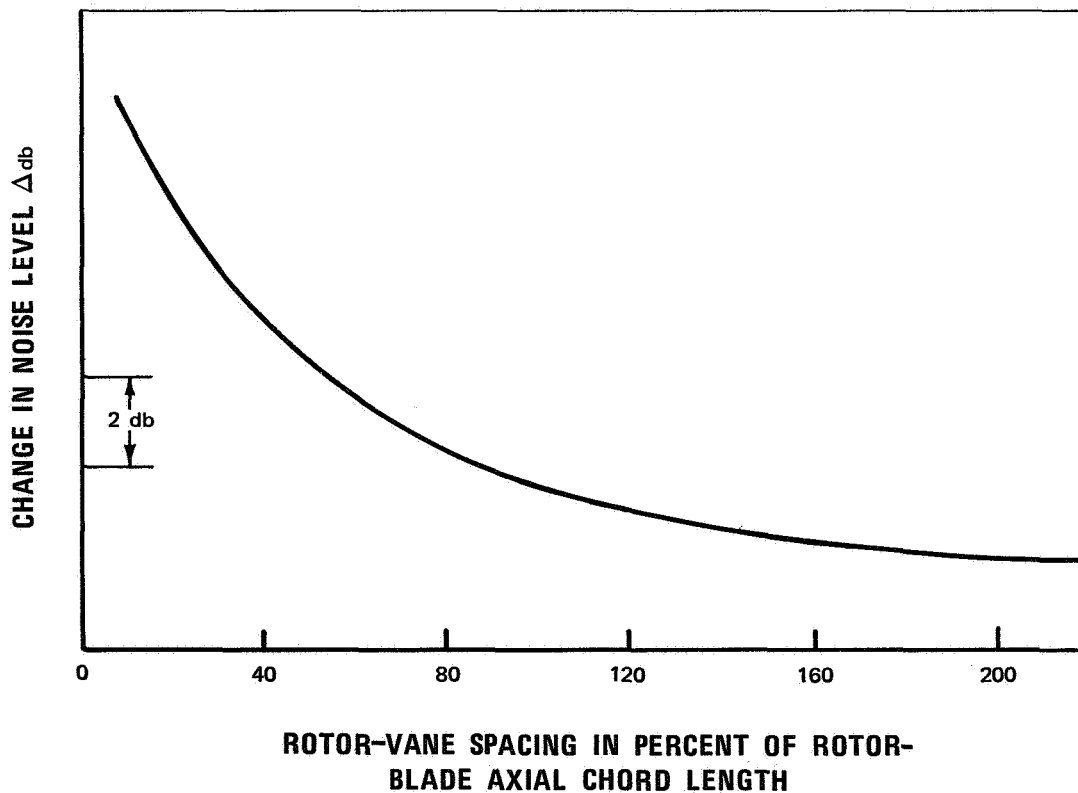
Figure 1   Effect of Rotor-Stator Spacing on Fan Fundamental Blade-Passing Frequency Noise Level

3

vanes used in adjacent rows, and on the rotor speed. Briefly, the interaction of the vanes with blade wakes causes the resulting pressure pattern to progress circumferentially around the duct, generally at some speed other than that of the rotor. When the circumferential speed of this pattern exceeds a certain value, which depends somewhat on duct geometry and axial flow velocity, the pattern passes through a cutoff speed. Above the cutoff speed the blade-passing noise is propagated forward and aft of the rotor. The cutoff speed for a given rotor speed and number of blades can be selected by the choice of the number of vanes. This phenomenon is discussed by Tyler and Sofrin[1].

The second type of fan noise is broadband noise generated by the air flowing through the blades and vanes. The level of this type of noise has been experimentally determined to increase at about the 5th power of the blade-tip speed. Therefore, by reducing the design tip speed it may be possible to reduce broadband noise.

The third type of fan noise is the so-called supersonic fan noise, also referred to as buzz-saw noise. As the fan blades pass through the transonic speed range, a shockwave pattern is formed by each blade in the rotor. Forward of the rotor, these waves decay to a system of Mach waves which propagate forward out of the inlet duct. Figure 2 illustrates this pattern. If each blade in the rotor were identical, wave propagation as described by Figure 2a would be suggested and the resulting radiated noise in the inlet would be at blade-passing frequency. In actual practice, the situation depicted in Figure 2a has not been noted. Small variations from blade to blade, within the
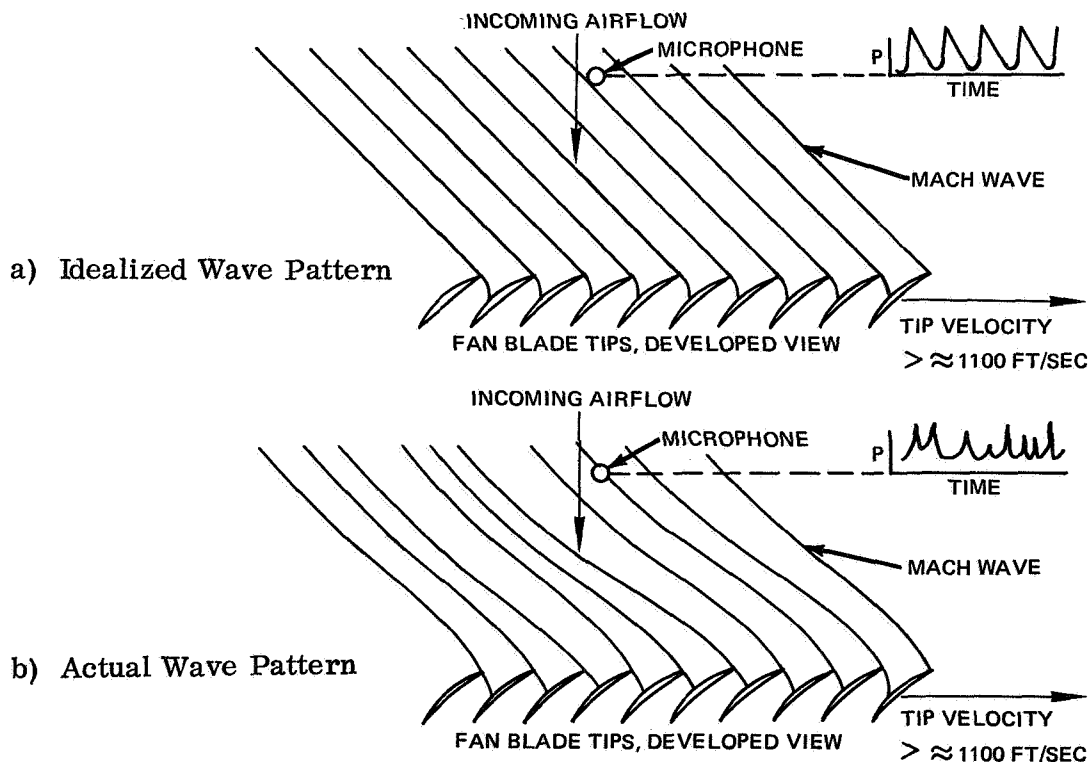
Figure 2   Supersonic Fan Blade Tip Noise

normal manufacturing and assembly tolerances, result in a wave pattern which is represented more nearly by Figure 2b. Spectral analysis of this type of wave pattern, which repeats once per engine revolution, produces all harmonics of engine rotational speed. The resulting buzz-saw noise is perceived as a low-pitched sound, quite unlike the typical noise generated by blade-vane interaction. A method used to reduce this type of noise is to design for the lowest possible tip speed, with subsonic relative velocities the ultimate goal.

B. <u>Flow Path and Vector Diagrams</u>

The design of this fan incorporates characteristics for low noise. Thus, no inlet-guide vanes are used, the tip speed has been kept low at 1000 ft/sec, the rotor and stator are widely spaced, and the number of rotor and stator blades were selected from noise-propagation considerations. The final-stage design parameters are tabulated below, along with the contract specifications.

TABLE 1
Design Parameters

	Final	Specifications
tip diameter, inches (meters)	31.0 (0.7874)	30.0 (0.762) min.
rotor inlet flow/unit annulus area, lb/sec/ft^2 (kg/sec/m^2)	42.0 (205.07)	
rotor inlet hub/tip ratio	0.392	0.4
rotor tip speed, ft/sec (meter/sec)	1000.0 (304.8)	1000 (304.8)
rotor aspect ratio (average length/root chord)	1.92	2
rotor taper ratio (tip chord/root chord)	1.22	
rotor tip solidity	1.358	1 minimum
stator aspect ratio (average length/root chord)	3.67	4
stator taper ratio (tip chord/root chord)	1.0	
stator root solidity	2.169	1.5 minimum
corrected speed, rpm	7400.0	
corrected flow, lb/sec (kg/sec)	185.0 (83.916)	
stage average pressure ratio	1.5	1.5
stage average efficiency, percent adiabatic	87.3	

The rotor-alone pressure ratio was set constant at 1.54 from root to tip. With stator losses, the average stage pressure ratio is 1.5 as specified by the contract. The inlet flow per unit annulus area was set at 42.0 lb/sec/ft^2 (205.07 kg/sec/m^2) to be consistent with typical advanced fan designs.

Boundary-layer growth on the flow-path walls was estimated using test data from several single-stage rigs of similar size. Effective end walls within the actual flow path were used to account for the displacement thickness of the wall boundary layers. The ratio of actual to effective area is 1.005 ahead of the rotor, 1.01 between the rotor and stator,

and 1.015 behind the stator. Effective endwalls were located at equal percentages of span inside of the actual walls.

The rotor-inlet hub/tip ratio of 0.392 is consistent with contractual specifications. The number of rotor blades was selected to be 24. The low rotor aspect ratio of 1.92 is not typical of advanced engine fans. However, this aspect ratio, along with a pin-root attachment to the rotor disc, was selected because it provides mechanical integrity over the complete operating range without the use of part-span shrouds. The unshrouded design yields the maximum amount of blade-element data and also eliminates a likely noise source.

The flowpath is shown by Figure 3. The procedure used to obtain the flowpath and velocity triangles was an iteration involving the flow-field calculation given in Appendix 1 and the loss system given in Appendix 2. The calculation procedure solves the continuity, energy, and radial equilibrium equations, including streamline curvature and slope terms. Stagnation pressures and temperatures are entered spanwise behind the rotor and stator. The iteration is required because the vector diagrams are dependent upon losses, which are in turn dependent upon the blade shape. In general, it takes three passes before the blade shape and aerodynamic calculation are consistent. Figures 4 and 5 show the spanwise variation of rotor efficiency and stator loss, respectively.

Overall flow-path convergence was determined by setting the inlet-to-exit axial velocity ratio at roughly unity. The schedule of convergence and wall curvature was used to control velocity profiles and wall loadings. One of the major aerodynamic problems inherent in a low-speed but high-loading design is large turnings past axial in the rotor root region. These sizable root turnings can be minimized by larger root exit diameters, but this tends to increase the tip exit diameters and tip aerodynamic loadings. A study determined that a constant rotor tip diameter did not result in excessive tip loadings as evidenced by a D-factor of 0.53 in Figure 6. Therefore, all of the flow convergence was taken at the root. The rotor-root convergency angle was set at 20 degrees, which, with the rotor-inlet hub/tip ratio and root chord, results in a rotor-exit-root wheel speed of 494 ft/sec (150.6 meter/sec). The root turns to 39.6 degrees past axial as shown in Figure 7. Past-axial turnings extend for the first 30 percent of span, measured from the root. Figure 8 shows the inlet and exit velocity profiles for both the rotor and stator. Figure 9 shows the rotor-inlet relative Mach number and the stator-inlet absolute Mach number.

Because of the unusually large axial separation between the rotor and stator, the rotor hub wall convergence could not be continued back to the stator without creating excessive axial velocities. Wall contour was set to attain a constant annulus for about one inch along the axial gap between the rotor and stator. Additional convergence was then used through the root (hub) of the stator to control velocity ratio and stator loadings. The stator-inlet air angles are shown in Figure 10. The stator discharge angle was set to zero across the entire span. The number of stator vanes was selected to be 64 in order to cut off the fundamental blade-vane interaction noise as previously discussed. Using a constant chord of 1.83 inches (0.0465 meter) the stator-root solidity is 2.169 and the aspect ratio is 3.67. The resulting stator loadings are shown by Figure 11.

DIMENSIONS IN INCHES UNLESS NOTED

Figure 3   Flow Path

7
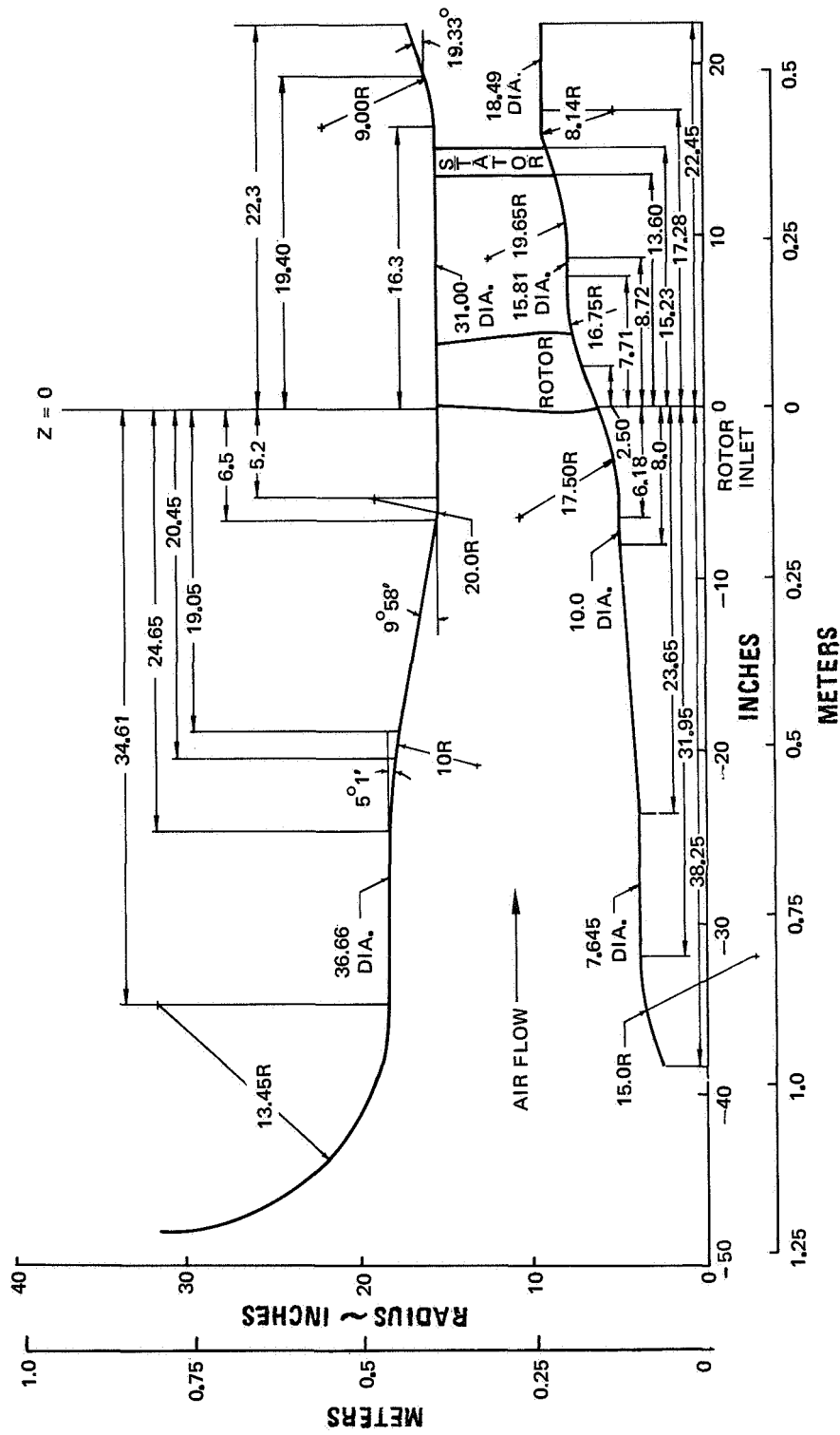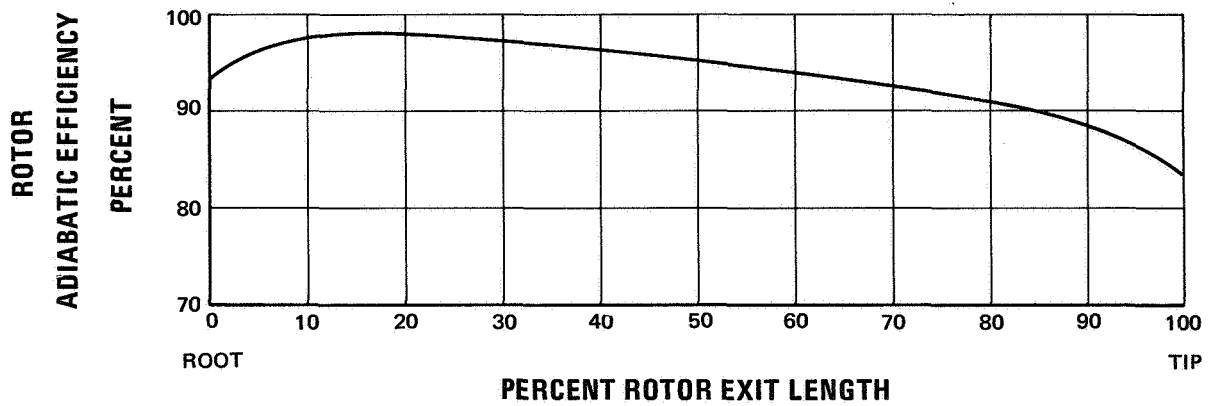
Figure 4   Rotor Spanwise Adiabatic Efficiency
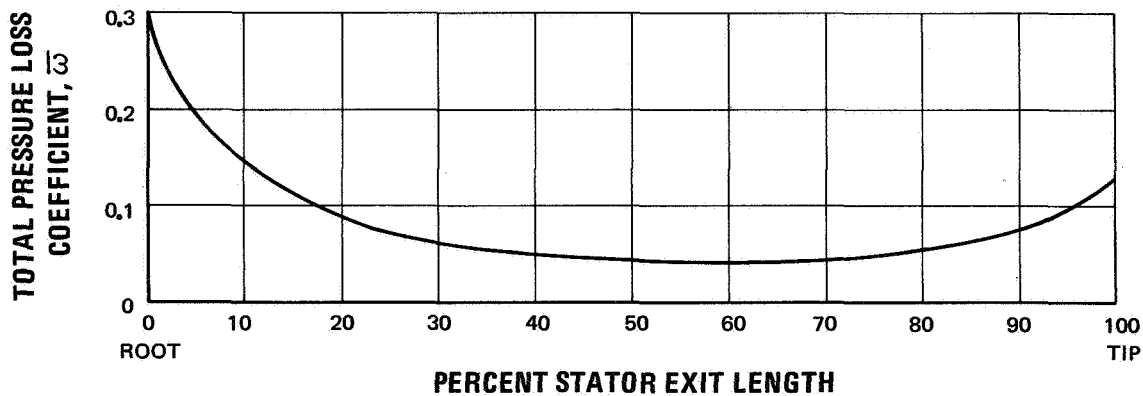
Figure 5   Stator Spanwise Loss
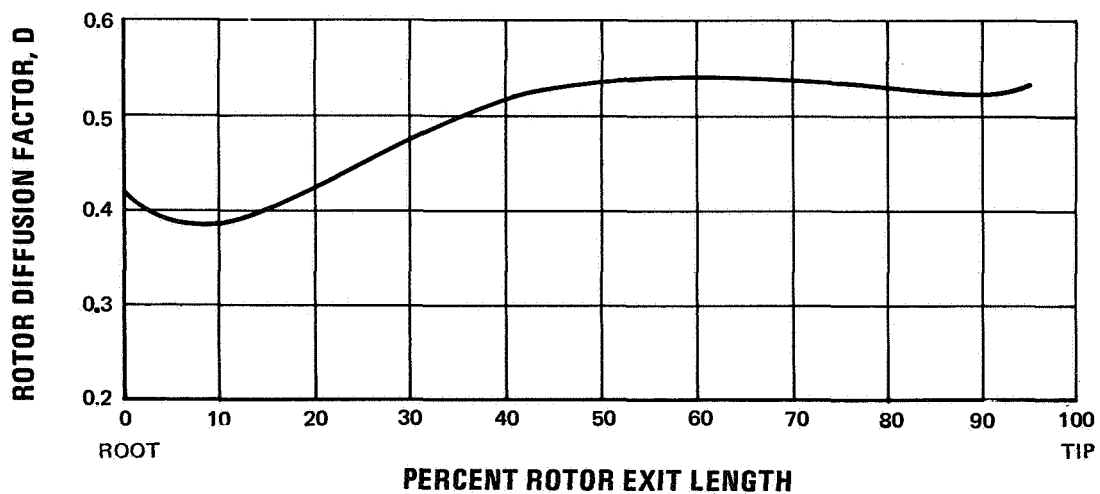
Figure 6   Rotor Diffusion Factor

8
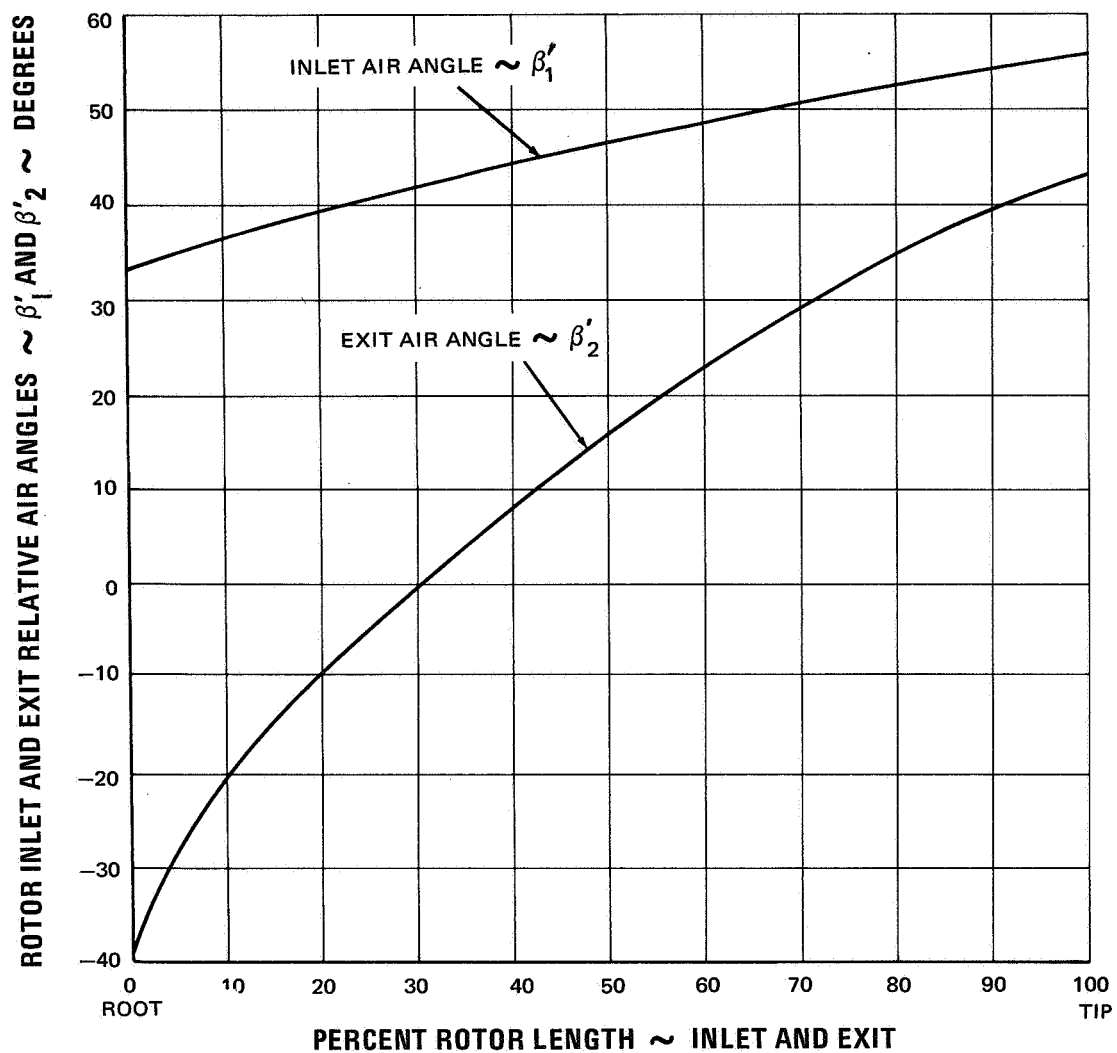
Figure 7   Rotor Inlet and Exit Relative Air Angle Profiles
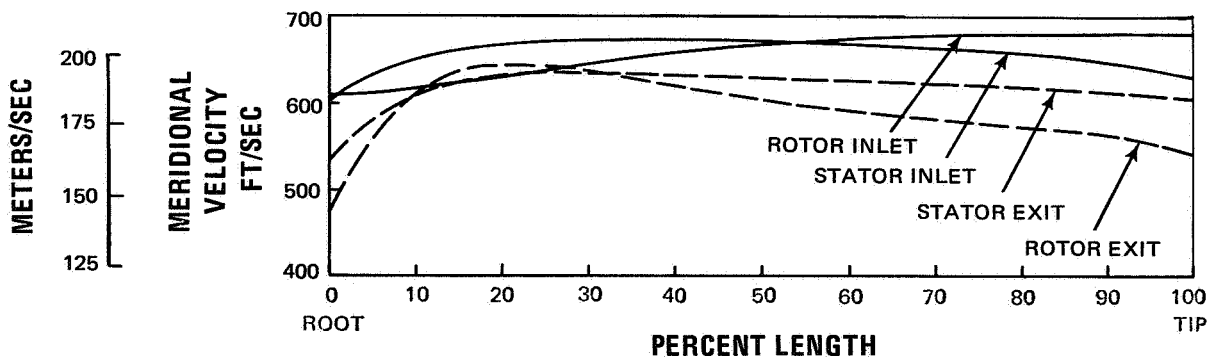
Figure 8   Rotor and Stator Inlet and Exit Velocity Profiles

9
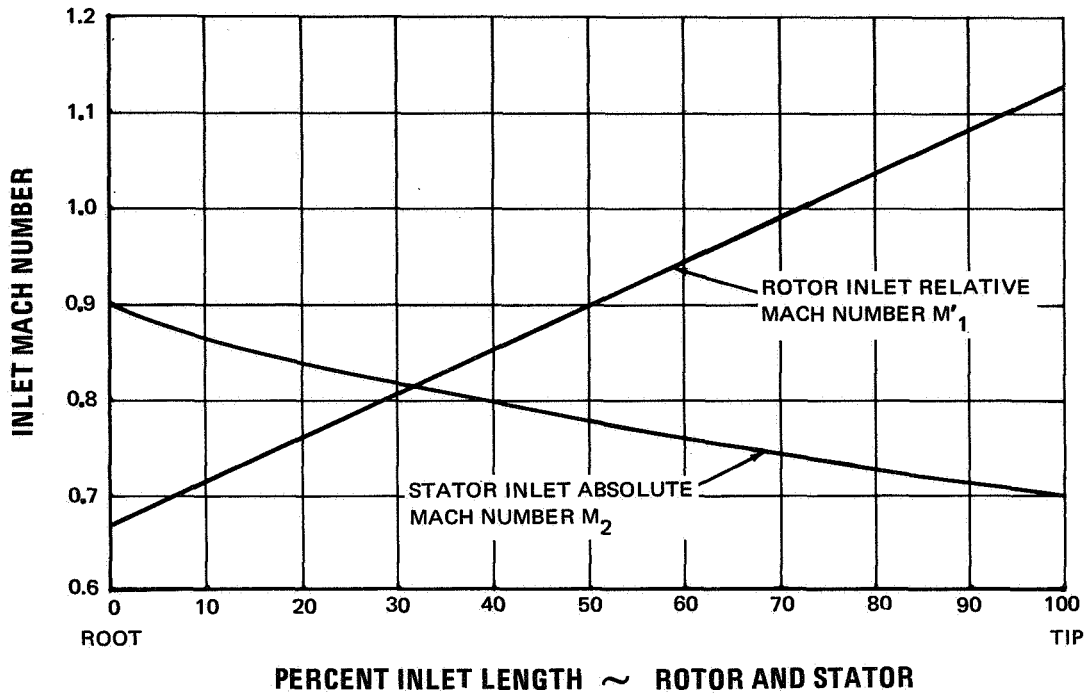
Figure 9   Rotor and Stator Inlet Mach Number Profiles
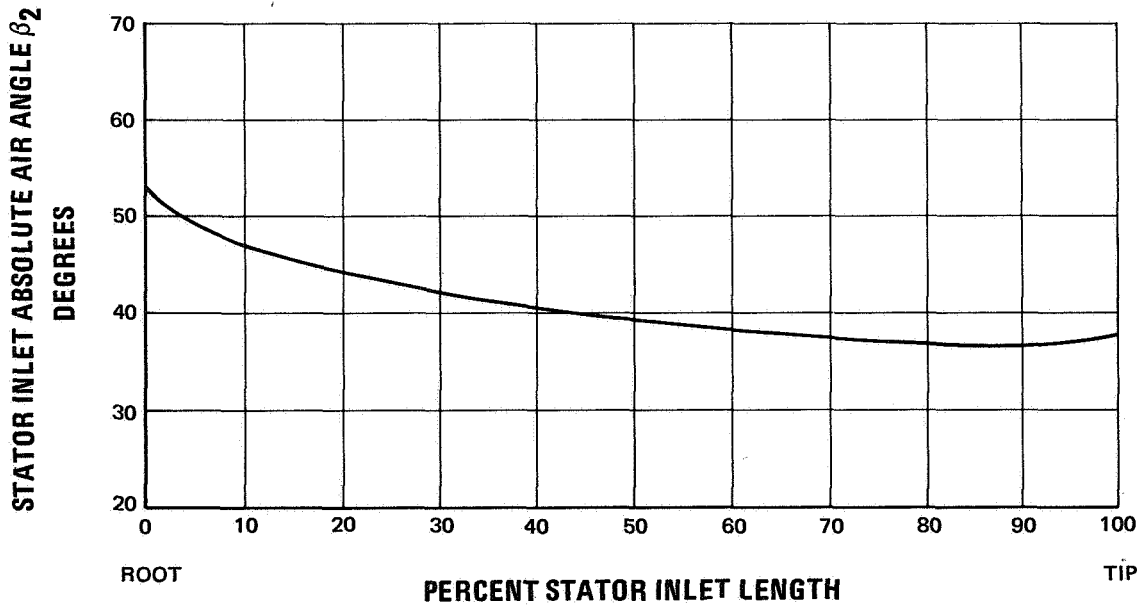
Figure 10   Stator-Inlet Absolute Air Angle Profile

10
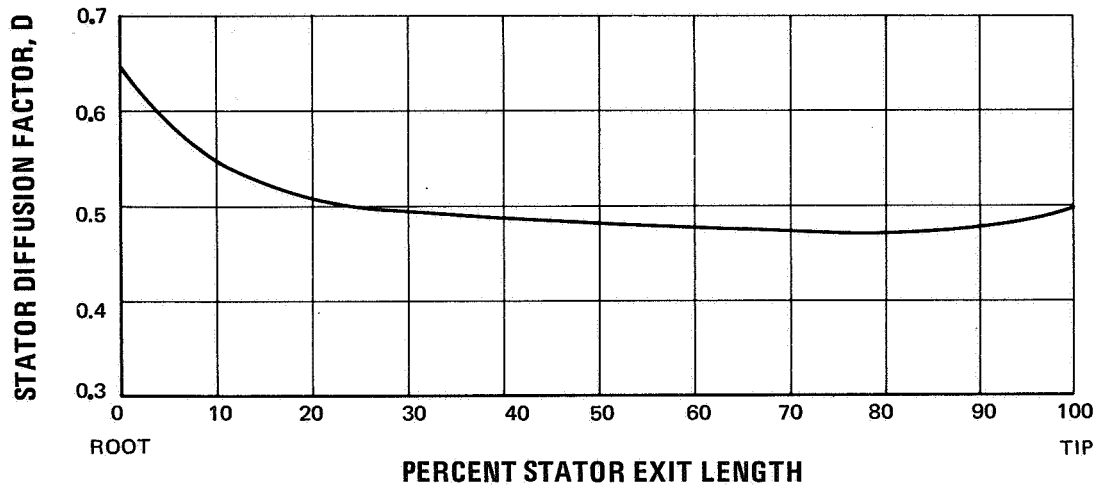
Figure 11   Stator Diffusion Factor

The value of an end-wall loading parameter defined as $1- (V^2_{m\ min}/V^2_{m\ max})$, where V_m is the end-wall meridional velocity between blade rows, was kept below values attained in previous compressor tests. Sharp curvatures were not used to control blade loadings since the resulting equivalent rise in wall loadings between blade rows is just as dangerous to stage performance as excessive blade loadings. Table 2 lists values of the wall-loading parameter for the present design as well as for other stages for which experimental data are available.

TABLE 2
Values of Maximum Wall-Loading Parameter

Compressor	Maximum Wall-Loading Parameter $1- (V^2_{m\ min}/V^2_{m\ max})$	Location
Contract NAS3-7614 design (Reference 3)	0.482	between rotor and stator
JT9D LPC	0.47	LPC transition duct
Present design	0.466	between rotor and stator

The design vector diagrams for the rotor and stator leading and trailing edges are presented in aerodynamic summary tables, Appendix 7, for every ten percent of flow radially.

11

IV. AIRFOIL DESIGN

A. Rotor

The rotor uses multiple-circular-arc airfoils designed on conical surfaces which are approximate streamlines of revolution. Airfoil sections were defined by specifying total and front chord, total and front camber, maximum thickness and its location, and leading and trailing edge radii as shown in Figure 12. The design of the multiple-circular-arc airfoil controls the relation between the amount of supersonic (front) turning and the amount of subsonic (rear) turning. With this control, minimum total loss can be achieved by proper optimization of shock losses with respect to subsonic diffusion losses. The multiple-circular-arc concept is discussed in detail in Reference 2. Figure 13 shows several views of this rotor and Figure 14 shows the rotor and disc assembly.

The chord and thickness ratio were selected to provide mechanical integrity without part-span shrouds. Even though the tip design speed is low at 1000 ft/sec (304.8 meter/sec), the design still presents a mechanical challenge because of the very large amount of blade twist. Between the root and tip the stagger angle γ varies 67 degrees (see
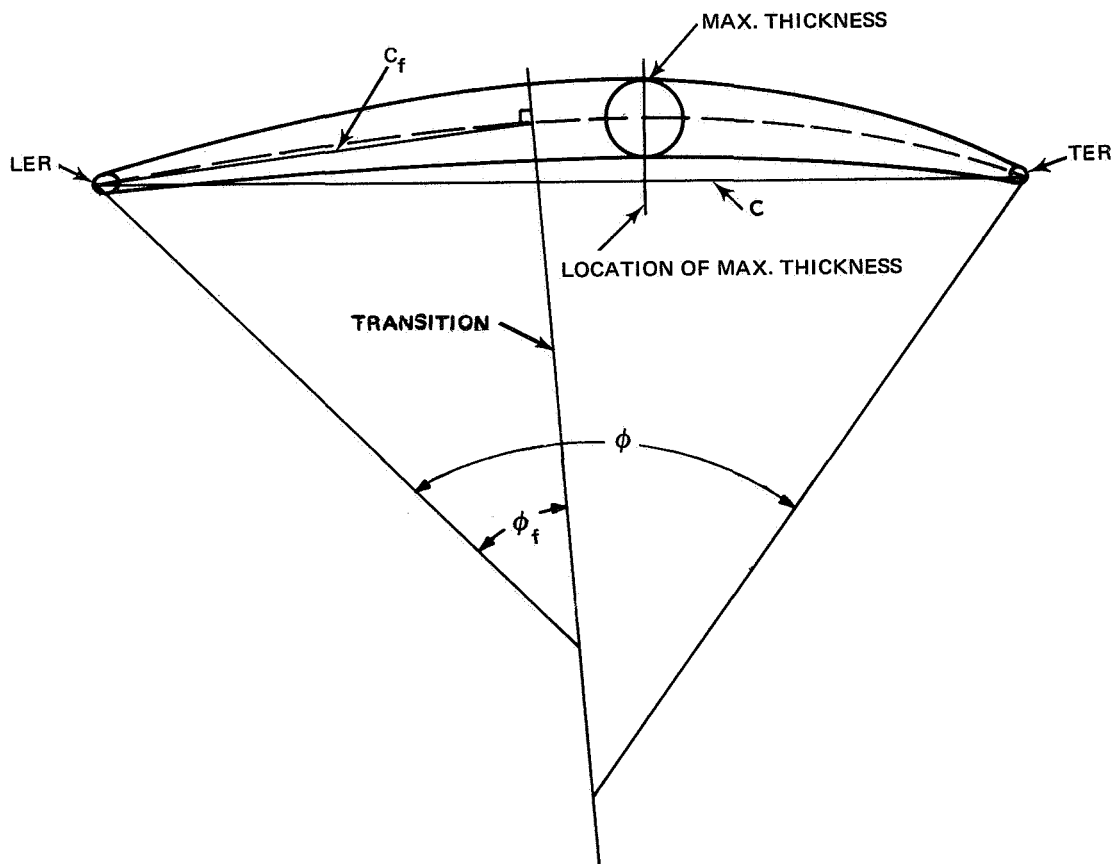
Figure 12   Multiple-Circular-Arc Airfoil Definitions

12
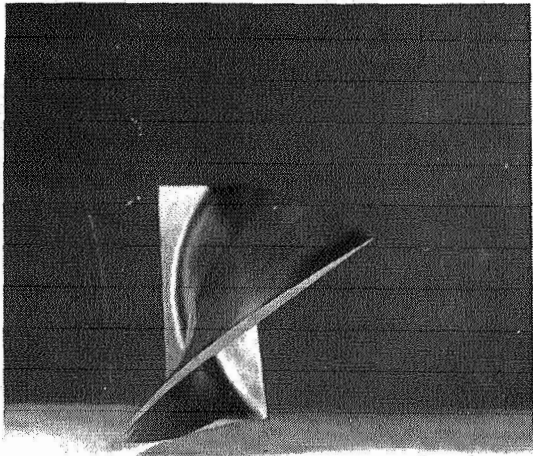
Top View Looking towards Platform
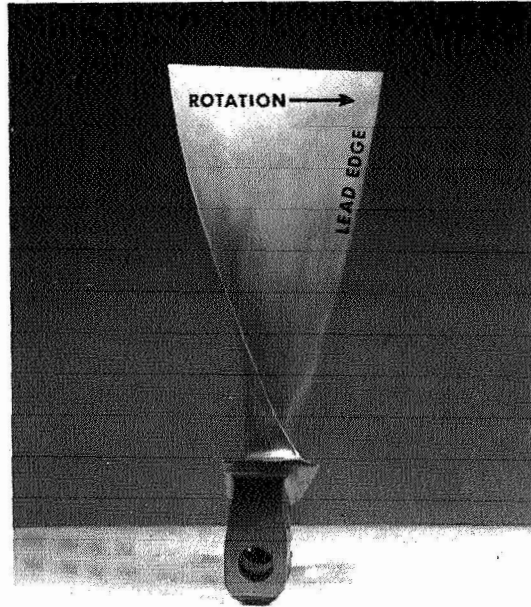
Trailing Edge
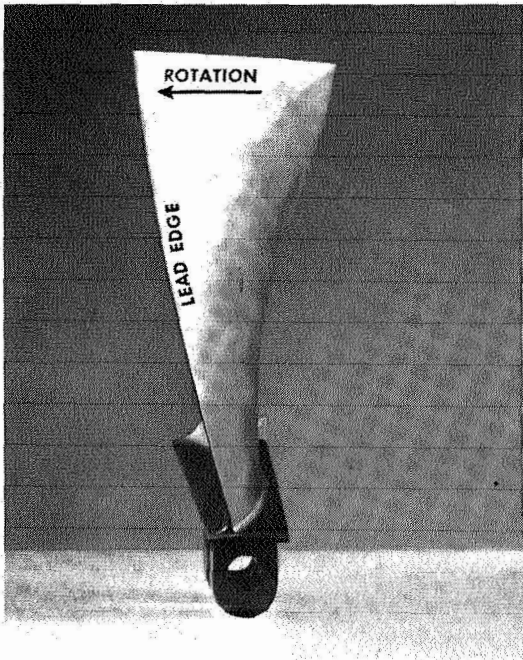
Leading Edge
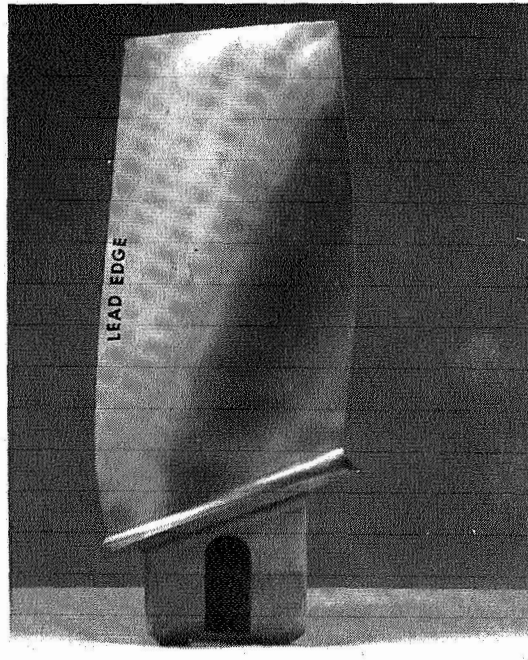
Side View Looking in Direction of Rotation

Figure 13   Four Views of Rotor
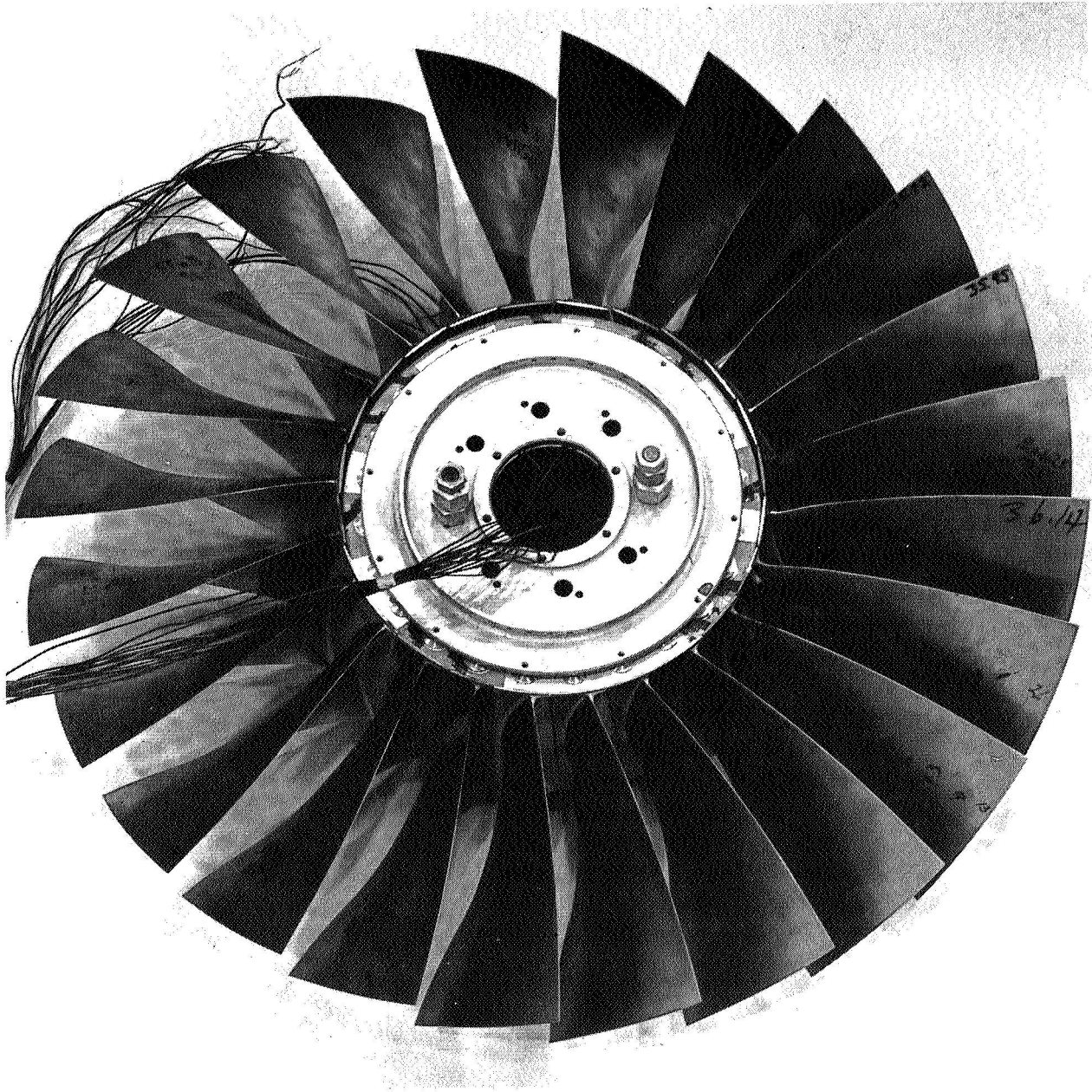
Figure 14   Rotor Assembly Looking into Rotor in Flow Direction

Figure 13) which produces substantial untwist stresses as discussed in Section V, below. In addition to mechanical problems, the thickness ratio selection was also affected by choking considerations. At the root, where the blade turns past axial, the throat area is controlled by the value and location of maximum thickness. The final value of chord and thickness ratios are 4.5 to 5.525 inches (0.1143 to 0.1403 meter) and 0.07 to 0.03, root to tip, respectively. Both chord and thickness are tapered linearly between root and tip. The number of rotor blades was set at 24 to provide a tip solidity of 1.358 which is consistent with the contract and results in a diffusion factor of 0.534 at 95 percent span from the root, as shown in Figure 6.

For the portion of span with supersonic inlet relative Mach numbers, the front chord was set to produce a transition point just aft of the assumed shock location, as shown in Figure 15 and discussed in Appendix 2. The ratio of front chord to full chord, C_f/C, may also be obtained from Appendix 8, Table 11. In the root section, chordwise camber distribution and transition location were determined by choking criteria. Because of the extreme past-axial turning at the root, the minimum passage area occurred at the trailing edge, and it was necessary to keep uncovered trailing edge turning to a minimum. This was accomplished by locating the transition point aft of mid-chord and putting little camber into the rear section of the airfoil. Maximum thickness and its chordwise location on the root airfoil were set to obtain the desired channel area distribution, as discussed in Appendix 4. A root maximum thickness of 7 percent chord, located at 40 percent chord gave the desired channel area. For the outer 80 percent of the flow annulus, maximum thickness is at 50 percent of chord, with a smooth fairing between 0 and 20 percent of the flow annulus from the root.

Incidence selection was based on three sources, 1) two-dimensional cascade data for the root section, 2) rotor data from Reference 3 for sections between the root and mid-span, and 3) a supersonic flow alignment technique to a neutral point B' for the outer 22 percent of span. Details of the incidence selection are discussed in Appendix 3. The spanwise variation of incidence is shown by Figure 16.

The front camber for the subsonic portion of the rotor was selected to produce a ratio of channel throat to critical area, (A/A*), of 1.03 times the A/A* for the inlet relative Mach number. The front camber for the supersonic portion of the blade was adjusted to set the blade-passage minimum A/A* at 1.03. This procedure is discussed in Appendix 4. The resultant local channel A/A* through the rotor passage for ten spanwise stream tubes is shown by Figure 18. The area ratios corresponding to the inlet and exit relative Mach numbers are also shown on Figure 18 for reference.

Deviation for most of the rotor was set using Carter's rule plus an experience factor as discussed in detail in Appendix 5. The rotor root was treated as a separate problem from the rest of the blade for deviation as was also the case for incidence angle. There is little information in the literature and Pratt & Whitney Aircraft has had no experience with a rotor that turns almost 40 degrees past axial. Root deviations were calculated using the method of NASA SP-36[4], Carter's rule (Appendix 5), and Ainley's turbine deviation system[5]. In addition, Pratt & Whitney Aircraft cascade data was reviewed. Cascade data in Figure 17 show an air turning angle ($\Delta\beta$) of 60 degrees at $i_{mc}= 0$, or

DIAMETER ~ METERS

DIAMETER ~ INCHES

SHOCK
INTERACTION
LOCATION

TRANSITION

AXIAL LOCATION ~ INCHES

AXIAL LOCATION ~ METERS
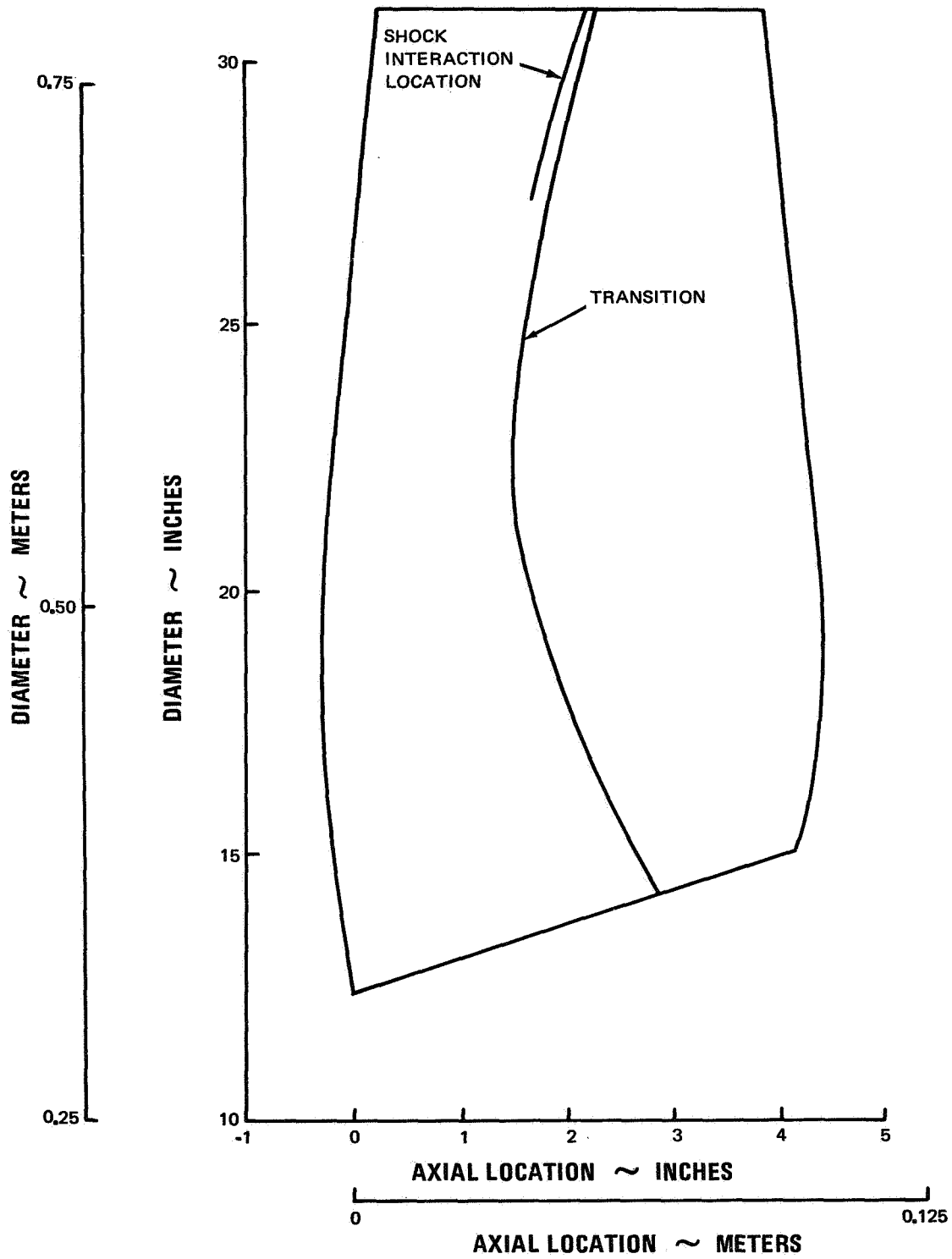
Figure 15   Rotor Axial Projection

16
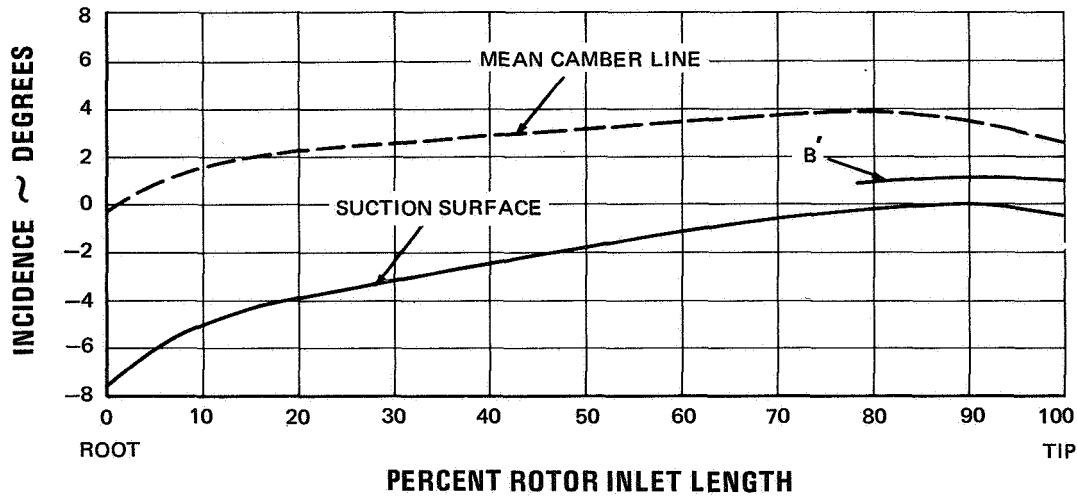
Figure 16   Rotor Incidence Referenced to Mean Camber Line and Suction Surface at Leading Edge and at Point B'

10 degrees of deviation ($\phi - \Delta \beta = 10°$). The subject rotor root airfoil has its maximum camber point located nearer the leading edge and also has higher solidity than the cascade of Figure 17, thus reducing the estimated deviation to about 7 degrees. The results of these deviation systems are tabulated below:

TABLE 3
Rotor Root Deviation System

Deviation System	Deviation, degrees
NASA SP-36	10
Carter's rule	14.8
Ainley's turbine system	9
P&WA cascade data	7

It was decided to use 7 degrees instead of the other predictions because of its more direct approach. Other systems cited are dependent on extrapolated corrections, made necessary by basic differences in the system operating ranges. Also of prime concern in predicting the proper deviation was the channel choking that might occur as a result of excessive camber, i.e., accelerated flow at the end of the channel between blades. Use of the 7-degree deviation does not cause choking in the blade channel. This root deviation was faired into the deviations calculated for the rest of the span using the modified Carter's rule. The spanwise variation of deviation is shown in Figure 19.

An additional correction was required to compensate for blade untwist due to centrifugal loading. Static blade angles were set so that the untwist at design speed produced the desired operating blade angles. Rotating as well as static blade angles are shown by Figure 20.

17
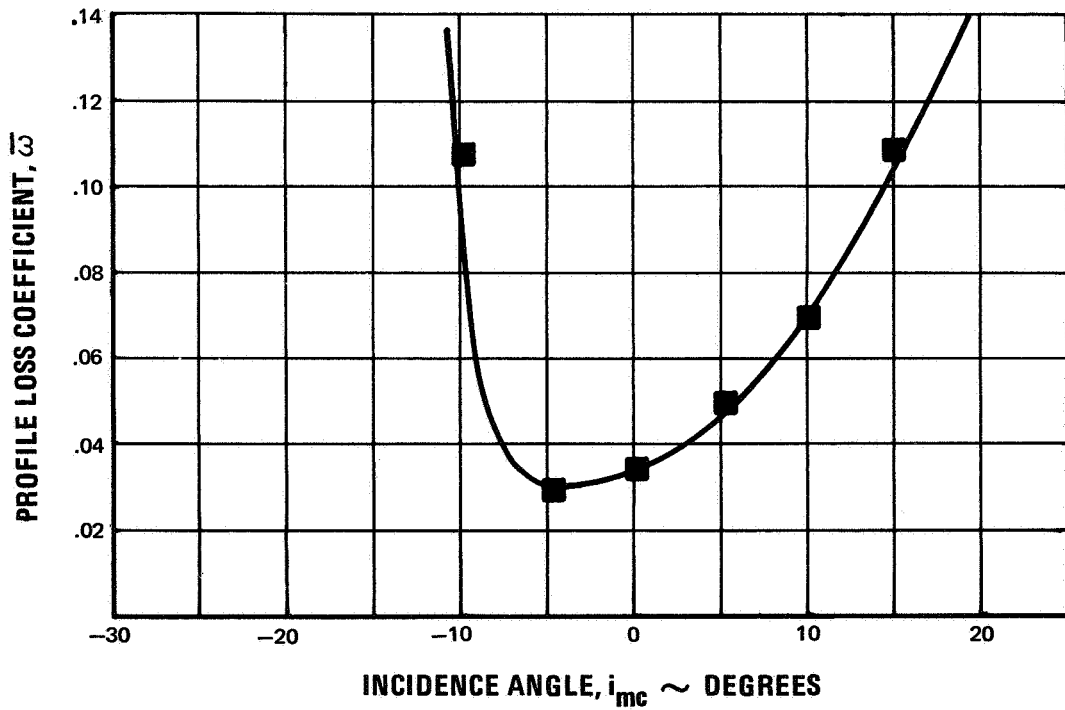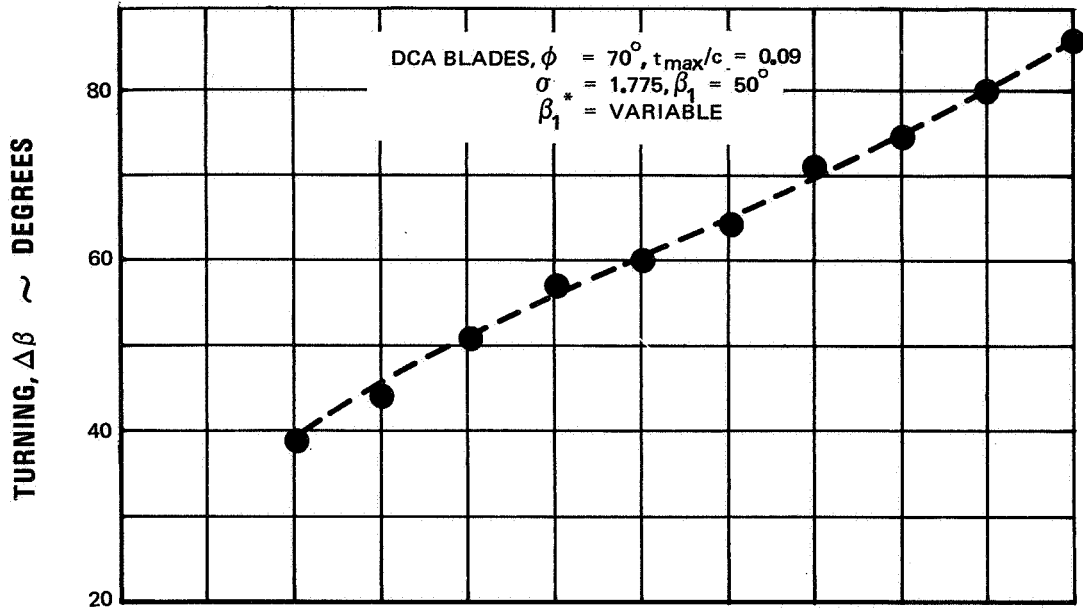
Figure 17   Two-Dimensional Cascade Data

18

RATIO OF ACTUAL TO CRITICAL AREA, A/A*

A/A* (INCLUDES SHOCK LOSS)

BETWEEN 0% AND 5% FLOW FROM ROOT STREAMLINE

$1.03 \ (A/A^*)_{M_1'}$

BETWEEN 10% AND 20% FLOW

$1.03 \ (A/A^*)_{M_1}$

BETWEEN 20% AND 30% FLOW

$1.03 \ (A/A^*)_{M_1'}$

BETWEEN 30% AND 40% FLOW

$1.03 \ (A/A^*)_{M_1'}$

BETWEEN 40% AND 50% FLOW

$1.03 \ (A/A^*)_{M_1'}$

BETWEEN 50% AND 60% FLOW

$1.03 \ (A/A^*)_{M_1'}$

BETWEEN 60% AND 70% FLOW

FIRST SUPERSONIC STREAM TUBE

BETWEEN 70% AND 80% FLOW

BETWEEN 80% AND 90% FLOW

BETWEEN 90% AND 100% FLOW

$Z-Z_{LE}$

$Z-Z_{LE}$

AXIAL LOCATION FROM LEADING EDGE, $Z-Z_{LE}$ ~ INCHES

Note: × = A/A* at rotor relative inlet Mach number
       ● = A/A* at rotor relative exit Mach number

Figure 18   Rotor A/A* Profile

19
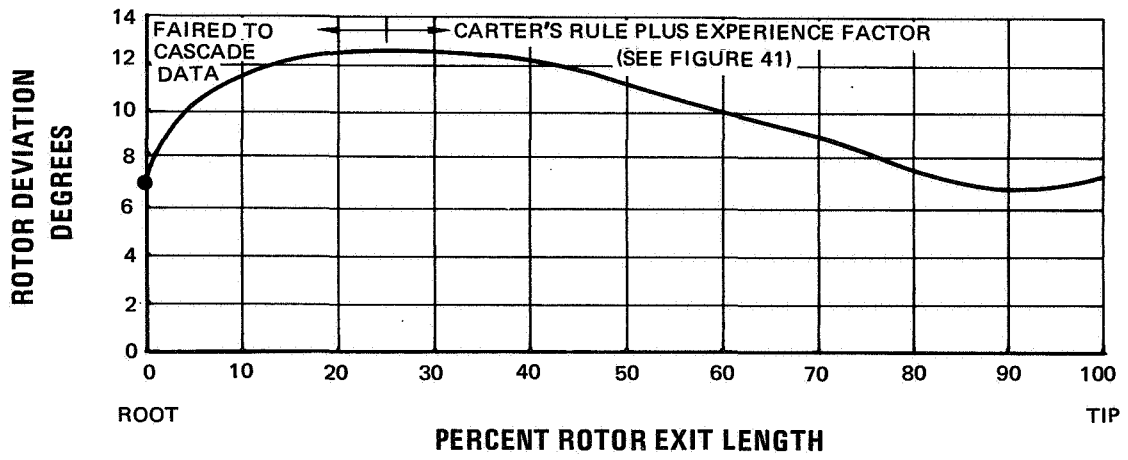
Figure 19   Rotor Spanwise Deviation on Conical Surface
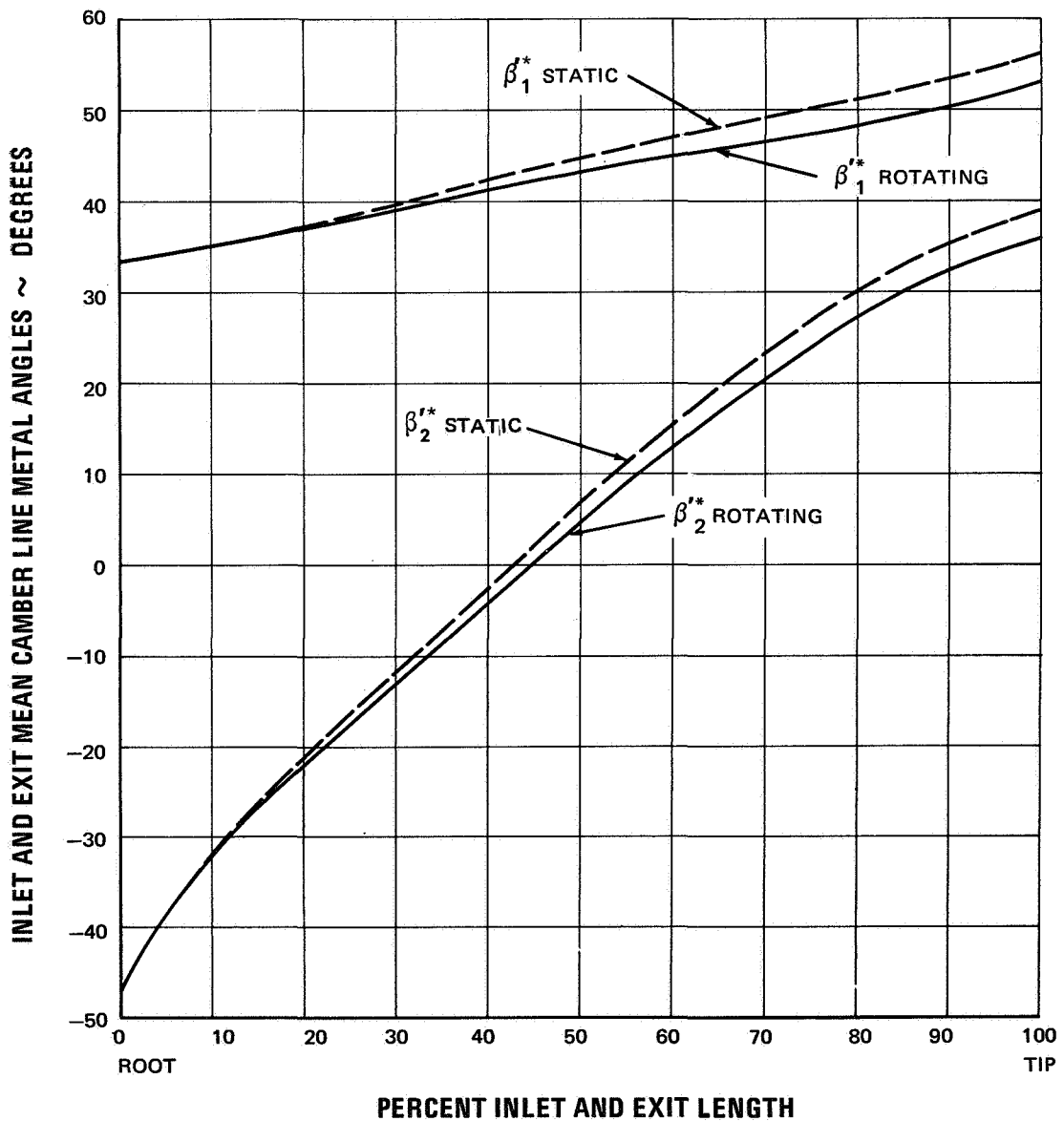
Figure 20   Rotor Spanwise Variation of Inlet and Exit Mean Camber Line Metal Angles on Conical Surface Including Untwist Effect

The rotor geometry on the conical surfaces is summarized in Appendix 8, Table 11. For manufacturing purposes the airfoil sections were redefined on planes normal to a radial line passing through the center of area of the root airfoil section. A computer program provided a smooth fit of the airfoil properties and produced a set of coordinates for manufacturing purposes. These coordinates are tabulated in Appendix 9, Tables 13 to 16.

B. Stator

The stator, like the rotor, is a multiple-circular-arc airfoil (Figure 12) and is designed on conical surfaces approximating stream surfaces. The design philosophy and final design is similar to that detailed in Reference 2. However, the aerodynamic requirements of the present stator are somewhat less severe than those of Reference 2. For example, loading or D-factor is 0.64 near the hub (root) and the inlet Mach number there is about 0.9.

Figure 21 shows the 64 stator vanes as an assembly. The number of stator vanes was set from noise considerations. Stator-root solidity was selected to be 2.169 and aspect ratio 3.67. With a constant radially-projected chord utilized, this chord length is 1.826 inches. The maximum thickness-to-chord ratio was set to vary linearly from 0.039 at the root to 0.07 at the tip. Maximum thickness was located at mid-chord to minimize edge bluntness. Leading and trailing-edge radii are about 8.5 percent of the maximum thickness. These values of maximum thickness and edge radius are small enough for low losses and yet large enough to provide mechanical integrity as discussed in Section V.

The incidence angle to the suction surface was set equal to zero because minimum loss was near this angle for similar transonic stators in References 3 and 8. Some of these loss results are repeated for convenience in Appendix 3. Figure 22 presents the suction surface and mean camber line incidence for the stator.

The transition location between front and rear cambers was selected to be at the stator suction-surface shock intersection point (defined in Appendix 2). The transition point is shown in an axially-projected view of the stator in Figure 23. The amount of supersonic camber or turning ahead of the transition location was set to be 6/10 of the supersonic turning for a double-circular-arc design. This is the same criterion utilized in Reference 2 which resulted in good transonic stator performance (References 3 and 8). A Prandtl-Meyer expansion from a Mach number of unity was used to estimate suction-surface Mach number ahead of the shock, although inlet Mach numbers were in general slightly subsonic (Figure 9). Although this technique overestimates the suction-surface Mach number, the inlet Mach number is averaged with it to yield a normal shock loss at the averaged value. However for the present stators, shock losses are almost negligible. Stator profile losses were estimated from recent results on similar designs (References 3 and 8), and are presented in Appendix 2.
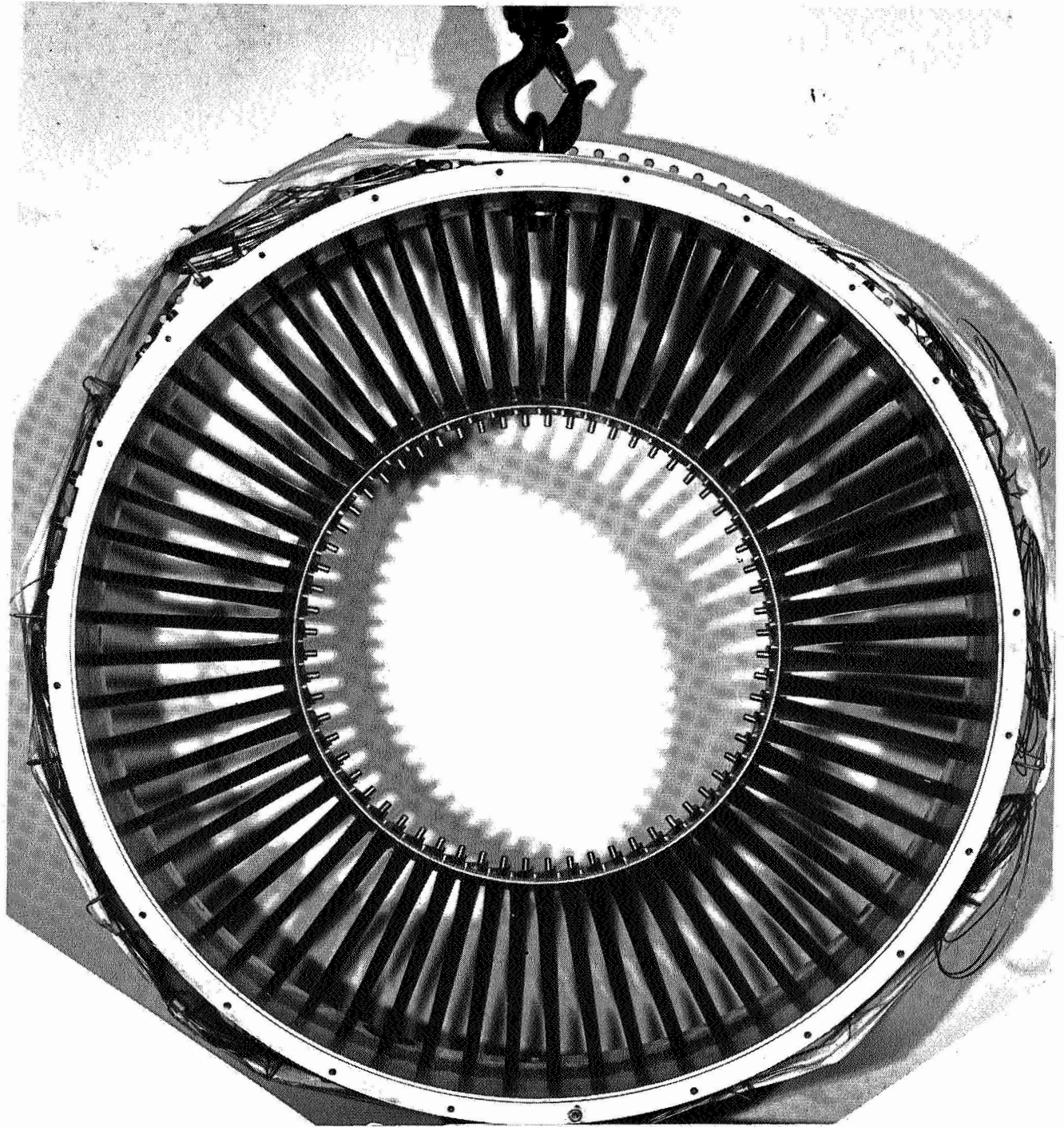
Figure 21   Assembly View of Stator Looking at Stator Leading Edge
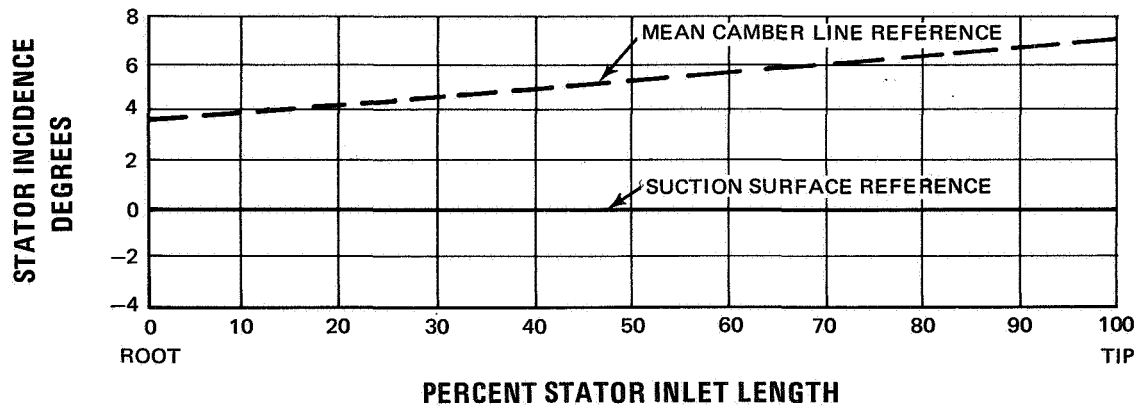
Figure 22   Stator Incidence Referenced to Mean Camber Line and Suction Surface at
Leading Edge

The cross-sectional flow areas through the stator vanes were not tailored by design as
was done for the rotor blades. However, the flow-area distribution was calculated to in-
sure unchoked conditions. Figure 24 presents the actual-to-critical area ratio as a func-
tion of axial location through the stators. The critical flow area is determined from lo-
cal conditions between the leading and trailing edges of the vane. The stream-tube anal-
ysis used for the stators is similar to that described for the rotor blades in Appendix 4.
The minimum area ratio is about 1.08 which occurs near the stator root. The minimum
area ratio moves slightly downstream from the stator leading edge as the span is trav-
ersed from root to tip (Figure 24).

Stator deviations are shown in Figure 25. These are based on Carter's rule plus an ex-
perience factor from similar stators as detailed in Appendix 5. The stator inlet and exit
mean camber line metal angles are presented in Figure 26. The stator is designed to
turn the flow back to the axial direction.

The stator geometry is tabulated in Appendix 8, Table 12, on the conical surfaces used
for design. For manufacturing purposes the airfoil sections were redefined on planes
normal to a radial line passing through the center of area of the root airfoil section.
These manufacturing coordinates are in Appendix 9, Tables 17 to 20.

C. Stator Root Slit Design

In order to reduce total pressure losses and attain higher lift coefficients in axial flow
turbomachinery, it is necessary to prevent end-wall boundary-layer separation. Data
from Reference 8 show that losses in the end-wall region limit stator loadings. Other
experimental data[6] show that substantial improvements in performance (2 points in
efficiency) can be gained by applying boundary-layer control in the corner of a blade or

23
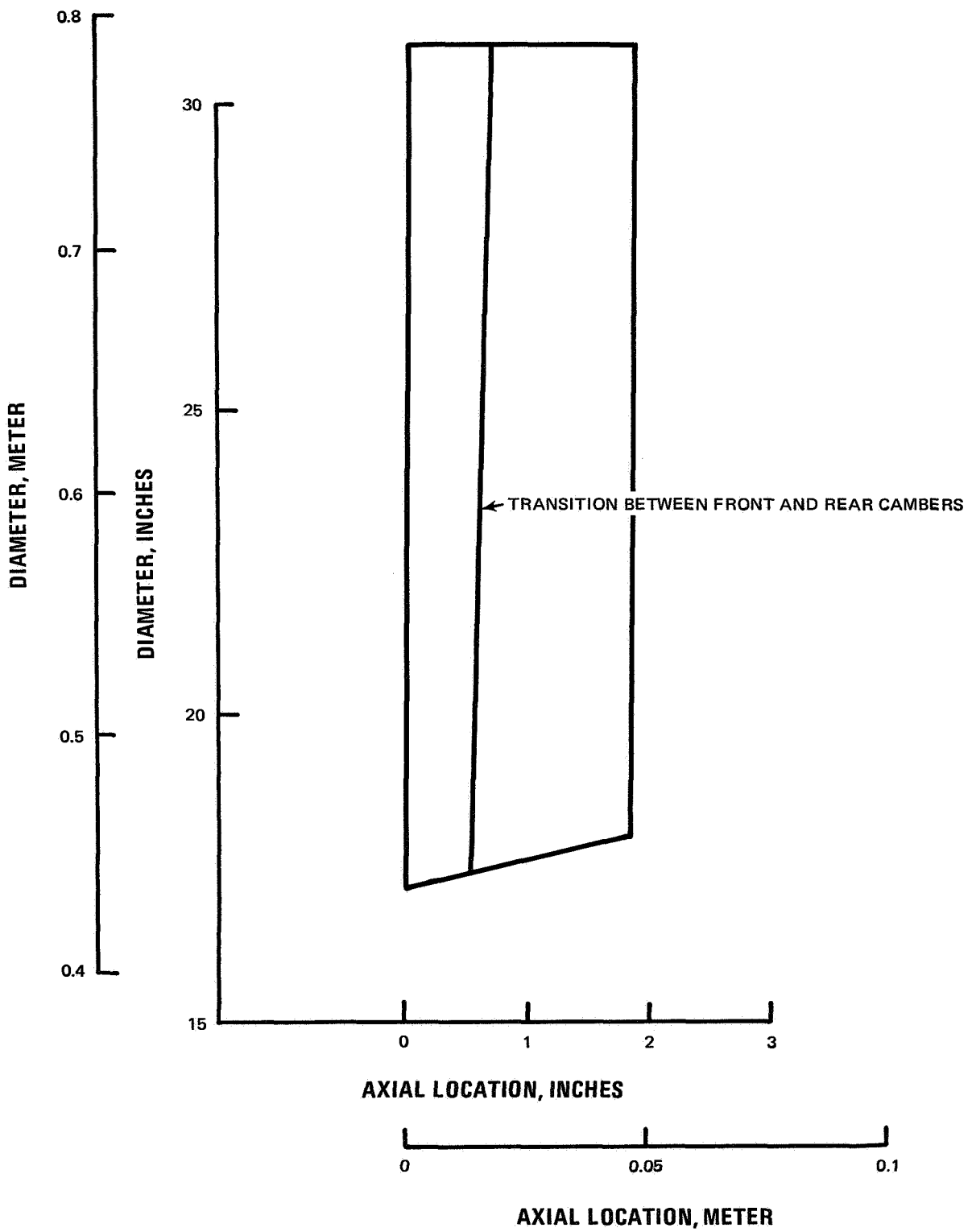
Figure 23   Stator Axial Projection
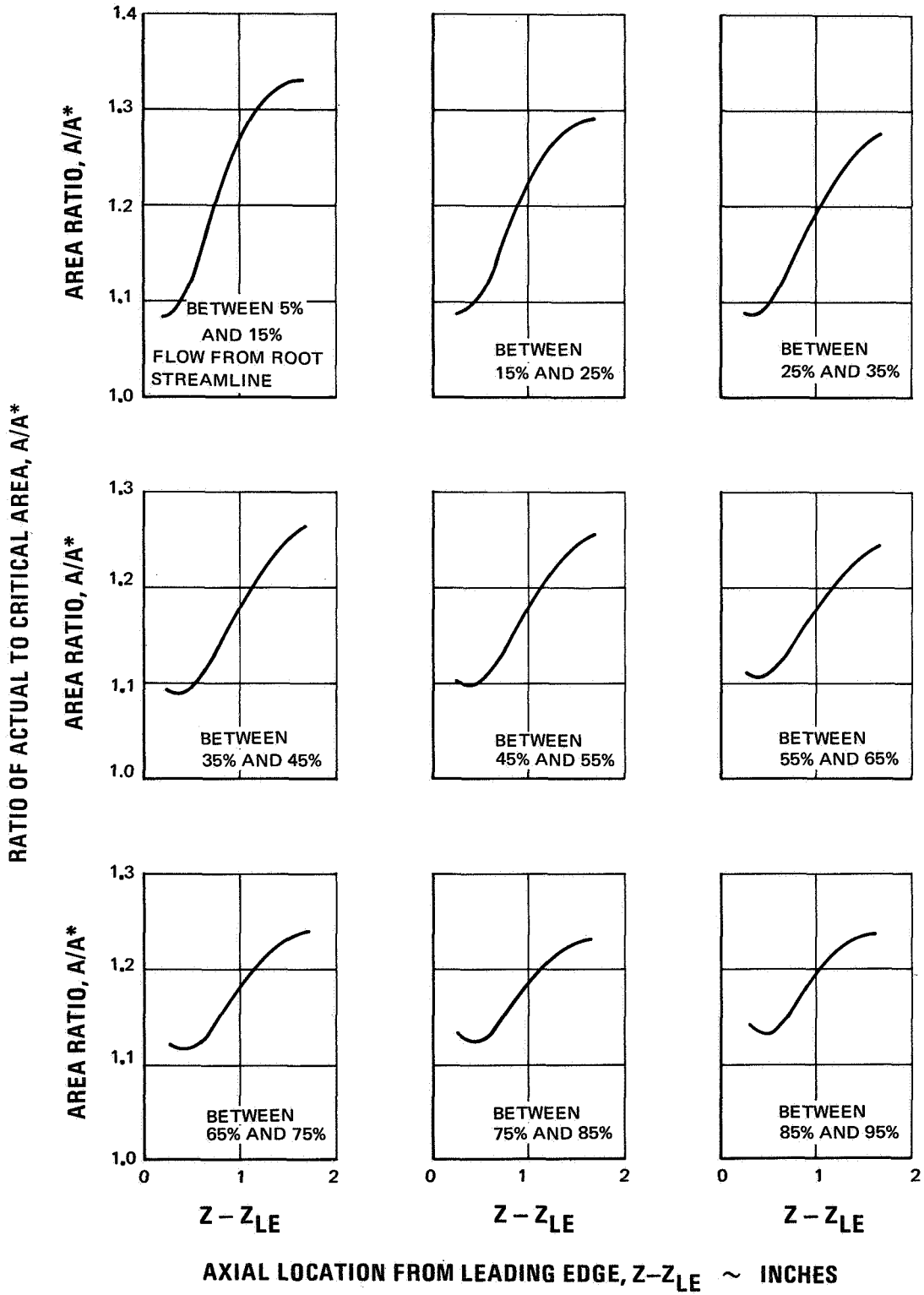
Figure 24 Stator A/A* Profile
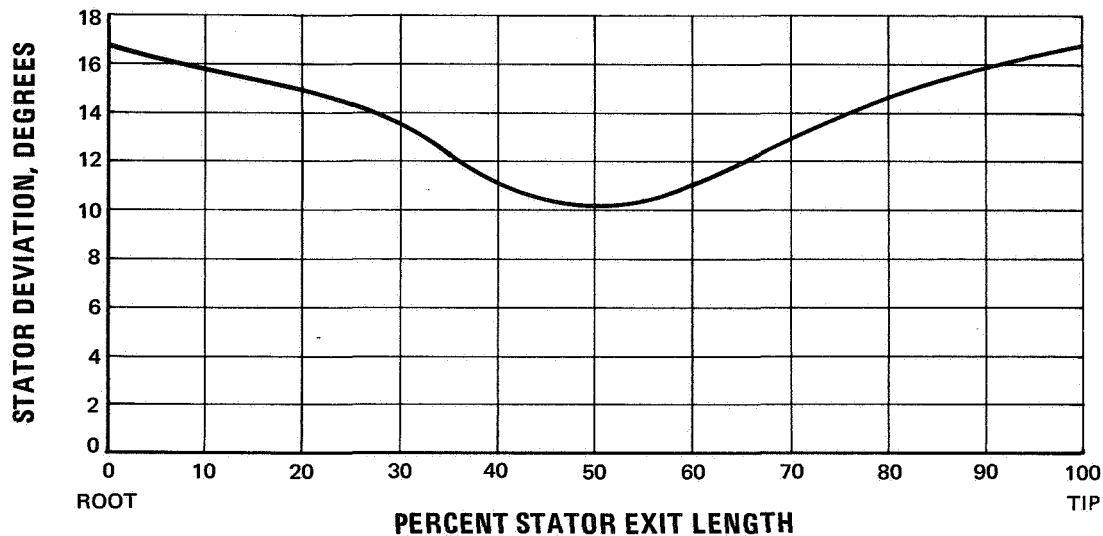
Figure 25   Stator Spanwise Deviation on Conical Surface

vane surface and the annular wall or casing. Peacock[6] reduced compressor cascade losses significantly by extracting a small amount of flow through a slit at the intersection of the wall and blade suction surface. His data were analyzed and slit design criteria were developed. It was found that most of the attainable benefit was obtained by bleeding off the flow within the displacement thickness growths on both the vane surface and the wall. This is the flow in which the direct and turbulent dissipation of kinetic energy is greatest[7]. Calculations of bleed flow requirements based on the analysis of Peacock's data are presented in Figure 27 for the hub (root) end only of this stator, which has an aspect ratio of 3.67 and a hub solidity of 2.169. The minimum slit bleed flow extracts only the air with the lowest energy. When the slot width extends beyond the boundary of this low-energy fluid, additional air is drawn in, and increased bleed flow is necessary to insure that the required amount of low-energy fluid is extracted.

With flow rate determined by slit width, (Figure 27), many combinations of slit length and flow velocity are possible. In this design, the slit extends from 15 percent to 85 percent of chord. This is further forward than the optimum configuration reported in Reference 6, but it provides suction closer to the minimum pressure point, and covers the area of possible shock impingement during transonic operation. Sonic bleed velocity was selected to prevent recirculation. A slit width of 0.017 inch (0.000432 m) or slit width to chord ratio of 0.0093, was selected to provide an adequate margin between slit flow capacity and the calculated ratio of slit bleed flow to total flow to prevent separation. A schematic of the stator root slit is shown in Figure 28.

26
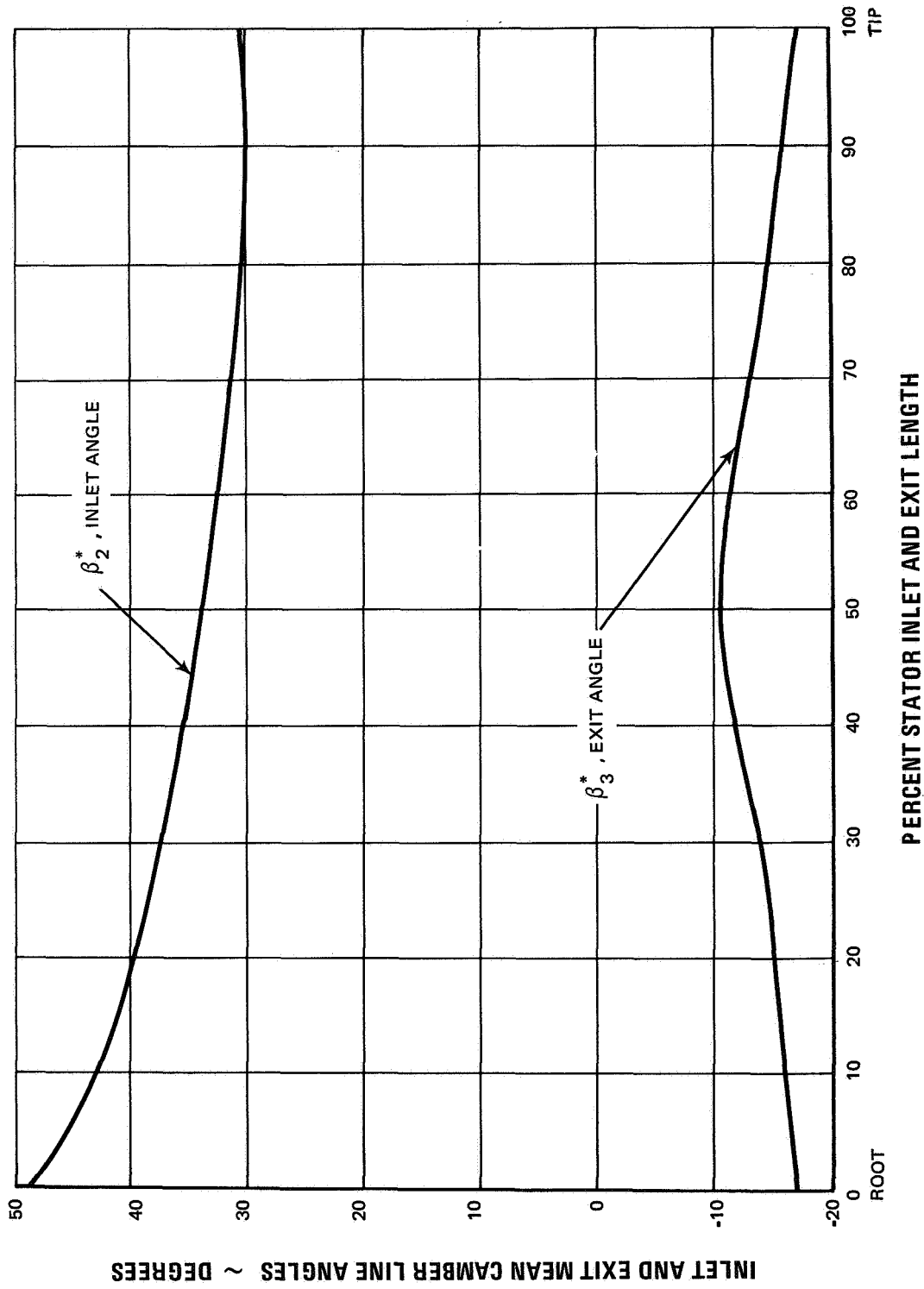
Figure 26   Stator Spanwise Variation of Inlet and Exit Mean Camber Line Metal Angles on Conical Surface
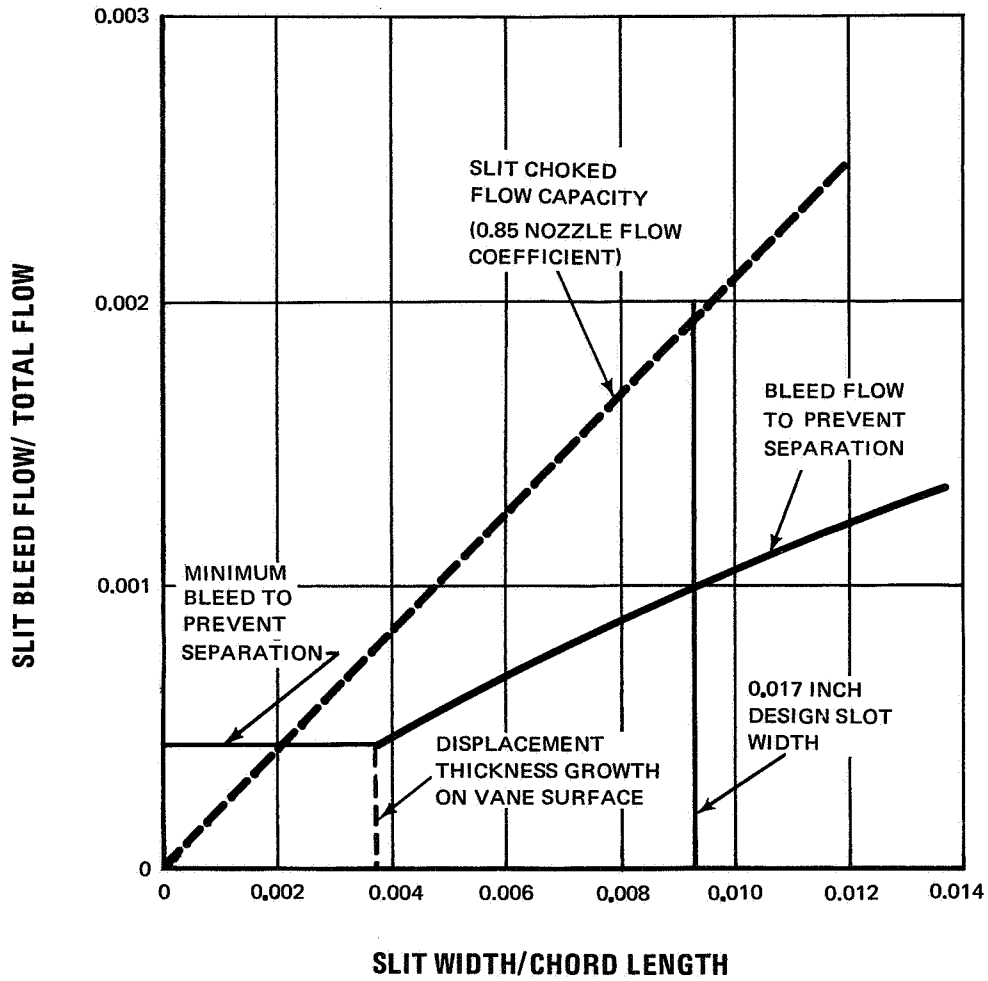
Figure 27   Calculated Minimum Bleed Flow Requirements to Prevent Corner Separation
at Root of Stator with Aspect Ratio of 3.67 and Root Solidity of 2.169
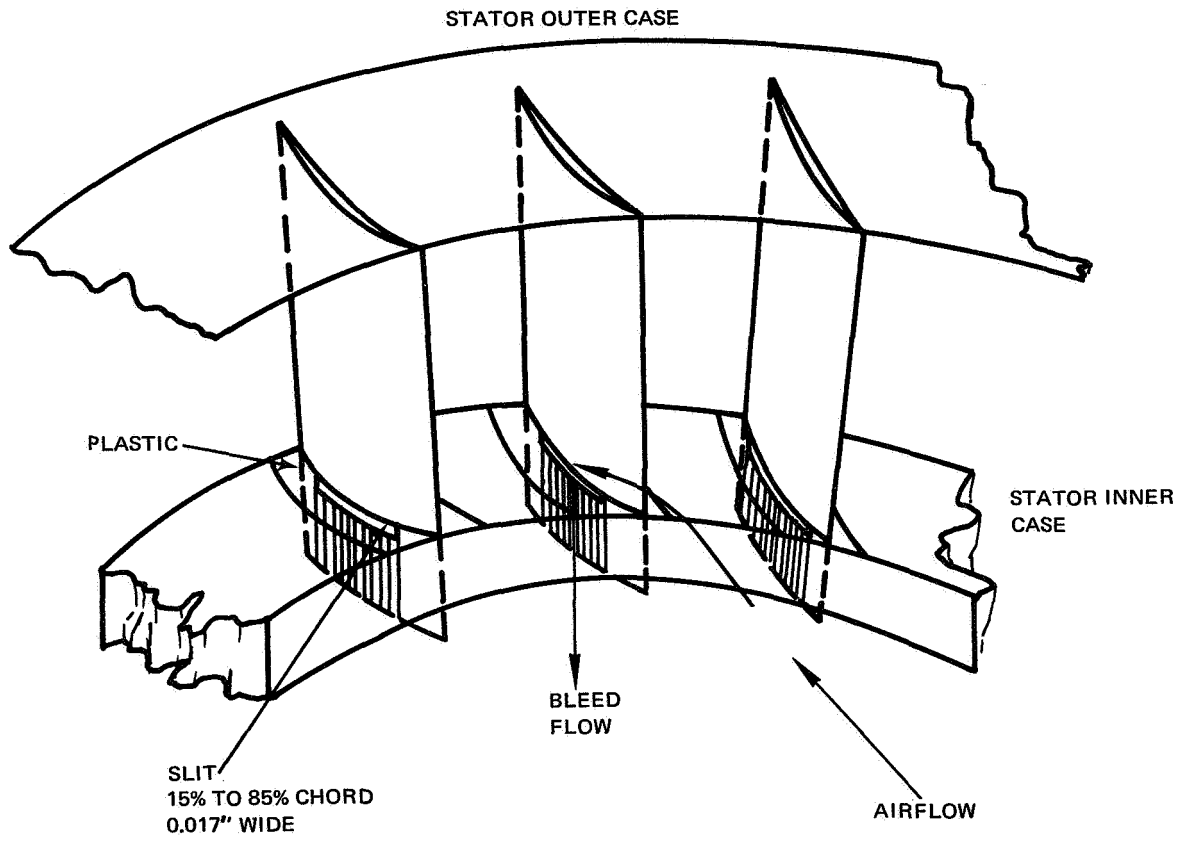
Figure 28   Schematic of Stator Root Slit

V. STRUCTURAL AND VIBRATION ANALYSIS

The aerodynamic design of a fan stage must be integrated with a satisfactory mechanical design. Although the design tip speed is low at 1000 ft/sec (304. 8 meter/sec), the blade twist is unconventionally high at 67 degrees. Stator aspect ratio is also high at 3. 67. The mechanical design of the stage follows:

A. Blade Attachment and Disc Stresses

Initial attempts to design conventional dovetail rotor attachments were unsuccessful. The frequency of the blade in first-mode bending fell in the range where it would re-sonate with two excitations per revolution while operating near design speed. Increasing root thickness-to-chord ratio to 0. 105 gave a barely-acceptable frequency margin at 110 percent of design speed, but was not acceptable aerodynamically because it caused choking in the channels between root-section airfoils near the trailing edge. Because circumferential distortion testing will require operation with two excitations per revolution, and because adequate margin could not be obtained with a conventional dovetail attachment, a pin-root blade attachment was used. The pin-root attachment was designed to produce a first-mode bending frequency falling between first and second-order excitation lines, thus eliminating resonance crossing. This characteristic is shown in Figure 29. Frequency tuning of this mode is accomplished by designing the right com-
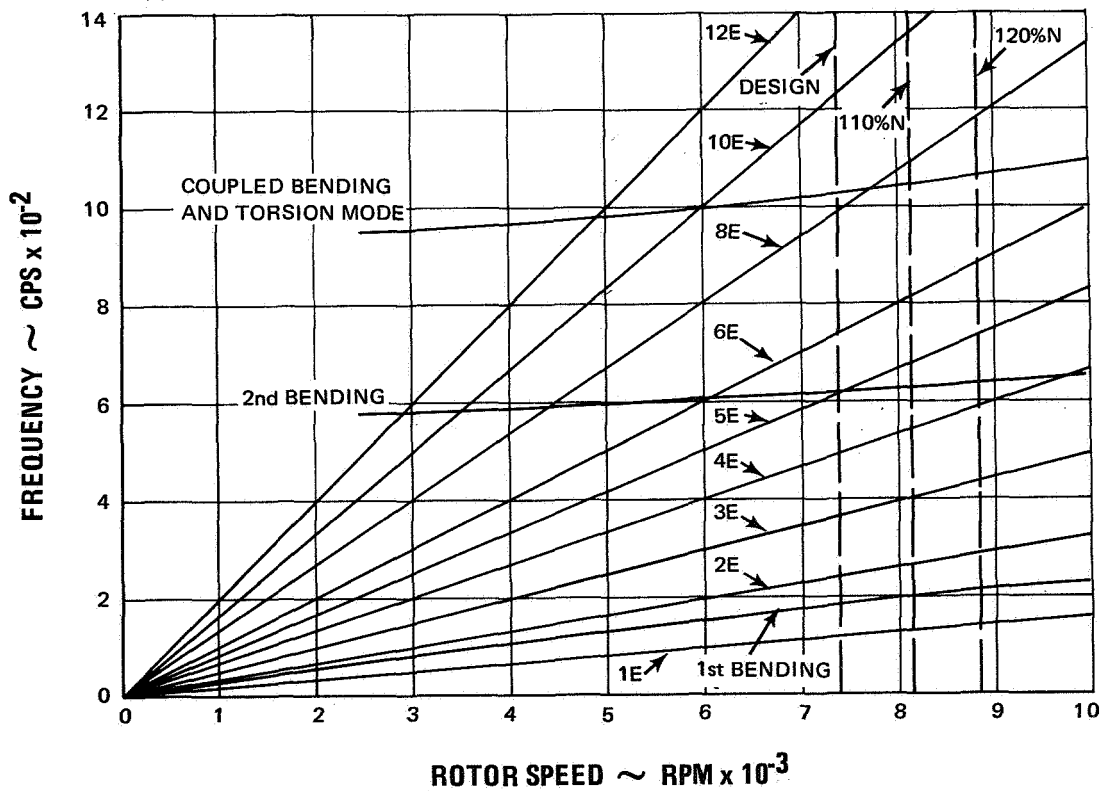
Figure 29   Blade and Disc Resonance Diagram

bination of pin diameter and the pin-to-blade clearance. A pin diameter of 0.70 inch (0.01778 meter) nominal and a clearance of 5 percent of the pin radius was required in this case.

For the type of pin root employed in this design, the attachment length dictates the disc thickness to such an extent that the disc is over-designed. At 120 percent of speed (8880 rpm) and 200°F (366.5°K) the disc burst and yield margins are 2.15 and 2.03, respectively. The tensile stress in the neck of the blade tang (see Table 4) is used as a design parameter and, with the appropriate stress concentration factor, is set near the allowable stress. From this point, the root is designed and optimized. The pin diameter is usually controlled by the blade pitch, thus resulting in the relative high bending stress in this element. Pratt & Whitney Aircraft has several pin-root attachments similar to this design running in the JT8D-1, JT4 and JT12 engines. Table 4 summarizes the disc and attachment stresses.

The pinned attachment also is beneficial in reducing flutter. The airfoil movement relative to the pin provides increased mechanical damping which helps to reduce the vibration amplitude. Also, the platform under the blade leading and trailing edges is not supported by the disc attachment (see sketch with Table 4). Some platform movement reduces blade stresses below what they would be with a completely rigid platform. This blade-disc design should be stable under all reasonable aerodynamic conditions.

B. Steady Stresses

Combined centrifugal pull (P/A) and untwisting stresses were calculated at 110 percent of design speed. A comparison was made to allowable stresses based on AMS 4928 titanium alloy at 150°F (338.7°K). There are two spanwise maximum stress locations, the root section which has high local stresses at the leading and trailing edges, which from past experience is not a problem, and the 10 percent span section. The left sketch in Figure 30 (pressure surface) shows the location and level of the maximum combined P/A and untwist stress and also some relative vibratory stress levels to be discussed later. Combined P/A and untwist stresses at 10 percent span and 110 percent of design speed were calculated to be 62,000 psi (426 x 10^6 N/m^2), which is well below the 0.2 percent yield strength of 100,000 psi (689 x 10^6 N/m^2).

Air loads were calculated for the rotor and stator. The results are presented below in Table 5.

TABLE 4

Disc and Attachment Stresses

Materials:

disc AMS 6415
blade AMS 4928
pin AMS 5615

Assumed Operating Conditions:

N = 8880 rpm (120 percent of design speed)
T = 200°F (366.5°K) (no radial temperature gradient)
pressure drop = 1.5 psi (10.3 x 10³ N/m2)
total disc rim load = 990,000 lb (449,064 kg)

Location	Stress Type	Calc. Stress, psi	Calc. Stress, N/m2	Percent Allowable Stress	Reference JT8D-1 2nd Stage Motor % of Allowable Stress
A – disc bore	tangential	46,298	319×10^6	37.05	
B – disc rim	radial	10,645	73.4×10^6	8.51	
	tangential	23,042	159×10^6	18.4	
C – pin	bending	101,000	695×10^6	88.6	93
	shear	28,500	196×10^6	45.5	
	ovalizing	80,000	551×10^6	80.0	
D – blade tang	tensile	97,500	671×10^6	97.5	100
	hertz (bearing stress)	104,500	720×10^6	69.7	
E – disc flanges					
1) over the holes	tensile	46,100	461×10^6	36.9	
2) holes	tearout shear	35,900	247×10^6	47.9	
3) holes	bearing	41,000	282×10^6	33.3	
F – flange bore	tangential	9,080	62.5×10^6	7.3	
G – diaphram bore	tangential	27,707	191×10^6	22.2	
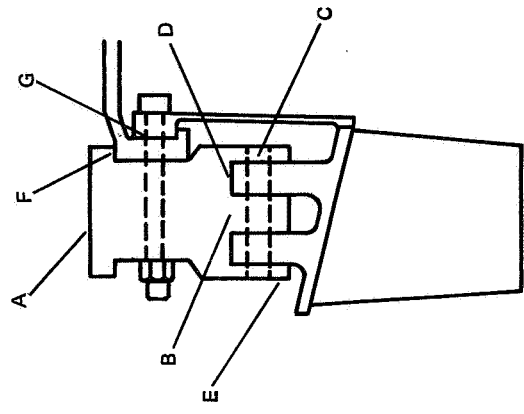
Total radial centrifugal growth at blade tip = 0.017 inch
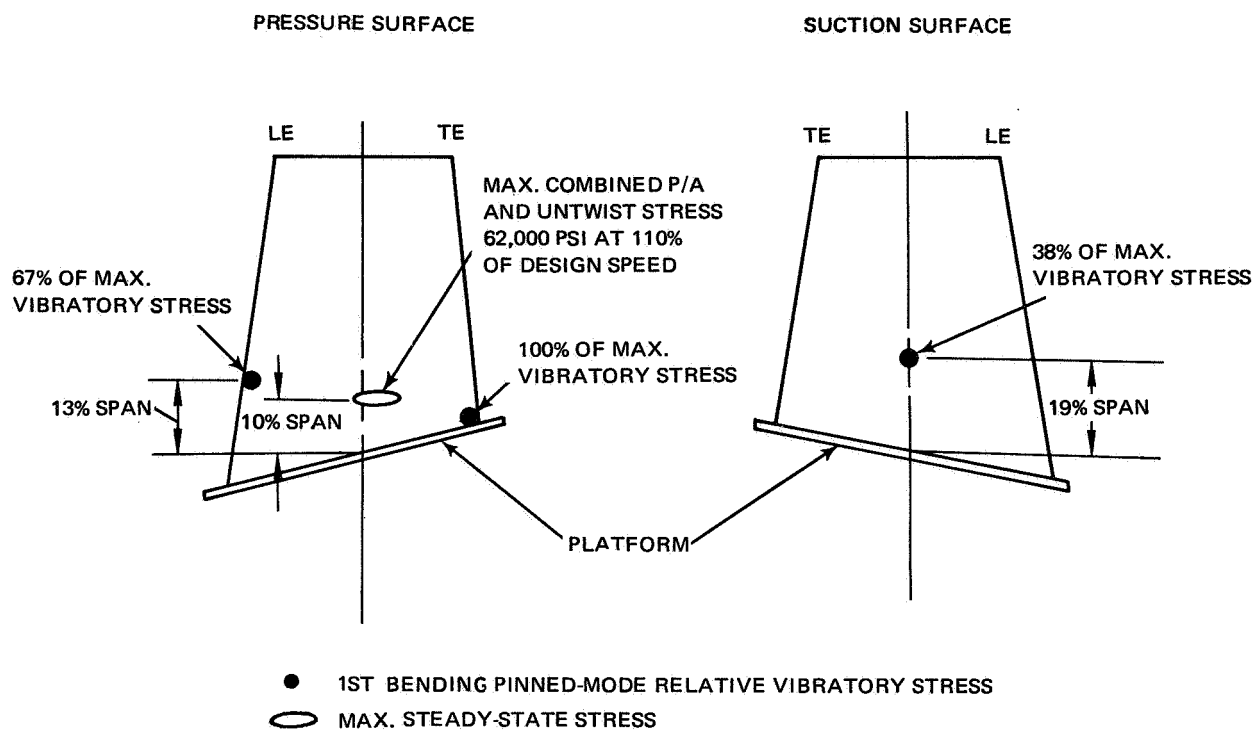
Figure 30 Maximum Combined P/A and Untwist, and Relative Vibratory Stresses

TABLE 5
Rotor and Stator Air Loads[1]

	Rotor	Stator[2]
material	AMS 4928 (titanium)	AMS 5613 (stainless steel)
number of airfoils	24	64
axial load, lb (kg)	2380 (1079.6)	1222.1 (554.3)
axial load diameter, in. (meter)	18.584 (0.4720)	24.542 (0.6234)
tangential load, lb (kg)	4171 (1892.0)	3243.2 (1471.1)
tangential load diameter, in. (meter)	24.769 (0.6291)	24.382 (0.6193)
maximum gas bending stress, psi (N/m^2)	4980 (34.3×10^6)	20484 (141×10^6)
root centrifugal force, lb (kg)	28873 (13,096.8)	---
tensile stress at airfoil root, lb/in^2 (N/m^2)	30490 (210×10^6)	---

[1] Loads are for entire row. Loads for single airfoils are obtained by dividing by number of airfoils.

[2] Stresses were calculated on the basis of a pinned inside diameter and fixed outside diameter, thus providing a more conservative design than with both ends fixed.

34

C. Vibration and Flutter

Rotor blade first-bending mode maximum vibratory stress location is at the root trailing-edge position. Vibratory stress levels relative to the maximum, and at several different locations on the blade, are indicated on Figure 30. The displacement of the maximum vibratory stress from the maximum combined steady-state stress location, also shown on Figure 30 (and previously discussed), improve fatigue life.

A Goodman diagram was developed for the blade material at 150°F (338.7°K) and is presented in Figure 31.
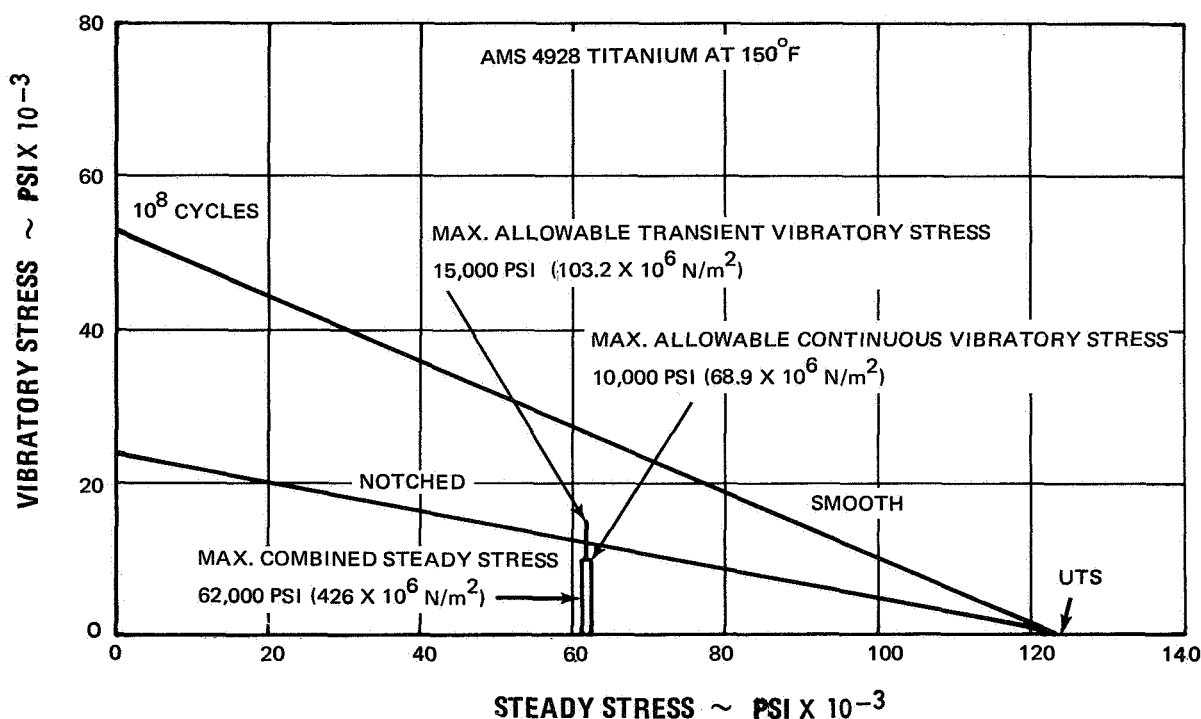
Figure 31   Rotor Goodman Diagram

The maximum allowable vibratory stresses are selected from the Goodman diagram at the calculated maximum combined steady stress of 62,000 psi (426 x 10^6 N/m^2). The maximum allowable transient vibratory stress is chosen as 15,000 psi (103.2 x 10^6 N/m^2) and the maximum allowable continuous vibratory stress as 10,000 psi (68.9 x 10^6 N/m^2). These vibratory stress limits are near to the notched fatigue limit of the material and well below the smooth limit.

The torsional flutter parameter bω_t (where b is the blade chord at 75 percent span from root and ω_t is the torsional frequency) was calculated for the rotor blade and is 1670 ft/ sec (509.0 m/sec). This is well above the values at which flutter problems occur.

Stator vibration frequency was calculated for, 1) hub end free and tip end fixed, i.e., cantilevered stator, 2) hub end pinned and tip end fixed, and 3) both ends fixed. The values of reduced velocity $(V/b\omega_t)$, calculated for the above-mentioned frequencies, showed that the cantilevered stator would be prone to torsional flutter, which could be prevented by fixing the hub end. Bending flutter should not be a problem with either a pinned or fixed hub end constraint. The hub end was therefore supported or fixed by a plastic which was also used for positioning the stator hub and for forming the slit. The amount of constraint provided by this plastic on the pressure surface and 15 percent chord from both edges on the suction surface, is not precisely known, but it is believed that the hub would be more typical of fixed than of free or pinned constraint.

D. Critical Speeds

A critical speed analysis was made for the rig. With a conventional undamped bearing, critical speeds occur at 4360 and 6900 rpm, as shown by Figure 32. The bearing-support
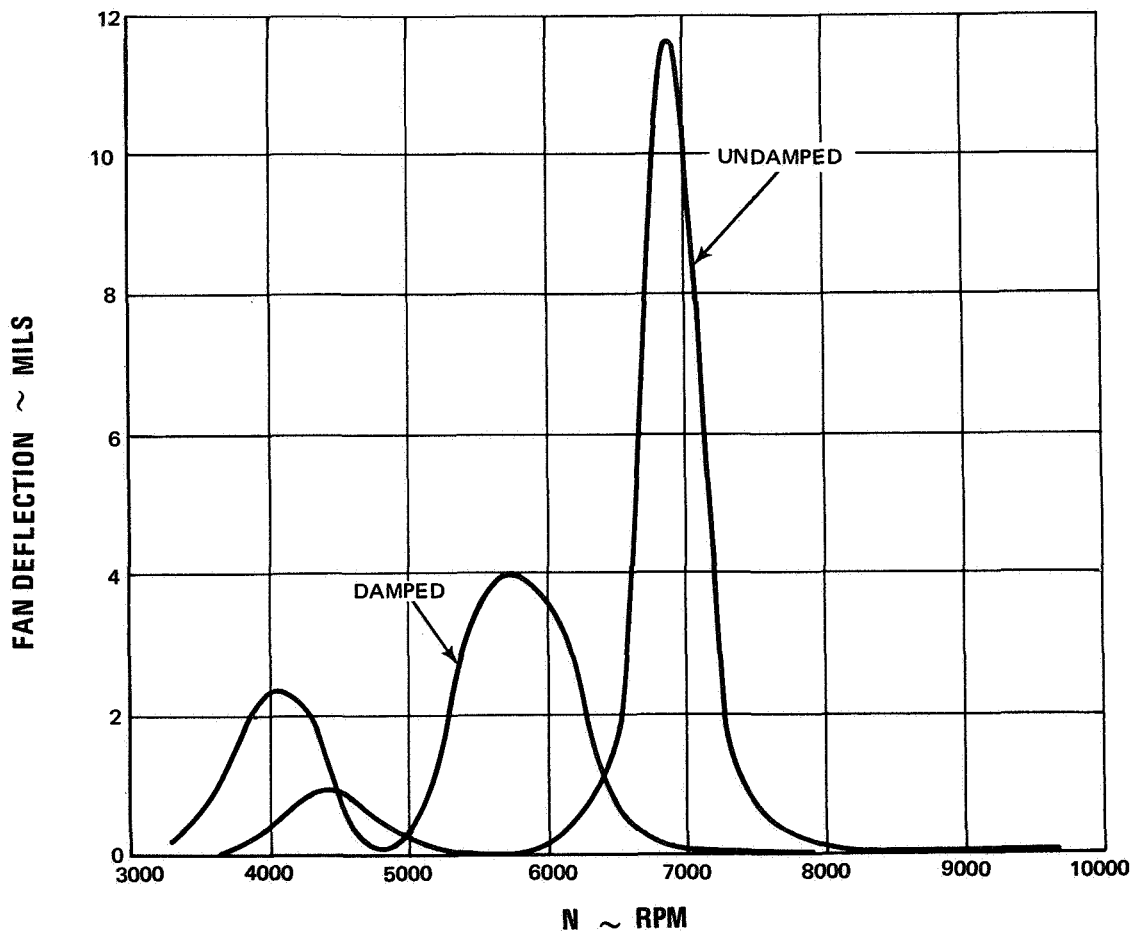
Figure 32   Fan Rig Vibration Amplitude with 1 1/2 oz-in. Unbalance in Fan

36

spring rates were calculated by using unit radial loads. The longitudinal support structures were applied to the calculation as frame members. Axial load was not considered in the bearing spring-rate calculations since experience has shown that applying such a load does not produce nonlinearities.

By using an oil-damped bearing the fan deflections are greatly reduced. Figure 32 shows that the amplitude of the second mode, which is a sensitive fan mode, is reduced by 60 percent with the oil-damped bearing. The first-mode amplitude is increased by the damper. This is because of a mode-shape change that accommodates the softer rate of the damped bearing. The amplitude of this first mode is still low with the damped bearing and will cause no problems. The third-mode amplitude is insignificant and is unaffected by the damper. With the oil-damped bearing used for this rig, critical speeds occur at 4100, 5740, and 12730 rpm, or 55.5, 77.5, and 172 percent of design speed. From past experience, there should be no difficulty in running through or operating near critical speeds with a properly balanced rotor. Figure 33 illustrates the configuration that was analyzed and shows the location and value of the springs that were used.
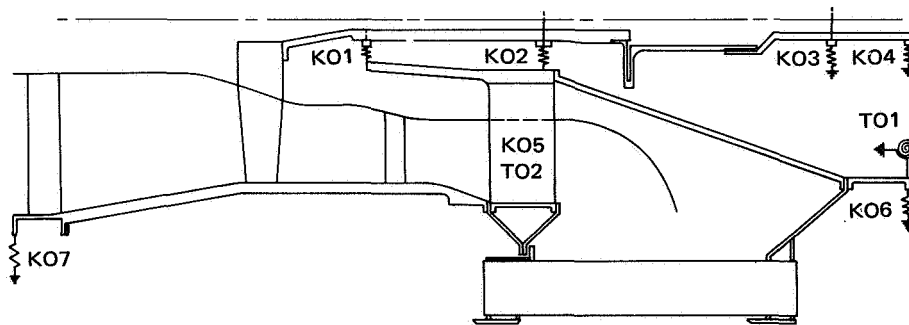
Spring Rates

KO1 (oil-damped bearing)
KO2 - 7.20 x 10^6 lb/in. (1.26 x 10^9 N/m^2)
KO3 - 2.07 x 10^6 lb/in. (3.62 x 10^8 N/m^2)
KO4 - 2.28 x 10^6 lb/in. (3.98 x 10^8 N/m^2)
KO5 - 1.50 x 10^6 lb/in. (2.62 x 10^8 N/m^2)
KO6 - 1.00 x 10^{10} lb/in. (1.75 x 10^{12} N/m^2)
KO7 - 1.7 x 10^7 lb/in. (2.98 x 10^9 N/m^2)
TO1 - 1.00 x 10^{10} lb/in. (1.75 x 10^{12} N/m^2)
TO2 - 1.75 x 10^8 lb/in. (3.06 x 10^{10} N/m^2)

Figure 33   Compressor Rig Spring Location and Spring Rates

VI. RESUME

The purpose of this report is to present the design of a highly-loaded low-speed compressor stage with low noise characteristics. The design features a rotor tip speed of 1000 feet per second (304.8 meters per second), no inlet guide vane, and a stator whose axial location and number of vanes were determined from noise considerations. Other characteristics are:

flow per annulus area at rotor leading edge	42 lb/sec/ft^2 (205.07 kg/sec/m^2)
stage pressure ratio	1.5
stage adiabatic efficiency	87.3 percent
hub/tip ratio at rotor inlet	0.392
rotor aspect ratio	1.92
stator aspect ratio	3.67
rotor tip solidity	1.358
stator hub solidity	2.169
tip diameter	31 inches (0.7874 meter)
number of rotor blades	24
number of stator vanes	64
rotor-stator axial spacing	2 rotor chords

APPENDIX 1

Inviscid Flow-Field Calculation Procedure

APPENDIX I

Inviscid Flow-Field Calculation Procedure

The aerodynamic flow-field calculation used in this design assumes axisymmetric flow and uses solutions of continuity, energy, and radial equilibrium equations. These equations account for streamline curvature and radial gradients of enthalpy and entropy, but viscous terms are neglected. Calculations for the rotor blades were performed on stations oriented at an angle with respect to the axial direction.

The equation of motion is in the form

$$\frac{1}{2} \frac{\partial V_m^2}{\partial m} \cos(\lambda - \epsilon) + \frac{V_m^2}{R_c} \sin(\lambda - \epsilon) - \frac{V_\theta^2}{r} + \frac{1}{\rho} \frac{\partial p}{\partial r} = 0$$

$$R_c = \frac{\partial \epsilon}{\partial m} = \text{streamline radius of curvature}$$

Enthalpy rise across a rotor for a streamline ψ is given by the Euler relationship

$$Jg_c \Delta H_{rotor} = (U_2 V_{\theta 2})_\psi - (U_1 V_{\theta 1})_\psi$$

Weight flow is calculated by the continuity equation

$$W = 2\pi \int_{y \text{ root}}^{y \text{ tip}} g K \rho V_m \frac{\sin(\lambda - \epsilon)}{\sin \lambda} y \, dy$$

where K is the local blockage factor and y is the radial dimension in the plane of station from the centerline or inner wall, to the point of interest.

40

APPENDIX 2

Loss System

Loss System

The loss model that was developed is an extension of the NASA model which combines a shock loss with a profile loss to obtain total loss[4]. To obtain shock loss a normal shock is assumed to originate at the leading edge and to be normal to a mean camber line at mid-gap as shown by Figure 34. To obtain the Mach number of the assumed normal shock, a Prandtl-Meyer expansion from the free-stream relative Mach number is calculated from the turning of the flow from the inlet to the suction-surface shock intersection point. The camber of the suction surface between the leading edge and the shock intersection point is termed the supersonic suction-surface camber $(\phi_{SS_{SS}})$. Thus the flow turns from the free-stream condition through an incidence angle i_{SS} to the suction-surface leading edge and is further turned through the angle $\phi_{SS_{SS}}$ to the shock interaction point. Three-dimensional effects were considered small and were ignored.

ROTATION

LEADING EDGE

SUPERSONIC SUCTION SURFACE CAMBER, $\phi_{SS_{SS}}$

LINE OF INLET
RELATIVE MACH
NUMBER M'

M'_{SHOCK}

ASSUMED NORMAL SHOCK

$M'_{AVERAGE}$

MEAN CAMBER LINE AT
MID—GAP
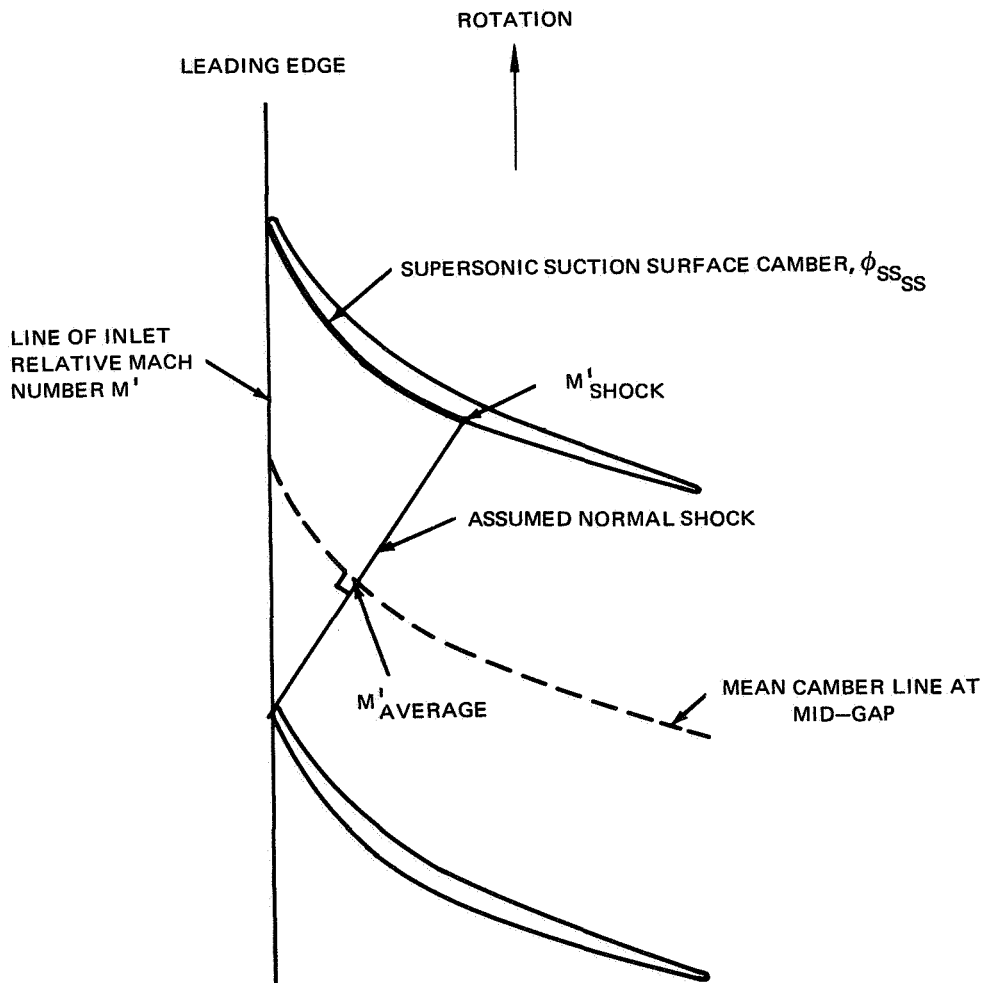
Figure 34   Location of Assumed Normal Shock for Loss Model

For a Prandtl-Meyer expansion, Mach number and turning are related by:

$$\mu = f(M) = \sqrt{\frac{k+1}{k-1}} \ \tan^{-1} \ \sqrt{\frac{k-1}{k+1}(M^2-1)} \ - \tan^{-1} \ \sqrt{M^2-1}$$

Then:

$$\mu_1 = f(M_1')$$

$$\mu_s = \mu_1 + \phi_{ss}s_{ss} + i_{ss}$$

$$M_s' = f^{-1}(\mu_s)$$

$$M_{s \ avg}' = \frac{M_s' + M_1'}{2}$$

Using the general loss model where total loss is equal to the sum of shock loss and profile loss, several previously-tested compressors were analyzed. Table 6 lists the compressors that were analyzed to obtain this correlation of profile loss. Aerodynamic conditions were calculated along the leading and trailing edges of both rotors and stators with a data reduction program that uses test data in the form of pressures and temperatures as input. This program provides a three-dimensional axisymmetric compressible flow solution of the continuity, energy, and radial equilibrium equations. It is discussed in Appendix 1. Spanwise values for profile loss ($\bar{\omega}_p$) were obtained by subtracting shock loss from the total loss. A profile loss parameter ($\bar{\omega}_p \cos\beta_2'/2\sigma$) was calculated and correlated against diffusion factor D. Compressors 1 through 5 were used for the rotor profile loss correlation shown in Figure 35. Compressor 4 was used for the stator profile loss correlation shown in Figure 36. Compressor 4 was a NASA-sponsored high-Mach-number stator research rig in which three different stators were evaluated.
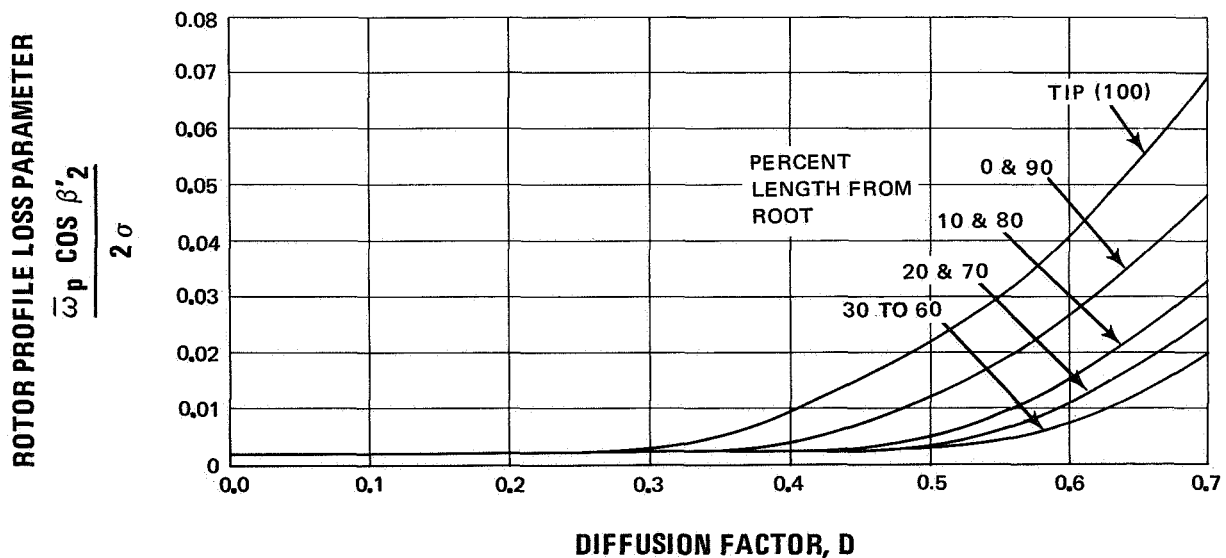
Figure 35   Rotor Profile Loss Parameter as Function of Diffusion Factor

TABLE 6

Compressors Analyzed for Profile Loss Correlation

No.	Compressor	Design	Rotor Series	Stator Series	Design Point Pres. Ratio	Tip Speeds Analyzed ft/sec (m/sec)			
1	JTF14F	single-stage fan	straight entry	not analyzed	—	(1) 1790 (545.6)	(2) 1630 (496.3)	(3) 1465 (446.5)	(4) 1300 (396.2)
2	JTF17	two-stage fan	straight entry	not analyzed	—	(1) 1550 (472.2)	(2) 1395 (425.1)		
3	JT9D	single-stage fan	straight entry	not analyzed	—	(1) 1570 (478.5)	(2) 1430 (435.9)	(3) 1287 (392.3)	
4	Contract NAS3-7614 (Ref. 2)	single-stage fan	C.A.*	C.A. & M.C.A.**	1.5	(1) 1315 (410.8)	(2) 1197 (364.8)	(3) 1075 (327.7)	(4) 995 (291.1)
5	Contract NAS3-7617 (Ref. 9)	single-stage fan	C.A. & M.C.A.	not analyzed	1.6	(1) 1400 (426.7)	(2) 1260 (384.0)		

*circular arc
**multiple-circular-arc
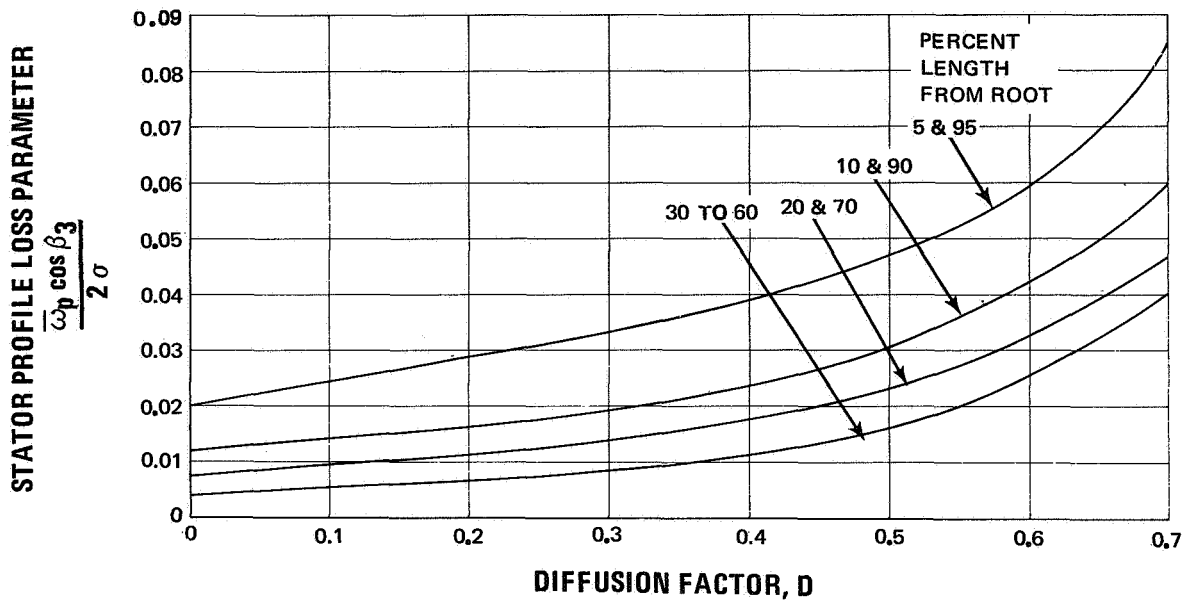
Figure 36   Stator Profile Loss Parameter as Function of Diffusion Factor

45

APPENDIX 3

Incidence Selection

APPENDIX 3

Incidence Selection

For blade elements with supersonic inlet relative Mach numbers, the absolute flow capacity
is established at some incidence and consequently the selection of incidence is of major
concern. However, this condition is relaxed for subsonic blade elements and additional
latitude is available in selecting incidence.

Subsonic Flow

Incidence at the rotor-root section was selected from the Pratt & Whitney Aircraft cas-
cade data of Figure 17. These cascade data are for a camber angle of 70 degrees which
approximates the design camber of 80 degrees better than any available rotor data. It
was assumed that the useful incidence range of this cascade data was bounded by the
positive and negative incidences at which loss is twice the minimum loss level. As
shown in Figure 16, the design incidence at the root was set at -1/2 degree, which is
in the center of the useful incidence range of Figure 17. This incidence to the mean
camber line becomes -7 1/2 degrees to the suction surface for the blade camber and
thickness of interest. Between the root and the mid-span location, incidence to the
rotor suction surface was obtained from the rotor data of Contract NAS3-7614 (Reference
3). Typical results are shown by Figure 37 for the 50 percent span location. An incidence
near -2 degrees to the suction surface was selected for mid-span as shown in Figure 16.

Stator incidence to the suction surface, root to tip, was set equal to zero, based on re-
sults from Reference 3. Typical results supporting this selection are shown by Figure
38. A summary of the stator incidence angles to the mean camber line and to the suction
surface is presented in Figure 22.

Supersonic Flow

Efficient alignment of supersonic flow to the suction surface in the entrance region of ro-
tor tip airfoils was a major design consideration. If the blade suction surface curvature
upstream of the first captured Mach wave does not correspond exactly to freestream flow,
then alignment with the surface causes expansion or compression waves, as shown in Fig-
ure 39. When meridional flow is subsonic, the waves formed between the leading edge
and the first captured Mach wave propagate forward and adjust upstream flow conditions.
Compression or expansion from this portion of the suction surface must be balanced by a
corresponding expansion or compression of equal strength respectively, in order for each
blade to have the same inlet flow conditions. Far upstream of the leading edge, compres-
sion and expansion waves cancel each other, and the flow is axisymmetric. Thus, a com-
pression at the leading edge (Figure 39a) must be followed by an expansion to a neutral
point B', where aligned flow angle equals the axisymmetric flow angle, followed by con-
tinued expansion to point B sufficient to cancel the entire leading-edge compression. Con-
versely, an expansion about the leading edge (Figure 39b) must be followed by a system
of cancelling compression waves. Thus, a repeating pattern of waves with a period of
one blade gap exists at any radial location, and only one Mach wave in expansion or com-
pression fields near the leading edge has the axisymmetric flow angle.

48

% DESIGN
SPEED   MACH NO. RANGE
☐ 110 _ _ _ .0.91 – 0.94
◇ 100 _ _ _ 0.82 – 0.84
◿ 95 _ _ _ 0.77 – 0.80
⬡ 90 _ _ _ 0.73 – 0.76
◇ 70 _ _ _ 0.55 – 0.57
△ 50 _ _ _ 0.39 – 0.40
◉ DESIGN PT.

TOTAL PRESSURE LOSS COEFFICIENT, $\overline{\omega}$

0.35
0.30
0.25
0.20
0.15
0.10
0.05
0

−8   −4   0   4   8   12

INCIDENCE ANGLE TO SUCTION SURFACE, i_{ss}, ~ DEGREES

0   4   8   12   16

INCIDENCE ANGLE TO MEAN CAMBER LINE i_{mc}
DEGREES
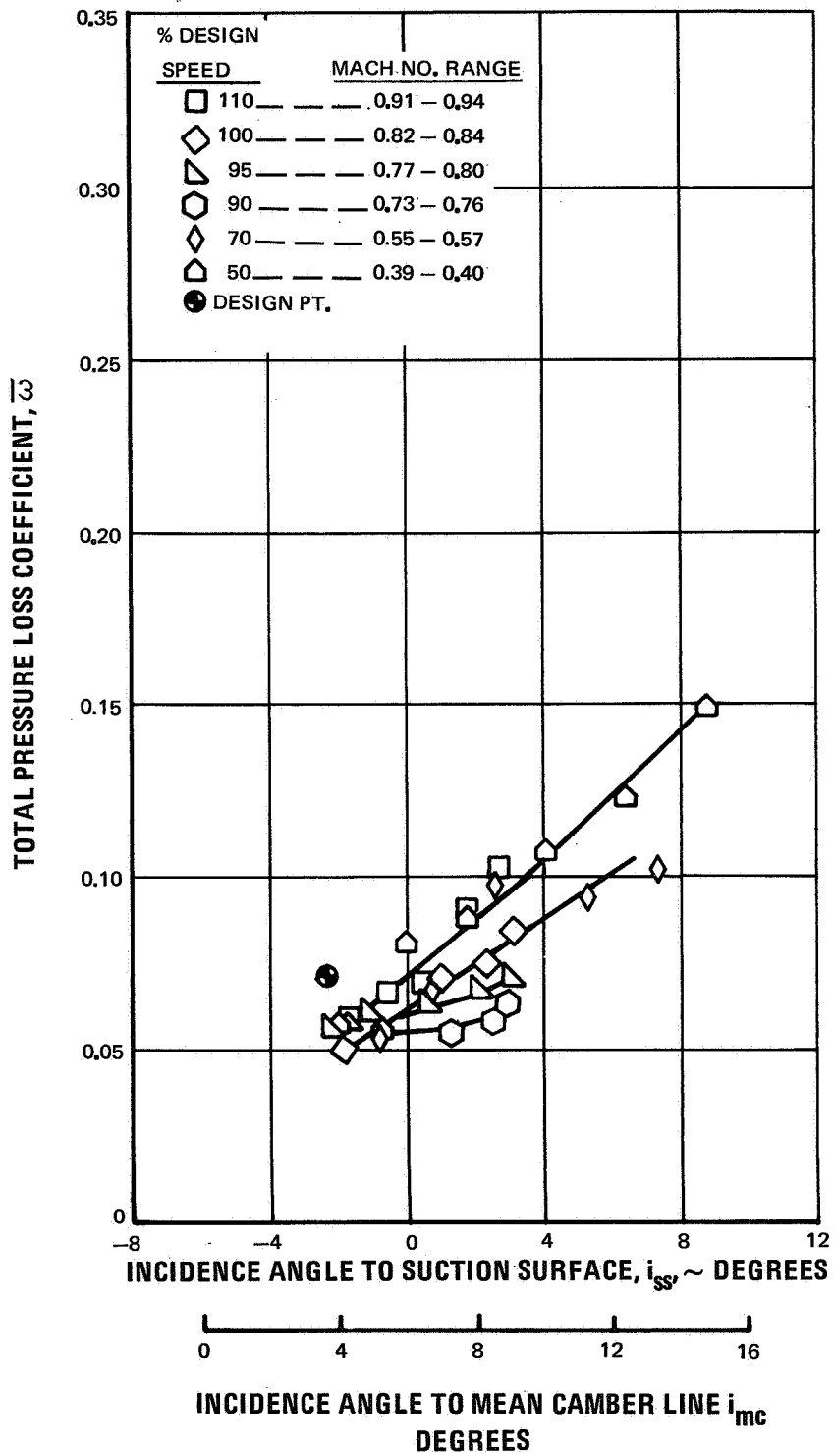
Figure 37   Typical Rotor Loss Bucket at 50 Percent Span from Reference 3

If entrance-region design of supersonic sections does not accomodate this adjustment, then it must take place through detached shocks or blade boundary-layer buildup, or a combination of both. This sort of inefficient adjustment can be a source of significant loss in supersonic blade elements.

It was assumed that the neutral point on the blade suction surface, where aligned flow angle equalled the axisymmetric flow angle, was halfway between the leading edge and the emanation point of the first captured Mach wave, as shown in Figure 39. A detailed construction of a typical flow pattern verified that this assumption is a good approximation.

Entrance-region relative flow angles for freestream flow were calculated by the flow-field calculation procedure discussed in Appendix 1. These angles were decreased by 1 degree to account for increased axial velocity due to blade leading-edge blockage, and for boundary-layer development on the suction surface. Then the blade-element suction sur-
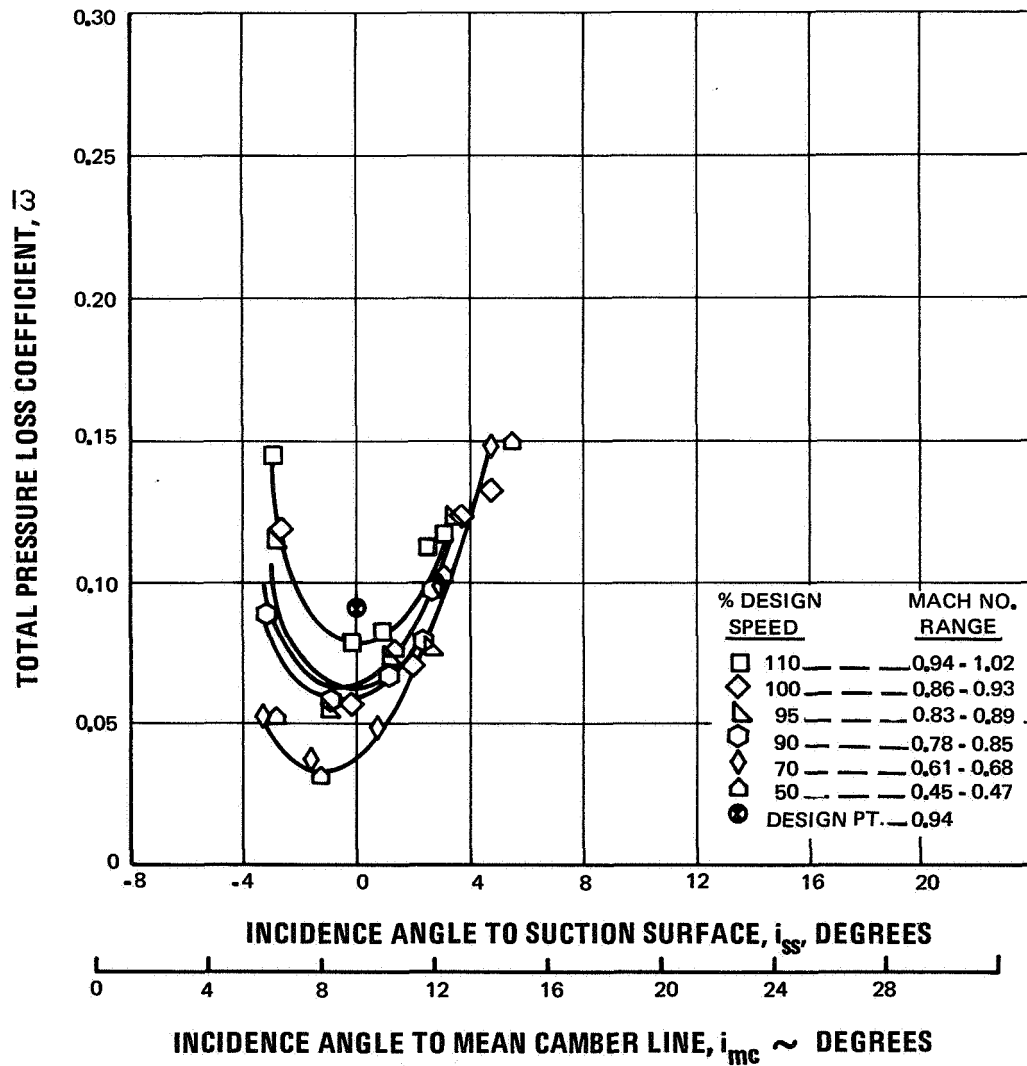
Figure 38   Typical Stator Loss Bucket at 50 Percent Span from Reference 3

50

face was set tangent to this adjusted free-stream flow angle at point B' in Figure 39, which is midway between the leading edge and the emanation point of the first captured Mach wave, point B. Thus for supersonic flow, the airfoil suction surface was aligned nominally with the axisymmetric flow angle at point B', with cancelling zones of expansion and compression on either side of this point. The resultant values of rotor incidence are summarized on Figure 16.
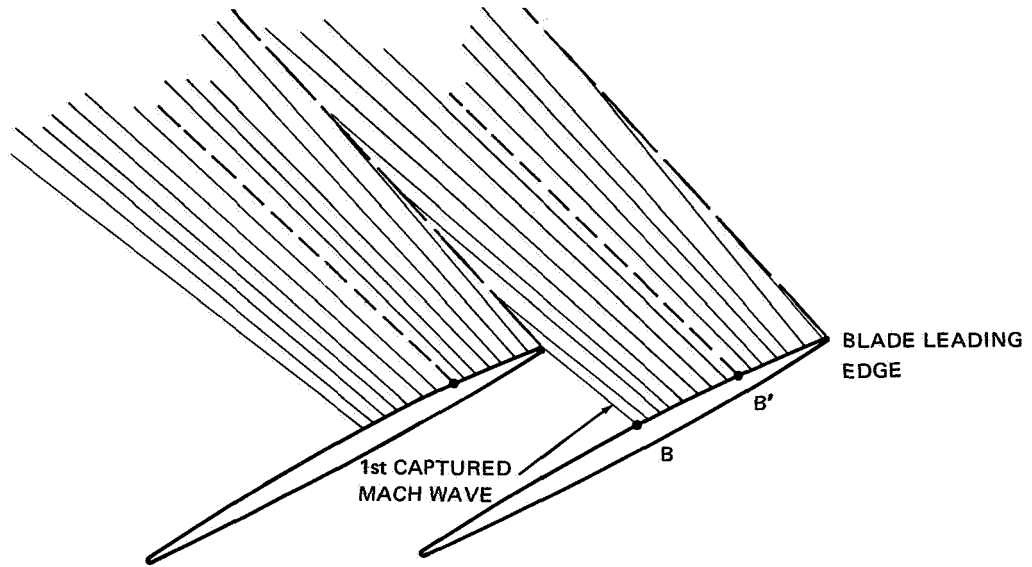
a) Convex Entrance Region (Inboard of 90% of Rotor Span from Root)
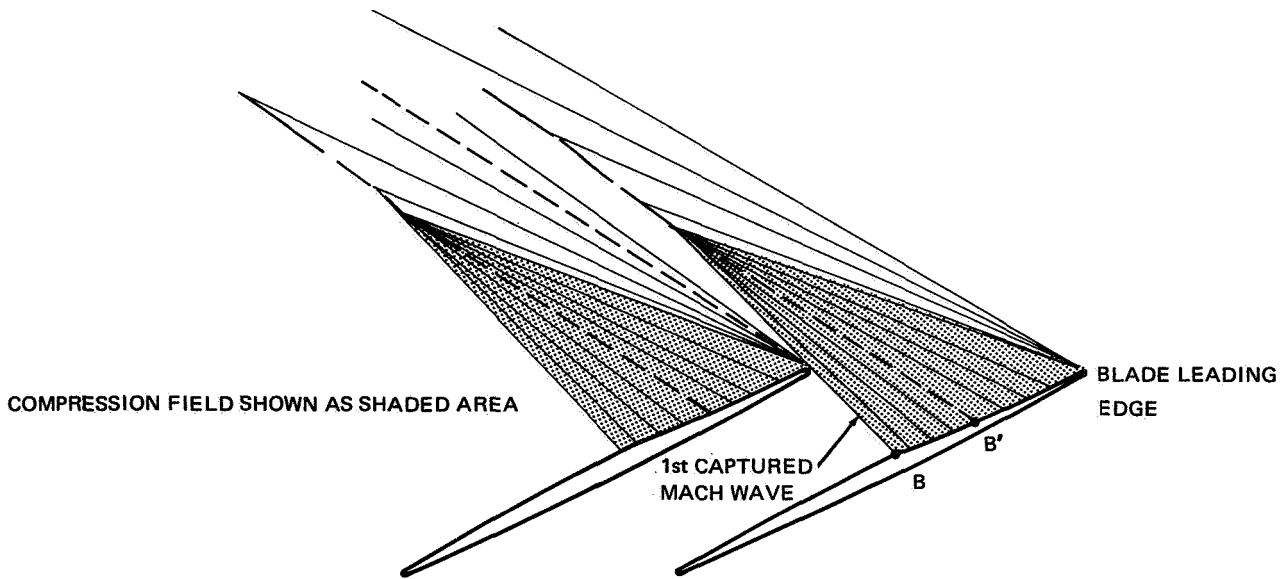
b) Concave Entrance Region (Rotor Tip)

Figure 39   Wave Pattern for Super-Critical Operation of Curved-Blade Entrance Regions

APPENDIX 4

Stream-Tube Analysis in Channels between Rotor Blades

APPENDIX 4

Stream-Tube Analysis in Channels between Rotor Blades

Supersonic blade-element data in References 11 through 14, show minimum loss occurring when blade-passage A/A* was approximately 1.03. Subsonic stator blade element data from References 3 and 8, and subsonic two-dimensional cascade data show minimum loss occurring when channel throat area was approximately $1.03 \text{ s } \cos\beta$. Thus channel area was considered of equal importance to incidence angle in designing for operation at minimum loss.

A stream-tube analysis was performed to obtain the local value of A/A* through the blade passage. The calculation used an average passage width, O, obtained by averaging passage widths of blade channels for stream lines defining the stream-tube annulus, shown by Figure 40. The calculation accounts for convergence, total relative enthalpy change due to radius changes, and distribution of losses within the channel. The distribution of losses within the channel assumed no loss until the first covered section at mid-gap, see Figure 41. At this point the shock loss described in Appendix 2 was applied. The profile loss was linearly applied from the first covered section to the full value at the trailing edge. Thus, at the first covered section the full shock loss was used and at the trailing edge the sum of the shock and profile loss, as shown by Figure 41.

Values of minimum channel A/A* were controlled by adjusting front camber. If the value of A/A* was not correct, the channel was opened or closed by increasing or decreasing, respectively, the value of front camber while holding incidence to a reference point constant, as follows. For supersonic relative inflow, incidence to the neutral point B' (Figure 39 and Appendix 3) was held constant while incidence to the leading edge changed as front camber was changed. For subsonic relative inflow, incidence to the leading edge point was held constant while that to other points changed as front camber was changed. In general, care was taken to design the blade so that minimum A/A* occurs near the leading edge to obtain a gradual diffusion in the channel.
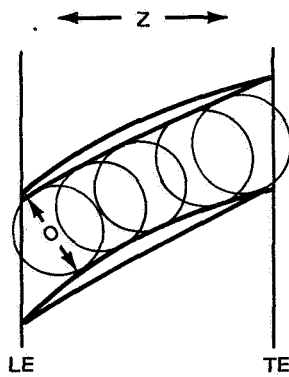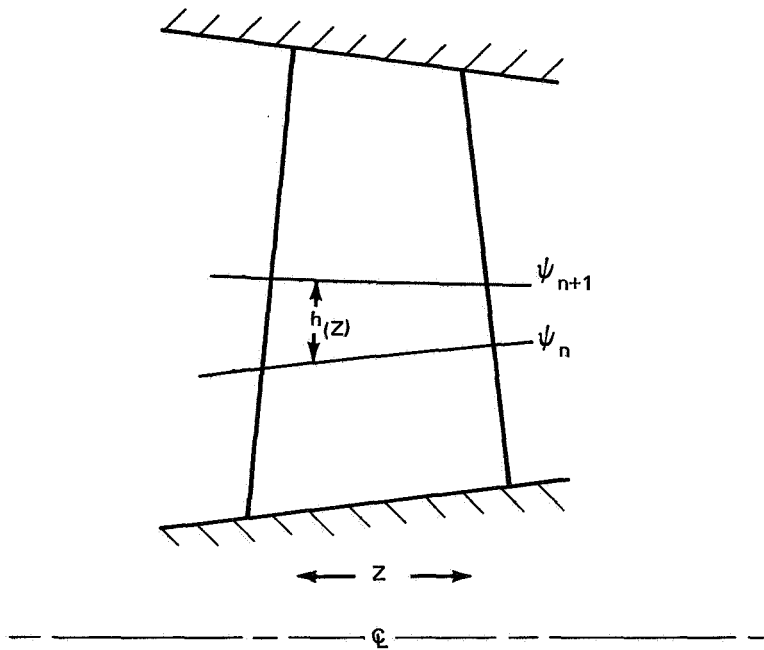
$$\text{STREAM TUBE AREA} = \frac{O_{(Z)}\psi_{n+1} + O_{(Z)}\psi_n}{2} \left[h_{(Z)} \right]$$

Figure 40   Channel Area
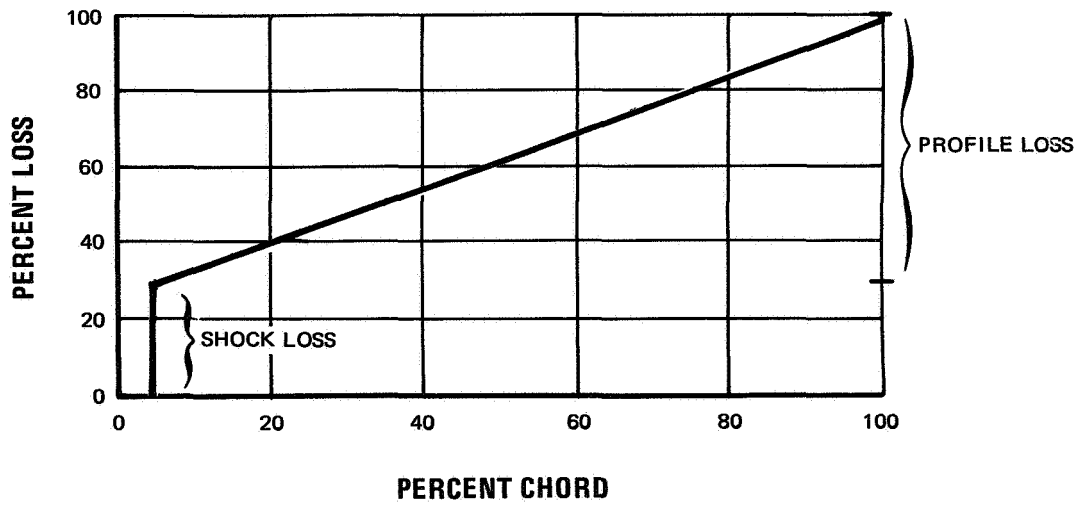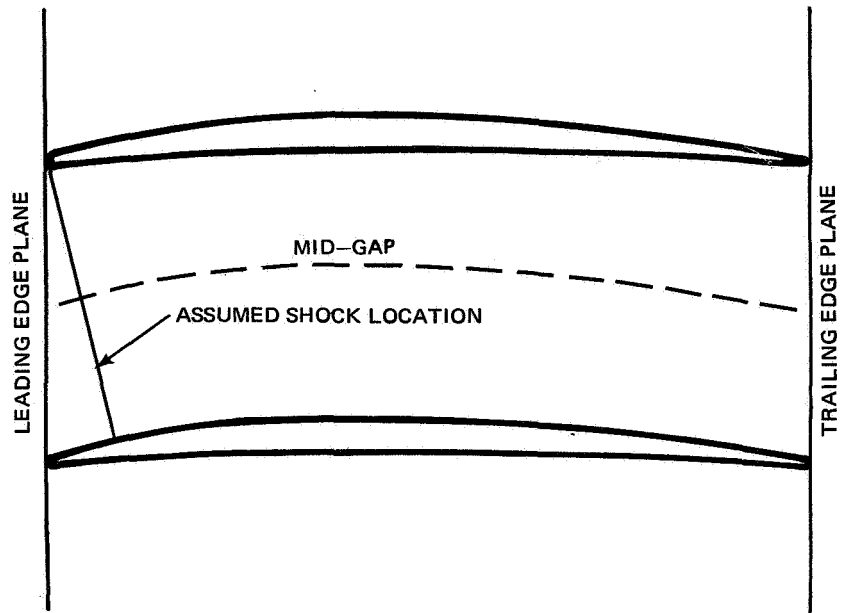
Figure 41   Loss Distribution through Channel

APPENDIX 5

Deviation System

Deviation System

Carter's rule plus an experience factor was used to obtain deviation for most of the rotor and the entire stator. Carter's rule $\delta^0 = m \, \phi \, /\sqrt{\sigma}$ and the definitions $\phi = \beta_1'^* - \beta_2'^*$, $\delta^0 = \beta_2'^* - \beta_2'$, and $i_{mc} = \beta_1'^* - \beta_1'$ were combined to give for the rotor:

$$\delta^0_{\text{Carter's rule}} = \frac{(\Delta\beta - i_{mc})\, m_c \sqrt{\frac{1}{\sigma}}}{1 - m_c \sqrt{\frac{1}{\sigma}}}$$

$$m_c = 0.92(a/c)^2 + 0.002\, \beta_2' \qquad\qquad \text{(Reference 10)}$$

$$\frac{a}{c} = \frac{\text{distance to maximum camber point from leading edge}}{\text{chord}}$$

For the rotor the modification to Carter's rule that was used is shown by Figure 42. Data from Contract NAS3-7617 (References 11 to 14) is shown in the figure. The rotor root was treated as a separate problem because of the large amount of turning past axial. The root is discussed in detail in the rotor airfoil design section (Page 15).
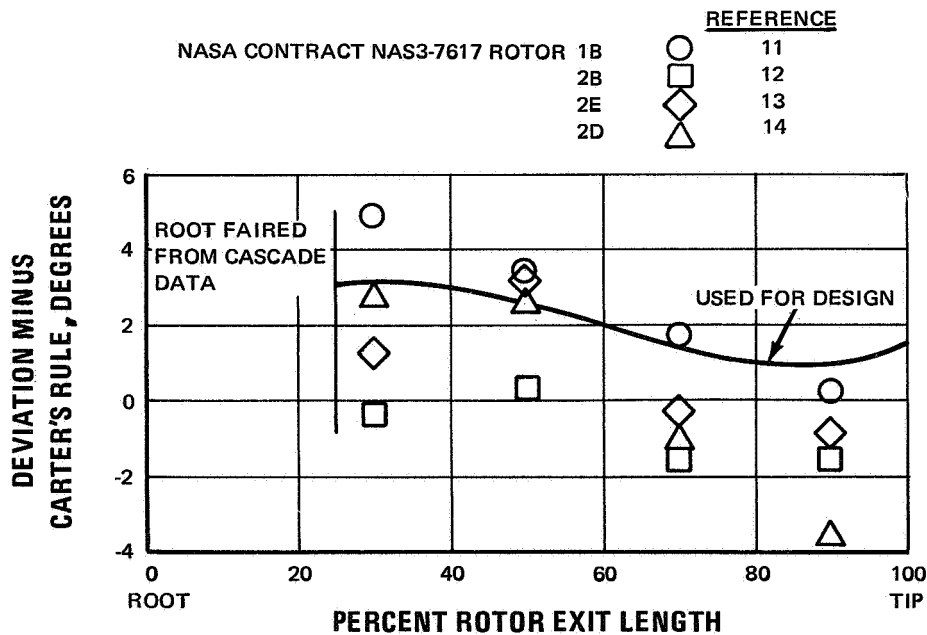
Figure 42   Modification to Carter's Rule Deviation Used for Rotor

For the stator, absolute air angles were used along with the modification to Carter's rule shown by Figure 43. This curve is based on data from Contract NAS3-7614 (References 3 and 8) which evaluated three stators with Mach numbers and loadings just slightly higher than those of the present design.
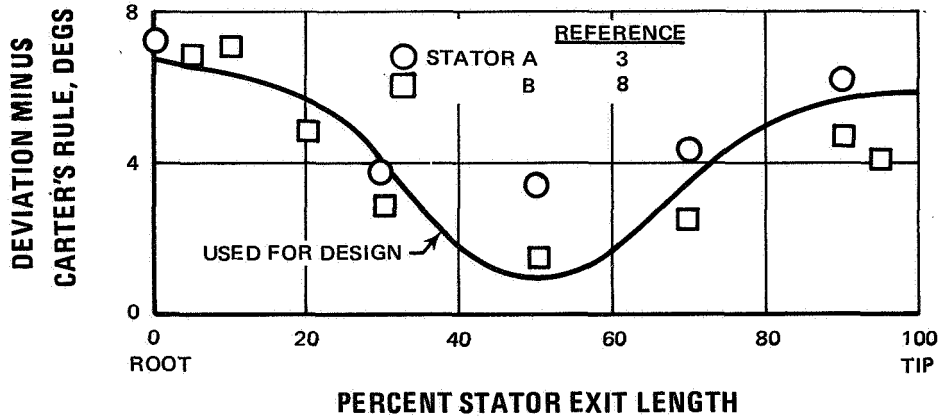
Figure 43   Modification to Carter's Rule Deviation Used for Stator

APPENDIX 6

Symbols

APPENDIX 6

Symbols

B $\quad=\quad$ location of first captured Mach wave on suction surface

B' $\quad=\quad$ point midway between leading edge and first captured Mach wave emanation point on suction surface

a $\quad=\quad$ distance to maximum camber point from leading edge, inches or meters

A/A* $\quad=\quad$ ratio of actual area to critical area (where local Mach number is 1.0)

b $\quad=\quad$ rotor chord at 75 percent of span from root, inches or meters

c $\quad=\quad$ chord (aerodynamic on flow surface), inches or meters

D $\quad=\quad$ diffusion factor for rotor $= 1 - V_2'/V_1' + \dfrac{r_2 V_{\theta 2} - r_1 V_{\theta 1}}{(r_1 + r_2) V_1' \sigma}$

$\quad\quad$ for stator $= 1 - V_3/V_2 + \dfrac{r_3 V_{\theta 3} - r_2 V_{\theta 2}}{(r_2 + r_3) V_2 \sigma}$

g $\quad=\quad$ acceleration due to gravity, 32.17 ft/sec^2 or 9.80 m/sec^2

g_c $\quad=\quad$ conversion factor, 32.17 lb mass ft/lb sec^2

h $\quad=\quad$ distance between streamlines

H $\quad=\quad$ total or stagnation entropy, Btu/lb mass (cal/kg)

i $\quad=\quad$ incidence angle between inlet air direction and, depending on subscript, tangent to blade mean camber line or to suction surface at leading edge, degrees or radians

J $\quad=\quad$ mechanical equivalent of heat, ft lb/Btu or 4.186 Joules/cal

k $\quad=\quad$ ratio of specific heats

K $\quad=\quad$ blockage factor

M $\quad=\quad$ Mach number

m_c $\quad=\quad$ correlation factor in Carter's rule , $0.92 (a/c)^2 + 0.002\ \beta_2$

O $\quad=\quad$ width of channel between adjacent blades

P $\quad=\quad$ total or stagnation pressure, lb/ft^2 or N/m^2

p $\quad=\quad$ static or stream pressure, lb/ft^2 or N/m^2

r $\quad=\quad$ radius

$R, \theta, Z \quad=\quad$ cylindrical coordinate system located with Z axis as rig centerline and with unit vectors $\bar{i}$, $\bar{j}$, and $\bar{k}$ respectively (see Figure 3 for $Z = 0$)

$R_c \quad=\quad$ streamline radius of curvature

s $\quad=\quad$ blade spacing, inches or meters

T $\quad=\quad$ total or stagnation temperature, °R or °K

$t_{max} \quad=\quad$ blade maximum thickness, inches or meters

U $\quad=\quad$ rotor speed, ft/sec or meter/sec

V $\quad=\quad$ air velocity, ft/sec or meter/sec

$\bar{V} \quad=\quad$ absolute air velocity vector, $V_R \bar{i} + V_\theta \bar{j} + V_z \bar{k}$, ft/sec or meter/sec

$V_m \quad=\quad$ meridional air velocity vector, $(V_R^2 + V_z^2)^{1/2}$, ft/sec or meter/sec

W $\quad=\quad$ weight flow rate, lb/sec or kg/sec

$\bar{X} \quad=\quad$ horizontal distance from leading edge along chord to airfoil center of gravity, inches or meters

X $\quad=\quad$ horizontal distance from leading edge along chord to airfoil coordinate, inches or meters

$\bar{Y} \quad=\quad$ vertical distance from chord to airfoil center of gravity, inches or meters

Y $\quad=\quad$ vertical distance from chord to airfoil coordinate, inches or meters

y $\quad=\quad$ length along calculation station from centerline to point of interest

$\alpha \quad=\quad$ conical surface angle approximating a streamline of revolution as measured from the axial direction, degrees or radians

β = absolute air angle = $\cot^{-1} (V_m/V_\theta)$, degrees or radians

β' = relative air angle = $\cot^{-1} (V_m/V_\theta)$, degrees or radians

$\Delta\beta$ = air turning angle = $\beta'_1 - \beta'_2$ for rotors and $\beta_2 - \beta_3$ for stators, degrees or radians

β'_z = relative air angle = $\cot^{-1} (V_z/V'_\theta)$, degrees or radians

β_z = absolute air angle = $\cot^{-1} (V_z/V_\theta)$, degrees or radians

β^* = stator vane metal angle on conical surface between tangent to mean camber line and axial direction at leading and trailing edge, degrees or radians

β'^* = rotor blade metal angle on conical surface between tangent to mean camber line and axial direction at leading or trailing edge, degrees or radians

δ^o = deviation angle, angle between exit air direction and tangent to blade mean camber line at trailing edge, degrees or radians

γ = blade chord angle (stagger angle), angle between chord and axial direction on cylindrical surface, degrees or radians

ϵ = angle between tangent to streamline projected on meridional plane and axial direction, degrees or radians

λ = angle of calculation station measured from axial direction

μ = Prandtl-Meyer function

ρ = density, lb mass/ft^3 or kg/m^3

σ = density, lb sec^2/ft^4 (slugs/ft^3) or kg/m^3

ϕ = blade camber angle, difference between blade angles at leading and trailing edges on conical surface, $\beta'^*_1 - \beta'^*_2$ for rotors and $\beta^*_2 - \beta^*_3$ for stators, degrees or radians

ψ = denotes a streamline

ω = angular velocity of rotor, radians/sec

ω_t = torsional frequency, radians/sec

$\bar{\omega}$ =   total pressure loss coefficient, mass average defect in relative total pressure divided by difference between inlet stagnation and static pressure

L.E.R. =   leading edge radius, inches or meters

T.E.R. =   trailing edge radius, inches or meters

Subscripts

f	=	front
p	=	profile
r	=	radial direction (normal to axis) with unit vector $\bar{i}$
s	=	shock
ss	=	suction surface
ss_{ss}	=	suction surface supersonic
t	=	total
m	=	meridional direction (in z-r plane)
mc	=	mean camber line
z	=	axial direction with unit vector $\bar{k}$
θ	=	coordinate in tangential direction with unit vector $\bar{j}$
1	=	station into rotor
2	=	station out of rotor or into stator
3	=	station out of stator

Superscript

'	=	relative to rotor

APPENDIX 7

Aerodynamic Summary Tables

TABLE 7

Aerodynamic Summary – Rotor Inlet (English Units)

		I.D.										O.D.
Percent Flow		0	10	20	30	40	50	60	70	80	90	100
Percent Length		0	16.9	30.3	41.8	52.1	61.4	70.0	78.1	85.8	93.1	100
		Z^1 I.D. = -0.73 inch										Z O.D. = 0.26 inch
diameter	inches	12.217	15.382	17.903	20.058	21.975	23.723	25.341	26.857	28.289	29.651	30.953
pressure ratio[2]	–	1.0	1.0	1.0	1.0	1.0	1.0	1.0	1.0	1.0	1.0	1.0
temperature ratio[2]	–	1.0	1.0	1.0	1.0	1.0	1.0	1.0	1.0	1.0	1.0	1.0
M	–	0.561	0.581	0.602	0.615	0.624	0.629	0.632	0.634	0.635	0.636	0.635
M'	–	0.669	0.741	0.806	0.860	0.908	0.950	0.990	1.027	1.061	1.095	1.127
V	ft/sec	607.7	628.3	649.0	662.2	670.7	676.1	679.5	681.5	682.4	682.6	682.4
V'	ft/sec	724.5	800.9	869.1	926.2	976.3	1021.6	1063.5	1102.8	1140.1	1175.8	1210.1
V_Z	ft/sec	575.5	609.5	638.2	655.9	667.1	674.1	678.5	681.0	682.3	682.6	682.4
V_m	ft/sec	607.7	628.3	649.0	662.2	670.7	676.1	679.5	681.5	682.4	682.6	682.4
V_θ	ft/sec	0	0	0	0	0	0	0	0	0	0	0
V'_θ	ft/sec	-394.4	-496.6	-597.9	-647.6	-709.5	-765.9	-818.1	-867.1	-913.3	-957.3	-999.3
β_z	degrees	34.43	39.17	42.16	44.63	46.76	48.65	50.33	51.85	53.24	54.51	55.67
β'_z	degrees	18.76	14.05	10.46	7.88	5.95	4.43	3.19	2.15	1.25	0.49	-0.10
ϵ	degrees											
U	ft/sec	394.4	496.6	578.0	647.6	709.5	765.9	818.2	867.1	913.3	951.3	999.3
M_m	–	0.561	0.581	0.602	0.615	0.624	0.629	0.632	0.634	0.635	0.636	0.635
M_z	–	0.531	0.564	0.592	0.609	0.620	0.627	0.631	0.634	0.635	0.636	0.635
β	degrees	0	0	0	0	0	0	0	0	0	0	0
β'	degrees	32.98	38.32	41.69	44.36	46.61	48.56	50.29	51.84	53.23	54.51	55.67

TABLE 7

Aerodynamic Summary – Rotor Inlet (SI Units)

		I.D.										O.D.
Percent Flow		0	10	20	30	40	50	60	70	80	90	100
Percent Length		0	16.9	30.3	41.8	52.1	61.4	70.0	78.1	85.8	93.1	100
		Z I.D. = -0.0185 meter										Z O.D. = 0.0066 meter
diameter	meters	0.3103	0.3907	0.4547	0.5095	0.5582	0.6026	0.6437	0.6822	0.7185	0.7531	0.7862
pressure ratio	–	1.0	1.0	1.0	1.0	1.0	1.0	1.0	1.0	1.0	1.0	1.0
temperature ratio	–	1.0	1.0	1.0	1.0	1.0	1.0	1.0	1.0	1.0	1.0	1.0
M	–	0.561	0.581	0.602	0.615	0.624	0.629	0.632	0.634	0.635	0.636	0.635
M'	–	0.669	0.741	0.806	0.860	0.908	0.950	0.990	1.027	1.061	1.095	1.127
V	m/sec	185.2	191.5	197.8	201.8	204.4	206.1	207.1	207.7	208.0	208.1	207.9
V'	m/sec	220.8	244.1	264.9	282.3	297.6	311.4	324.2	336.1	347.5	358.4	368.8
V_Z	m/sec	175.4	185.8	194.5	199.9	203.3	205.5	206.8	207.6	207.9	208.1	207.9
V_m	m/sec	185.2	191.5	197.8	201.8	204.4	206.1	207.1	207.7	208.0	208.1	207.9
V_θ	m/sec	0	0	0	0	0	0	0	0	0	0	0
V'_θ	m/sec	-120.2	-151.4	-176.2	-197.4	-216.2	-233.4	-249.4	-264.3	-278.4	-291.8	-304.6
β_z	radians	0.602	0.684	0.736	0.779	0.816	0.849	0.878	0.905	0.929	0.951	0.972
β'_z	radians	0.327	0.245	0.183	0.138	0.104	0.077	0.056	0.038	0.022	0.009	-0.002
ϵ	radians											
U	m/sec	120.2	151.4	176.2	197.4	216.2	233.4	249.4	264.3	278.4	291.8	304.6
M_m	–	0.561	0.581	0.602	0.615	0.624	0.629	0.632	0.634	0.635	0.636	0.635
M_z	–	0.531	0.564	0.592	0.609	0.620	0.627	0.631	0.634	0.635	0.636	0.635
β	radians	0	0	0	0	0	0	0	0	0	0	0
β'	radians	0.576	0.669	0.728	0.774	0.814	0.848	0.878	0.905	0.929	0.951	0.972

1 See Figure 3 for flow path

2 Calculations based on an inlet pressure of 2116 psf and an inlet temperature of 518.6°R

TABLE 8
Aerodynamic Summary – Rotor Exit (English Units)

Z' I.D. = 4.66 inches   Z O.D. = 3.84 inches

		Percent Flow → I.D. 0	10	20	30	40	50	60	70	80	90	O.D. 100
	Percent Length	0	15.9	28.1	39.1	49.2	58.7	67.4	76.2	84.4	92.3	100
diameter	inches	15.308	17.787	19.699	21.411	22.994	24.477	25.878	27.211	28.486	29.716	30.922
pressure ratio[2]	–	1.540	1.540	1.540	1.540	1.540	1.540	1.540	1.540	1.540	1.540	1.540
temperature ratio[2]	–	1.141	1.134	1.135	1.136	1.138	1.139	1.141	1.143	1.146	1.150	1.157
M	–	0.912	0.875	0.826	0.778	0.742	0.714	0.692	0.674	0.659	0.646	0.634
M'	–	0.559	0.595	0.577	0.558	0.557	0.565	0.581	0.601	0.622	0.639	0.644
V	ft/sec	1006.9	968.8	921.9	874.7	838.3	810.4	788.1	769.9	755.0	742.7	732.3
V'	ft/sec	617.0	658.4	643.1	626.9	629.1	641.8	662.1	686.9	712.9	734.3	744.3
V_z	ft/sec	464.1	634.4	639.1	620.1	605.9	594.4	585.5	578.3	571.3	561.5	543.9
V_m	ft/sec	475.4	640.5	642.6	622.3	607.2	595.2	585.9	578.5	571.4	561.5	543.9
V_θ	ft/sec	887.6	726.9	661.0	614.7	578.0	549.9	527.1	508.1	493.5	486.1	490.3
V'_θ	ft/sec	393.3	152.7	25.0	-76.6	-164.4	-240.3	-308.4	-370.4	-426.2	-473.3	-508.0
β_z	degrees	62.39	48.89	45.97	44.75	43.65	42.78	41.99	41.31	40.82	40.89	42.03
β'_z	degrees	-40.28	-13.53	-2.24	7.04	15.18	22.11	27.78	32.64	36.72	40.12	43.04
ϵ	degrees	12.52	7.89	6.02	4.78	3.76	2.90	2.15	1.48	0.89	0.38	-0.05
U	ft/sec	494.2	574.3	635.9	691.3	742.4	790.2	835.5	878.5	919.7	959.4	998.3
M_m	–	0.431	0.579	0.576	0.554	0.537	0.524	0.514	0.506	0.499	0.488	0.471
M_z	–	0.420	0.573	0.573	0.552	0.536	0.524	0.514	0.506	0.498	0.488	0.471
β	degrees	61.82	48.62	45.81	44.65	43.89	42.74	41.98	41.30	40.81	40.89	42.03
β'	degrees	-39.60	-13.41	-2.23	7.01	15.15	21.98	27.76	32.63	36.72	40.13	43.04

TABLE 8
Aerodynamic Summary – Rotor Exit (SI Units)

Z I.D. = 0.1184 meter   Z O.D. = 0.0975 meter

		I.D. 0	10	20	30	40	50	60	70	80	90	O.D. 100
diameter	meters	0.3888	0.4518	0.5084	0.5438	0.5840	0.6217	0.6573	0.6912	0.7235	0.7548	0.7854
pressure ratio	–	1.540	1.540	1.540	1.540	1.540	1.540	1.540	1.540	1.540	1.540	1.540
temperature ratio	–	1.141	1.134	1.135	1.136	1.138	1.139	1.141	1.143	1.146	1.150	1.157
M	–	0.912	0.875	0.826	0.778	0.742	0.714	0.692	0.674	0.659	0.646	0.634
M'	–	0.559	0.595	0.577	0.558	0.557	0.565	0.581	0.601	0.622	0.639	0.644
V	m/sec	306.9	295.3	280.9	266.6	255.5	247.0	240.2	234.7	230.1	226.4	223.2
V'	m/sec	188.1	200.6	196.0	191.1	191.7	195.6	201.8	209.4	217.3	223.8	226.9
V_z	m/sec	141.5	193.4	194.8	189.0	184.7	181.2	178.4	176.3	174.1	171.1	165.8
V_m	m/sec	144.9	195.2	195.9	187.7	185.1	181.4	178.6	176.3	174.2	171.1	165.8
V_θ	m/sec	270.5	221.6	201.5	187.4	176.2	167.6	160.7	154.9	150.4	148.2	149.4
V'_θ	m/sec	119.9	46.5	7.6	-23.3	-50.1	-73.2	-93.9	-112.9	-129.9	-144.3	-154.9
β_z	radians	1.089	0.853	0.802	0.781	0.762	0.747	0.733	0.721	0.712	0.714	0.734
β'_z	radians	-0.703	-0.236	-0.039	0.123	0.265	0.386	0.485	0.570	0.641	0.700	0.751
ϵ	radians	0.219	0.138	0.105	0.083	0.066	0.051	0.038	0.026	0.016	0.007	-0.001
U	m/sec	150.6	175.0	193.9	210.7	226.3	240.9	254.7	267.8	280.3	292.4	304.3
M_m	–	0.431	0.579	0.576	0.554	0.537	0.524	0.514	0.506	0.499	0.488	0.471
M_z	–	0.420	0.573	0.573	0.552	0.536	0.524	0.514	0.506	0.498	0.488	0.471
β	radians	1.079	0.849	0.799	0.779	0.766	0.746	0.733	0.721	0.712	0.714	0.734
β'	radians	-0.691	-0.234	-0.039	0.122	0.264	0.384	0.485	0.570	0.641	0.700	0.751

[1] See Figure 3 for flow path
[2] Calculations based on an inlet pressure of 2116 psf and an inlet temperature of 518.6°F

TABLE 9

Aerodynamic Summary – Stator Inlet (English Units)

		I.D.										O.D.
Percent Flow		0	10	20	30	40	50	60	70	80	90	100
Percent Length		0	14.8	27.2	38.4	48.6	58.2	67.2	75.9	84.1	92.2	100
		Z' I.D. = 13.50 inches										Z O.D. = 13.50 inches
diameter	inches	17.169	19.206	20.915	22.447	23.856	25.174	26.420	27.609	28.749	29.851	30.931
pressure ratio[2]	–	1.540	1.540	1.540	1.540	1.540	1.540	1.540	1.540	1.540	1.540	1.540
temperature ratio[2]	–	1.141	1.134	1.135	1.136	1.138	1.140	1.141	1.143	1.146	1.150	1.157
M	–	0.899	0.849	0.821	0.798	0.778	0.761	0.745	0.732	0.719	0.708	0.697
M'	–	0.586	0.597	0.604	0.615	0.629	0.644	0.660	0.677	0.694	0.706	0.707
V	ft/sec	994.9	944.0	916.5	894.3	875.1	858.3	843.3	829.9	818.1	807.9	799.4
V'	ft/sec	647.8	663.9	674.6	689.3	707.6	726.6	747.0	768.5	789.4	805.4	810.8
V_z	ft/sec	584.5	650.2	665.9	671.7	672.9	670.3	666.4	661.7	655.9	646.9	631.5
V_m	ft/sec	602.9	661.8	672.5	675.3	674.8	671.3	666.8	661.9	655.9	646.9	631.5
V_θ	ft/sec	791.4	673.2	622.6	586.3	557.1	534.8	516.3	500.8	488.9	483.9	490.1
V_θ'	ft/sec	237.1	53.1	-52.7	-138.4	-213.1	-277.9	-336.7	-390.6	-439.2	-479.8	-508.5
β_z	degrees	53.55	45.99	43.07	41.12	39.62	38.58	37.77	37.12	36.71	36.80	37.82
β_z'	degrees	-22.08	-4.67	4.52	11.64	17.57	22.53	26.81	30.55	33.81	36.57	38.84
ϵ	degrees	14.21	10.75	8.00	5.88	4.31	3.11	2.17	1.40	0.77	0.23	-0.27
U	ft/sec	554.3	620.1	675.2	724.7	770.2	812.8	853.0	891.4	928.2	963.8	998.6
M_m	–	0.545	0.596	0.602	0.602	0.600	0.595	0.589	0.583	0.577	0.567	0.551
M_z	–	0.528	0.585	0.597	0.599	0.598	0.594	0.589	0.583	0.577	0.567	0.551
β	degrees	52.69	45.49	42.79	40.97	39.54	38.54	37.75	37.11	36.70	36.80	37.82
β'	degrees	-21.47	-4.59	4.48	11.58	17.53	22.50	26.79	30.54	33.81	36.57	38.84

TABLE 9

Aerodynamic Summary – Stator Inlet (SI Units)

		I.D.										O.D.
Percent Flow		0	10	20	30	40	50	60	70	80	90	100
Percent Length		0	14.8	27.2	38.4	48.6	58.2	67.2	75.9	84.1	92.2	100
		Z I.D. = 0.3429 meter										Z O.D. = 0.3429 meter
diameter	meters	0.4361	0.4878	0.5312	0.5702	0.6059	0.6394	0.6711	0.7013	0.7302	0.7582	0.7856
pressure ratio	–	1.540	1.540	1.540	1.540	1.540	1.540	1.540	1.540	1.540	1.540	1.540
temperature ratio	–	1.141	1.134	1.135	1.136	1.138	1.140	1.141	1.143	1.146	1.150	1.157
M	–	0.899	0.849	0.821	0.798	0.778	0.761	0.745	0.732	0.719	0.708	0.697
M'	–	0.586	0.597	0.604	0.615	0.629	0.644	0.660	0.677	0.694	0.706	0.707
V	m/sec	303.2	287.7	279.3	272.6	266.7	261.6	257.1	252.9	249.4	246.2	243.7
V'	m/sec	197.5	202.4	205.6	210.1	215.7	221.5	227.7	234.2	240.6	245.5	247.1
V_z	m/sec	178.1	198.2	202.9	204.7	205.1	204.3	203.1	201.7	199.9	197.2	192.5
V_m	m/sec	183.8	201.7	204.9	205.8	205.7	204.6	203.3	201.7	199.9	197.2	192.5
V_θ	m/sec	241.2	205.2	189.8	178.7	169.8	162.9	157.4	152.6	149.0	147.5	149.4
V_θ'	m/sec	72.3	16.2	-16.0	-42.2	-64.9	-84.7	-102.6	-119.0	-133.9	-146.3	-154.9
β_z	radians	0.935	0.803	0.752	0.718	0.692	0.673	0.659	0.648	0.641	0.642	0.660
β_z'	radians	-0.385	-0.082	0.079	0.203	0.307	0.393	0.468	0.533	0.590	0.638	0.678
ϵ	radians	0.248	0.188	0.140	0.103	0.075	0.054	0.038	0.024	0.014	0.004	-0.005
U	m/sec	168.9	189.0	205.8	221.8	234.8	247.7	259.9	271.7	282.9	293.8	304.4
M_m	–	0.545	0.596	0.602	0.602	0.600	0.595	0.589	0.583	0.577	0.567	0.551
M_z	–	0.528	0.585	0.597	0.599	0.598	0.594	0.589	0.583	0.577	0.567	0.551
β	radians	0.919	0.794	0.747	0.715	0.690	0.673	0.659	0.648	0.641	0.642	0.660
β'	radians	-0.375	-0.080	0.078	0.202	0.306	0.393	0.468	0.533	0.590	0.638	0.678

[1]See Figure 3 for flow path
[2]Calculations based on an inlet pressure of 2116 psf and an inlet temperature of 518.6°R

70

TABLE 10

Aerodynamic Summary – Stator Exit (English Units)

		I.D.	10	20	30	40	50	60	70	80	90	O.D.
Percent Flow		0	10	20	30	40	50	60	70	80	90	100
Percent Length		0	14.2	26.0	36.8	46.9	56.6	65.9	74.8	83.4	91.8	100
		Z I.D. = 15.30 inches.										Z O.D. = 15.30 inches
diameter	inches	18.096	19.910	21.422	22.807	24.109	25.349	26.536	27.677	28.779	29.852	30.904
pressure ratio[2]	–	1.375	1.473	1.504	1.513	1.516	1.516	1.515	1.513	1.509	1.503	1.493
temperature ratio[2]	–	1.141	1.134	1.135	1.136	1.138	1.139	1.141	1.143	1.146	1.149	1.157
M	–	0.456	0.537	0.551	0.549	0.546	0.542	0.539	0.536	0.533	0.527	0.518
M'	–	0.677	0.773	0.814	0.841	0.866	0.891	0.915	0.938	0.961	0.981	0.998
V	ft/sec	532.8	620.6	635.9	634.8	631.2	628.1	625.4	622.6	619.2	614.4	606.5
V'	ft/sec	790.7	893.5	939.5	972.2	1002.9	1031.7	1060.7	1089.1	1116.6	1142.9	1167.6
V_z	ft/sec	520.5	612.8	631.7	632.5	630.0	627.5	625.1	622.5	619.2	614.4	606.5
V_m	ft/sec	532.8	620.6	635.9	634.8	631.2	628.1	625.4	622.6	619.2	614.4	606.5
V_θ	ft/sec	0	0	0	0	0	0	0	0	0	0	0
V_θ'	ft/sec	-584.2	-642.8	-691.6	-736.3	-778.4	-818.4	-856.7	-893.6	-929.2	-963.8	-997.7
β_z	degrees	0	0	0	0	0	0	0	0	0	0	0
β_z'	degrees	48.3	46.4	47.6	49.3	51.0	52.5	53.9	55.1	56.3	57.5	58.7
ϵ	degrees	12.34	9.09	6.63	4.82	3.51	2.52	1.74	1.11	0.60	0.17	-0.23
U	ft/sec	584.2	642.8	691.6	736.3	778.4	818.4	856.7	893.6	929.2	963.8	997.8
M_m	–	0.456	0.537	0.551	0.549	0.546	0.542	0.539	0.536	0.533	0.527	0.518
M_z	–	0.446	0.530	0.547	0.547	0.545	0.542	0.539	0.536	0.533	0.527	0.518
β	degrees	0	0	0	0	0	0	0	0	0	0	0
β'	degrees	46.64	46.01	47.40	49.24	50.96	52.50	53.87	55.13	56.32	57.48	58.71

TABLE 10

Aerodynamic Summary – Stator Exit (SI Units)

		I.D.	10	20	30	40	50	60	70	80	90	O.D.
		Z I.D. = 0.3886 meter										Z O.D. = 0.3886 meter
diameter	meters	0.4596	0.5057	0.5441	0.5793	0.6124	0.6439	0.6740	0.7029	0.7309	0.7582	0.7850
pressure ratio	–	1.375	1.473	1.504	1.513	1.516	1.516	1.515	1.513	1.509	1.503	1.493
temperature ratio	–	1.141	1.134	1.135	1.136	1.138	1.139	1.141	1.143	1.146	1.149	1.157
M	–	0.456	0.537	0.551	0.549	0.546	0.542	0.539	0.536	0.533	0.527	0.518
M'	–	0.677	0.773	0.814	0.841	0.866	0.891	0.915	0.938	0.961	0.981	0.998
V	m/sec	162.4	189.2	193.8	193.5	192.4	191.4	190.6	189.8	188.7	187.3	184.8
V'	m/sec	241.0	272.3	286.4	296.3	305.7	314.4	323.3	331.9	340.3	348.4	355.9
V_z	m/sec	158.6	186.8	192.5	192.8	192.0	191.3	190.5	189.7	188.7	187.3	184.8
V_m	m/sec	162.4	189.2	193.8	193.4	192.4	191.4	190.6	189.8	188.7	187.3	184.8
V_θ	m/sec	0	0	0	0	0	0	0	0	0	0	0
V_θ'	m/sec	-161.0	-195.9	-210.8	-224.4	-237.3	-249.5	-261.1	-272.4	-283.2	-293.8	-304.1
β_z	radians	0	0	0	0	0	0	0	0	0	0	0
β_z'	radians	0.843	0.809	0.831	0.861	0.890	0.917	0.940	0.962	0.983	1.003	1.025
ϵ	radians	0.215	0.159	0.116	0.084	0.061	0.044	0.030	0.019	0.011	0.003	-0.004
U	m/sec	178.1	195.9	210.8	224.4	237.3	249.5	261.7	272.4	283.2	293.8	304.1
M_m	–	0.456	0.537	0.551	0.549	0.546	0.542	0.539	0.536	0.533	0.527	0.518
M_z	–	0.446	0.530	0.547	0.547	0.545	0.542	0.539	0.536	0.533	0.527	0.518
β	radians	0	0	0	0	0	0	0	0	0	0	0
β'	radians	0.814	0.820	0.827	0.859	0.889	0.916	0.940	0.962	0.983	1.003	1.025

[1] See Figure 3 for flow path
[2] Calculations based on an inlet pressure of 2116 psf and an inlet temperature of 518.6°R

APPENDIX 8

Airfoil Definitions on Flow Surfaces (Assumed Conical)

TABLE 11

Airfoil Definitions on Flow Surfaces (Assumed Conical) – Rotor[1] (English Units)

Percent Flow	0 Root	10	20	30	40	50	60	70	80	90	100 Tip
diameter at leading edge, inches	12.217	15.382	17.903	20.058	21.975	23.723	25.341	26.857	28.289	29.651	30.95
cone angle α, degs	18.20	14.40	10.80	8.20	6.20	4.60	3.30	2.20	1.20	0.40	-0.20
aerodynamic chord c, inches	4.5	4.671	4.800	4.910	5.008	5.101	5.189	5.275	5.352	5.421	5.525
front chord c_f, inches	3.1	2.62	2.203	1.959	1.858	1.898	2.076	2.318	2.580	2.842	3.097
blade angle β_1^*, degs	33.26	36.22	39.07	41.50	43.36	45.18	46.53	47.95	49.46	50.97	52.88
blade angle β_{1ss}^*, degs	40.60	42.40	44.80	46.90	48.40	49.90	50.90	52.00	53.20	54.40	56.00
blade camber angle ϕ, degs	80.45	62.07	53.84	46.57	39.02	33.10	27.82	23.25	19.73	17.76	17.21
front camber angle ϕ_f, degs	60.82	30.69	18.80	12.22	7.89	5.51	4.02	3.31	2.56	2.16	2.79
max. thickness-to-chord ratio, t_{max}/c	0.07	0.0633	0.0581	0.0537	0.0494	0.0458	0.0422	0.0390	0.0359	0.0329	0.03
percent chord location of t_{max}	40.0	49.0	50.0	50.0	50.0	50.0	50.0	50.0	50.0	50.0	50.0
edge radii, L.E.R. - T.E.R., inch	0.0146	0.0137	0.0129	0.0122	0.0115	0.0108	0.0101	0.0095	0.0089	0.0083	0.0076
maximum camber location, a/c	0.4794	0.5337	0.5392	0.5378	0.5403	0.5470	0.5610	0.5773	0.5984	0.6203	0.6343
solidity, σ	2.513	2.155	1.953	1.812	1.704	1.616	1.550	1.493	1.443	1.397	1.359

TABLE 11

Airfoil Definitions on Flow Surfaces (Assumed Conical) – Rotor (SI Units)

Percent Flow	0 Root	10	20	30	40	50	60	70	80	90	100 Tip
diameter at leading edge, cm	0.31031	0.39070	0.45473	0.50947	0.55817	0.60256	0.64366	0.68217	0.71854	0.75314	0.78621
cone angle α, radians	0.3176	0.2513	0.1885	0.1431	0.1082	0.0803	0.0576	0.0384	0.0209	0.0070	-0.0035
aerodynamic chord c, cm	0.1143	0.1186	0.1219	0.1247	0.1272	0.1296	0.1318	0.1340	0.1359	0.1377	0.1403
front chord c_f, cm	0.0787	0.0665	0.0560	0.0498	0.0472	0.0482	0.0527	0.0589	0.0655	0.0722	0.0787
blade angle β_1^*, radians	0.5804	0.6320	0.6818	0.7242	0.7566	0.7884	0.8119	0.8367	0.8631	0.8894	0.9228
blade angle β_{1ss}^*, radians	0.7085	0.7399	0.7818	0.8184	0.8446	0.8708	0.8882	0.9074	0.9283	0.9493	0.9772
blade camber angle ϕ, radians	1.4039	1.0831	0.9395	0.8126	0.6809	0.5776	0.4855	0.4057	0.3443	0.3099	0.3003
front camber angle ϕ_f, radians	1.0613	0.5355	0.3281	0.2132	0.1377	0.0961	0.0701	0.0578	0.0447	0.0377	0.0487
max. thickness-to-chord ratio, t_{max}/c	0.07	0.0633	0.0581	0.0537	0.0494	0.0458	0.0422	0.0390	0.0359	0.0329	0.03
percent chord location of t_{max}	40.0	49.0	50.0	50.0	50.0	50.0	50.0	50.0	50.0	50.0	50.0
edge radii, L.E.R. - T.E.R., cm	0.000373	0.000348	0.000328	0.000310	0.000292	0.000274	0.000257	0.000241	0.000226	0.000210	0.000193
maximum camber location, a/c	0.4794	0.5337	0.5392	0.5378	0.5403	0.5470	0.5610	0.5773	0.5984	0.6203	0.6343
solidity, σ	2.513	2.155	1.953	1.812	1.704	1.616	1.550	1.493	1.443	1.397	1.359

[1] The rotor is a multiple-circular-arc airfoil on conical surfaces approximating streamlines of revolution

Number of rotor blades = 24

TABLE 12

Airfoil Definitions on Flow Surfaces (Assumed Conical) – Stator[1] (English Units)

Percent Flow	0 Root	10	20	30	40	50	60	70	80	90	100 Tip
diameter at leading edge, inches	17.198	19.214	20.918	22.456	23.854	25.172	26.421	27.611	28.750	29.851	30.931
cone angle α, degs	14.42	11.16	8.06	5.55	4.13	2.86	1.91	1.11	0.48	0.09	-0.43
aerodynamic chord c, inches	1.877	1.858	1.842	1.834	1.830	1.828	1.827	1.826	1.826	1.826	1.826
front chord c_f, inches	0.601	0.580	0.587	0.598	0.608	0.619	0.626	0.635	0.650	0.672	0.706
blade angle β_1^*, degs	48.82	41.11	38.02	35.78	34.02	32.82	31.74	30.83	30.20	30.12	30.71
blade angle β_{1ss}^*, degs	52.91	45.38	42.74	40.90	39.50	38.54	37.73	37.11	36.70	36.83	37.32
blade camber angle ϕ, degs	65.73	56.45	52.58	47.45	44.38	43.62	44.09	44.90	45.10	46.11	47.55
front camber angle ϕ_f, degs	9.72	7.89	7.23	6.41	5.85	5.68	5.84	5.64	5.60	5.74	5.97
max. thickness-to-chord ratio, t_{max}/c	0.039	0.0431	0.0472	0.0507	0.0541	0.0564	0.0591	0.0619	0.0641	0.0663	0.07
percent chord location of t_{max}	50.0	50.0	50.0	50.0	50.0	50.0	50.0	50.0	50.0	50.0	50.0
edge radii, L.E.R. - T.E.R., inch	0.0034	0.0038	0.0041	0.0043	0.0046	0.0048	0.0051	0.0053	0.0053	0.0057	0.0059
maximum camber location, a/c	0.5309	0.5304	0.5328	0.5356	0.5381	0.5405	0.5425	0.5445	0.5470	0.5510	0.5577
solidity, σ	2.169	1.935	1.773	1.651	1.555	1.474	1.405	1.346	1.293	1.246	1.203

TABLE 12

Airfoil Definitions on Flow Surfaces (Assumed Conical) – Stator (SI Units)

Percent Flow	0 Root	10	20	30	40	50	60	70	80	90	100 Tip
diameter at leading edge, cm	43.683	48.804	53.132	57.038	60.589	63.937	67.109	70.132	73.025	75.822	78.565
cone angle α, radians	.25167	.19478	.14067	.09686	.07208	.04992	.03334	.019303	-.00838	.00157	-.00750
aerodynamic chord c, cm	4.7676	4.7193	4.6787	4.6584	4.6482	4.6431	4.6406	4.6380	4.6380	4.6380	4.6380
front chord c_f, cm	1.527	1.473	1.491	1.519	1.544	1.572	1.590	1.613	1.651	1.707	1.793
blade angle β_1^*, radians	.85205	.71749	.66353	.62447	.59375	.57281	.55396	.53808	.52708	.52568	.53598
blade angle β_{1ss}^*, radians	.90773	.79202	.74594	.71383	.68939	.67264	.65850	.64768	.64053	.64279	.65135
blade camber angle ϕ, radians	1.1475	.9852	.9176	.8281	.7746	.7613	.7695	.7836	.7871	.8048	.8299
front camber angle ϕ_f, radians	.16964	.137704	.12619	.11187	.10210	.09913	.09843	.09843	.097736	.10018	.10419
max. thickness-to-chord ratio, t_{max}/c	0.039	0.0431	0.0472	0.0507	0.0541	0.0564	0.0591	0.0619	0.0641	0.0663	0.07
percent chord location of t_{max}	50.0	50.0	50.0	50.0	50.0	50.0	50.0	50.0	50.0	50.0	50.0
edge radii, L.E.R.-T.E.R., cm	.008636	.009652	.010414	.010922	.011684	.012192	.012954	.013462	.013462	.014478	.014986
maximum camber location, a/c	0.5309	0.5304	0.5328	0.5356	0.5381	0.5405	0.5425	0.5445	0.5470	0.5510	0.5577
solidity, σ	2.169	1.935	1.773	1.651	1.555	1.474	1.405	1.346	1.293	1.246	1.203

[1]The stator is a multiple-circular-arc airfoil on conical surfaces approximating streamlines of revolution

Number of stator vanes = 64

APPENDIX 9

Airfoil Coordinates on Manufacturing Surfaces

TABLE 13

Rotor Coordinates on Manufacturing Surfaces (Constant Radius)
Sections A, B, C and D (English Units)

Sect.		A–A		B–B		C–C		D–D	
Radius	inches	8.0		8.5		9.0		9.5	
c	inches	4.5180		4.5570		4.6054		4.6976	
γ	degrees	1° 53' 24"		7° 45 22"		12° 1' 17"		15° 58' 55"	
Ȳ	inches	0.7310		0.6280		0.5846		0.5430	
X̄	inches	2.2362		2.3104		2.3624		2.4060	

STA	X	Y	X	Y	X	Y	X	Y
1	0.0000	0.0000	0.0000	0.0000	0.0000	0.0000	0.0000	0.0000
2	0.0000	-0.0192	0.0000	-0.0226	0.0000	-0.0194	0.0000	-0.0212
3	0.4518	0.2230	0.4557	0.1836	0.4605	0.1630	0.4698	0.1490
4	0.9036	0.4346	0.9114	0.3640	0.9211	0.3266	0.9395	0.2980
5	1.3554	0.5974	1.3671	0.5038	1.3816	0.4552	1.4093	0.4158
6	1.8072	0.7114	1.8228	0.6022	1.8422	0.5486	1.8790	0.5036
7	2.2590	0.7776	2.2785	0.6570	2.3027	0.6052	2.3488	0.5560
8	2.7108	0.7892	2.7342	0.6598	2.7632	0.6110	2.8186	0.7620
9	3.1626	0.7394	3.1899	0.6030	3.2238	0.5620	3.2883	0.5182
10	3.6144	0.6110	3.6456	0.4822	3.6843	0.4500	3.7581	0.4142
11	4.0662	0.3692	4.1013	0.2824	4.1449	0.2652	4.2278	0.2418
12	4.5180	-0.0140	4.5570	-0.0144	4.6054	-0.0150	4.6976	-0.0136
13	4.5180	0.0200	4.5570	0.0174	4.6054	0.0144	4.6976	0.0148
14	4.0662	0.5080	4.1013	0.4354	4.1449	0.4206	4.2278	0.3896
15	3.6144	0.8282	3.6456	0.7082	3.6843	0.6756	3.7581	0.6288
16	3.1626	1.0040	3.1899	0.8720	3.2238	0.8430	3.2883	0.7706
17	2.7108	1.0800	2.7342	0.9478	2.7632	0.8910	2.8186	0.8354
18	2.2590	1.0764	2.2785	0.9486	2.3027	0.8880	2.3488	0.8330
19	1.8072	1.0030	1.8228	0.8816	1.8422	0.8012	1.8790	0.6516
20	1.3554	0.8630	1.3671	0.7550	1.3816	0.6972	1.4093	0.6516
21	0.9036	0.6536	0.9114	0.5680	0.9211	0.5208	0.9395	0.4868
22	0.4518	0.3656	0.4557	0.3162	0.4605	0.2882	0.4698	0.2700
23	0.0000	0.0236	0.0000	0.0220	0.0000	0.0214	0.0000	0.0192
LER	0.0214		0.0211		0.0203		0.0194	
TER	0.0115		0.0130		0.0126		0.0125	

TABLE 13

Rotor Coordinates on Manufacturing Surfaces (Constant Radius)
Sections A, B, C and D (SI Units)

Sect.		A–A		B–B		C–C		D–D	
Radius	meters	0.20320		0.21590		0.22860		0.24130	
c	meters	0.11476		0.11575		0.11698		0.11932	
γ	radians	0.032987		0.135369		0.209809		0.278934	
Ȳ	meters	0.018567		0.015951		0.014849		0.013792	
X̄	meters	0.056800		0.058684		0.060005		0.061112	

STA	X	Y	X	Y	X	Y	X	Y
1	0.0000	0.0000	0.0000	0.0000	0.0000	0.0000	0.0000	0.0000
2	0.0000	-0.000488	0.0000	-0.000574	0.0000	-0.000493	0.0000	-0.000538
3	0.011476	0.005642	0.011575	0.004663	0.011697	0.004140	0.011933	0.003785
4	0.022951	0.011039	0.023150	0.009225	0.023396	0.008296	0.023863	0.007569
5	0.034427	0.015174	0.034724	0.012797	0.035093	0.011562	0.035796	0.010561
6	0.045902	0.019594	0.046299	0.015296	0.046792	0.013934	0.047727	0.012791
7	0.057379	0.019751	0.057874	0.016688	0.058489	0.015372	0.059660	0.014122
8	0.068854	0.020460	0.069449	0.016759	0.070185	0.015519	0.071592	0.019355
9	0.080330	0.018781	0.081023	0.015316	0.081885	0.014229	0.083523	0.013162
10	0.091806	0.015519	0.092598	0.012248	0.093581	0.011430	0.095456	0.010521
11	0.103281	0.009378	0.104173	0.007173	0.105280	0.006736	0.107386	0.006142
12	0.114757	-0.000356	0.115748	-0.000366	0.116977	-0.000381	0.119319	-0.000345
13	0.114757	0.000508	0.115748	0.000442	0.116977	0.000367	0.119319	0.000376
14	0.103281	0.012903	0.104173	0.011059	0.105280	0.010683	0.107386	0.009896
15	0.091806	0.021036	0.092598	0.017988	0.093581	0.017160	0.095456	0.010597
16	0.080330	0.025502	0.081023	0.022149	0.081885	0.021412	0.083523	0.019573
17	0.068854	0.027432	0.069449	0.024074	0.070185	0.022631	0.071592	0.021219
18	0.057379	0.027341	0.057874	0.024094	0.058489	0.022555	0.059660	0.021158
19	0.045902	0.025476	0.046299	0.022393	0.046792	0.030350	0.047727	0.019512
20	0.034427	0.021920	0.034724	0.019177	0.035093	0.017709	0.035796	0.016551
21	0.022951	0.016601	0.023150	0.014427	0.023396	0.013228	0.023863	0.012365
22	0.011476	0.009286	0.011575	0.008031	0.011697	0.007320	0.011933	0.006858
23	0.0000	0.000599	0.0000	0.000559	0.0000	0.000544	0.0000	0.000488
LER	0.000544		0.000536		0.000516		0.000493	
TER	0.000292		0.000330		0.000320		0.000318	

TABLE 14
Rotor Coordinates on Manufacturing Surfaces (Constant Radius)
Sections E, F, G and H (English Units)

Sect.		E–E		F–F		G–G		H–H	
Radius	inches	10.0		10.5		11.5		12.5	
c	inches	4.7820		4.8620		5.0184		5.1588	
γ	degrees	19° 51′ 1″		23° 32′ 60″		30° 55′ 9″		37° 15′ 41″	
Ȳ	inches	0.5060		0.4704		0.3872		0.3080	
X̄	inches	2.4446		2.4774		2.5472		2.6036	

STA	X	Y	X	Y	X	Y	X	Y
1	0.0000	0.0000	0.0000	0.0000	0.0000	0.0000	0.0000	0.0000
2	0.0000	-0.0174	0.0000	-0.0162	0.0000	-0.0132	0.0000	-0.0096
3	0.4782	0.1368	0.4862	0.1226	0.5018	0.0932	0.5159	0.0630
4	0.9564	0.2722	0.9724	0.2456	1.0037	0.1874	1.0318	0.1322
5	1.4346	0.3830	1.4586	0.3488	1.5055	0.2724	1.5476	0.1948
6	1.9128	0.4686	1.9448	0.4304	2.0074	0.3420	2.0635	0.2516
7	2.3910	0.5176	2.4310	0.4758	2.5092	0.3818	2.5794	0.2898
8	2.8692	0.5214	2.9172	0.4786	3.0110	0.3816	3.0953	0.2940
9	3.3474	0.4762	3.4034	0.4362	3.5129	0.3462	3.6112	0.2656
10	3.8256	0.3778	3.8896	0.3446	4.0147	0.2720	4.1270	0.2080
11	4.3038	0.2186	4.3758	0.1996	4.5166	0.1546	4.6429	0.1160
12	4.7820	-0.0120	4.8620	-0.0120	5.0184	-0.0098	5.1588	-0.0092
13	4.7820	0.0152	4.8620	0.0144	5.0184	0.0126	5.1588	0.0124
14	4.3038	0.3586	4.3758	0.3300	4.5166	0.2692	4.6429	0.2182
15	3.8256	0.5826	3.8896	0.5404	4.0147	0.4478	4.1270	0.3660
16	3.3474	0.7200	3.4034	0.6700	3.5129	0.5616	3.6112	0.4616
17	2.8692	0.7846	2.9172	0.7328	3.0010	0.6186	3.0953	0.5110
18	2.3910	0.7848	2.4310	0.7350	2.5092	0.6238	2.5794	0.5130
19	1.9128	0.7250	1.9448	0.6790	2.0074	0.5756	2.0635	0.4680
20	1.4346	0.6132	1.4586	0.5708	1.5055	0.4796	1.5476	0.3864
21	0.9564	0.4558	0.9424	0.4212	1.0037	0.3520	1.0318	0.2820
22	0.4782	0.2534	0.4862	0.2326	0.5018	0.1948	0.5159	0.1572
23	0.0000	0.0206	0.0000	0.0150	0.0000	0.0124	0.0000	0.0114

LER		0.0179		0.0161		0.0128		0.0105
TER		0.0126		0.0124		0.0118		0.0108

TABLE 14
Rotor Coordinates on Manufacturing Surfaces (Constant Radius)
Sections E, F, G and H (SI Units)

Sect.		E–E		F–F		G–G		H–H	
Radius	meters	0.25400		0.26670		.29210		.31750	
c	meters	0.12146		0.12349		0.12747		0.13103	
γ	radians	0.346448		0.411019		0.539634		0.650324	
Ȳ	meters	0.012852		0.011948		0.009835		0.007823	
X̄	meters	0.062093		0.062926		0.064699		0.066131	

STA	X	Y	X	Y	X	Y	X	Y
1	0.0000	0.0000	0.0000	0.0000	0.0000	0.0000	0.0000	0.0000
2	0.0000	-0.000441	0.0000	-0.000411	0.0000	-0.000335	0.0000	-0.000244
3	0.012146	0.003474	0.012349	0.003114	0.012746	0.002367	0.013104	0.001600
4	0.024293	0.006913	0.024699	0.006238	0.025494	0.004691	0.026208	0.003358
5	0.036439	0.009728	0.037048	0.008860	0.038240	0.006919	0.039309	0.004948
6	0.048585	0.011902	0.049398	0.010932	0.050988	0.008687	0.052413	0.006391
7	0.060731	0.013147	0.061747	0.013085	0.063734	0.009698	0.065517	0.007361
8	0.072878	0.013244	0.074097	0.012156	0.076479	0.009698	0.078621	0.007468
9	0.085024	0.012095	0.086446	0.011079	0.089228	0.008793	0.091724	0.006746
10	0.097170	0.009596	0.098796	0.008753	0.101973	0.006909	0.104826	0.005283
11	0.109316	0.005552	0.111145	0.005070	0.114722	0.003932	0.117930	0.002946
12	0.121462	-0.000305	0.123495	-0.000305	0.127467	-0.000249	0.131034	-0.000234
13	0.121462	0.000386	0.123495	0.000366	0.127467	0.000320	0.131034	0.000315
14	0.109316	0.009108	0.111145	0.008382	0.114722	0.006838	0.117930	0.005542
15	0.097170	0.014798	0.098796	0.013726	0.101973	0.011374	0.104826	0.009296
16	0.085024	0.018288	0.086446	0.017018	0.089228	0.014265	0.091724	0.011725
17	0.027878	0.019929	0.074097	0.018613	0.076479	0.015712	0.078621	0.012979
18	0.060731	0.019929	0.061747	0.018669	0.063734	0.015845	0.065517	0.013030
19	0.048585	0.018415	0.049398	0.017247	0.050988	0.014620	0.052413	0.011887
20	0.036439	0.015575	0.037048	0.014498	0.038240	0.012182	0.039309	0.009815
21	0.024293	0.011577	0.024699	0.010698	0.025494	0.008941	0.026208	0.007163
22	0.012146	0.006436	0.012349	0.005908	0.012746	0.004948	0.013104	0.003993
23	0.0000	0.000523	0.0000	0.000381	0.0000	0.000315	0.0000	0.000290

LER		0.000455		0.000409		0.000325		0.000267
TER		0.000320		0.000315		0.000300		0.000274

TABLE 15

Rotor Coordinates on Manufacturing Surfaces (Constant Radius)
Sections J, K, L and M (English Units)

Sect.		J–J		K–K		L–L		M–M	
Radius	inches	13.5		14.5		15.4		6.0	
c	inches	5.2916		5.4032		5.5140		4.7462	
γ	degrees	42° 39′ 45″		47° 45′ 6″		50° 52′ 54″		−28° 59′ 20″	
Ȳ	inches	0.2334		0.1750		0.1552		1.1040	
X̄	inches	2.6614		2.7082		2.7600		1.5948	

STA	X	Y	X	Y	X	Y	X	Y
1	0.0000	0.0000	0.0000	0.0000	0.0000	0.0000	0.0000	0.0000
2	0.0000	-0.0086	0.0000	-0.0076	0.0000	-0.0084	0.0000	-0.0324
3	0.5292	0.0390	0.5403	0.0192	0.5514	0.0170	0.4746	0.6205
4	1.0583	0.0836	1.0806	0.0464	1.1028	0.0400	0.9492	1.0168
5	1.5875	0.1266	1.6210	0.0738	1.6542	0.0614	1.4239	1.2352
6	2.1166	0.1682	2.1613	0.1010	2.2056	0.0836	1.8985	1.3116
7	2.6458	0.2028	2.7016	0.1290	2.7570	0.1066	2.3731	1.3686
8	3.1750	0.2102	3.2419	0.1492	3.3084	0.1280	2.8477	1.1292
9	3.7041	0.1936	3.7822	0.1422	3.8598	0.1304	3.3223	0.9212
10	4.2333	0.1516	4.3226	0.1144	4.4112	0.1082	3.7970	0.6540
11	4.7624	0.0840	4.8629	0.0636	4.9626	0.0610	4.2716	0.3418
12	5.2916	-0.0092	5.4032	-0.0080	5.5140	-0.0076	4.7462	-0.0066
13	5.2916	0.0092	5.4032	0.0084	5.5140	0.0078	4.7462	0.0040
14	4.7624	0.1738	4.8629	0.1424	4.9626	0.1316	4.2716	0.3642
15	4.2333	0.2922	4.3226	0.2406	4.4112	0.2200	3.7970	0.6984
16	3.7041	0.3706	3.7822	0.3006	3.8598	0.2720	3.3223	1.0088
17	3.1750	0.4088	3.2419	0.3266	3.3084	0.2878	2.8477	1.2818
18	2.6458	0.4066	2.7016	0.3150	2.7570	0.2738	2.3731	1.4970
19	2.1166	0.3662	2.1613	0.2792	2.2056	0.2442	1.8985	1.6016
20	1.5875	0.3020	1.6210	0.2310	1.6542	0.2036	1.4239	1.5670
21	1.0583	0.2220	1.0806	0.1702	1.1028	0.1516	0.9492	1.3646
22	0.5292	0.1238	0.5403	0.0966	0.5514	0.0868	0.4746	0.9338
23	0.0000	0.0094	0.0000	0.0086	0.0000	0.0080	0.0000	0.0348
LER	0.0094		0.0085		0.0075		0.0145	
TER	0.0098		0.0087		0.0076		0.0052	

TABLE 15

Rotor Coordinates on Manufacturing Surfaces (Constant Radius)
Sections J, K, L and M (SI Units)

Sect.		J–J		K–K		L–L		M–M	
Radius	meters	0.34290		0.36830		0.39116		0.15240	
c	meters	0.13441		0.13724		0.14006		0.12055	
γ	radians	0.744589		0.833411		0.888039		-0.505944	
Ȳ	meters	0.005928		0.004445		0.003942		0.028042	
X̄	meters	0.067600		0.068788		0.070104		0.040508	

STA	X	Y	X	Y	X	Y	X	Y
1	0.0000	0.0000	0.0000	0.0000	0.0000	0.0000	0.0000	0.0000
2	0.0000	-0.000218	0.0000	-0.000193	0.0000	-0.000213	0.0000	-0.000823
3	0.013442	0.000991	0.013724	0.000488	0.014006	0.000432	0.012055	0.015761
4	0.026881	0.002123	0.027447	0.001179	0.028011	0.001016	0.024110	0.025827
5	0.040323	0.003216	0.041173	0.001875	0.042017	0.001560	0.036167	0.031374
6	0.053762	0.004272	0.054897	0.002565	0.056045	0.002123	0.048222	0.033315
7	0.067203	0.005151	0.068621	0.003277	0.070028	0.002708	0.060277	0.032222
8	0.080645	0.005339	0.082344	0.003790	0.084033	0.003251	0.072332	0.028682
9	0.094084	0.004917	0.096068	0.003612	0.098039	0.003312	0.084386	0.023398
10	0.107526	0.003851	0.109794	0.002906	0.112044	0.002748	0.096444	0.016612
11	0.120965	0.002134	0.123264	0.001615	0.126050	0.001549	0.108504	0.008682
12	0.134407	-0.000234	0.137241	-0.000203	0.140056	-0.000193	0.130553	-0.000168
13	0.134407	0.000234	0.137241	0.000213	0.140056	0.000198	0.120553	0.000102
14	0.120965	0.004415	0.123264	0.003617	0.126050	0.003343	0.108504	0.009251
15	0.107526	0.007422	0.109794	0.006111	0.112044	0.005588	0.096444	0.017739
16	0.094084	0.009413	0.096068	0.007635	0.098039	0.006909	0.084386	0.025624
17	0.080645	0.010384	0.082344	0.008194	0.084033	0.007310	0.072332	0.032558
18	0.067203	0.010328	0.068621	0.008001	0.070028	0.006955	0.060277	0.038024
19	0.053762	0.009301	0.054897	0.007092	0.056045	0.006203	0.048222	0.040681
20	0.040323	0.007671	0.041173	0.005867	0.042017	0.005171	0.036167	0.039802
21	0.026881	0.005639	0.027447	0.004323	0.028011	0.003851	0.024110	0.034661
22	0.013442	0.003145	0.013724	0.002454	0.014006	0.002205	0.012055	0.023719
23	0.0000	0.000239	0.0000	0.000218	0.0000	0.000203	0.0000	0.000884
LER	0.000239		0.000216		0.000191		0.000368	
TER	0.000249		0.000221		0.000193		0.000132	

TABLE 16
Rotor Coordinates on Manufacturing Surfaces (Constant Radius)
Sections N, P and R (English Units)

Sect.		N-N		P-P		R-R	
Radius	inches	6.85		7.5		16.0	
c	inches	4.5292		4.4996		5.5844	
γ	degrees	−16° 8' 22"		−6° 18' 20"		52° 47' 6"	
Ȳ	inches	1.0602		.9124		.1430	
X̄	inches	1.8812		2.1072		2.7888	

STA	X	Y	X	Y	X	Y
1	0.0000	0.0000	0.0000	0.0000	0.0000	0.0000
2	0.0000	-0.0240	0.0000	-0.0224	0.0000	-0.0074
3	0.4529	0.4126	0.4500	0.2932	0.5584	0.0164
4	0.9058	0.7592	0.8999	0.5598	1.1169	0.0384
5	1.3588	1.0112	1.3499	0.7674	1.6753	0.0580
6	1.8177	1.1646	1.7998	0.9164	2.2338	0.0766
7	2.2646	1.2124	2.2498	1.0052	2.7922	0.0958
8	2.7175	1.1524	2.6998	1.0180	3.3506	0.1164
9	3.1704	0.9906	3.1497	0.9366	3.9091	0.1226
10	3.6234	0.7346	3.5997	0.7422	4.4675	0.1028
11	4.0763	0.3982	4.0496	0.4182	5.0260	0.0590
12	4.5292	-0.0104	4.4996	-0.0146	5.5844	-0.0060
13	4.5292	0.0096	4.4996	0.0166	5.5844	0.0056
14	4.0763	0.4516	4.0496	0.5114	5.0260	0.1230
15	3.6234	0.8400	3.5997	0.9114	4.4675	0.2056
16	3.1704	1.1648	3.1497	1.1786	3.9091	0.2528
17	2.7175	1.4022	2.6998	1.3054	3.3506	0.2650
18	2.2646	1.5118	2.2498	1.3116	2.7922	0.2498
19	1.8117	1.4864	1.7998	1.2244	2.2338	0.2260
20	1.3588	1.3328	1.3499	1.0560	1.6753	0.1898
21	0.9058	1.0528	0.8999	0.8056	1.1169	0.1418
22	0.4529	0.6296	0.4500	0.4590	0.5584	0.0804
23	0.0000	0.0262	0.0000	0.0280	0.0000	0.0060
LER	0.0175		0.0204		0.0069	
TER	0.0080		0.0109		0.0067	

TABLE 16
Rotor Coordinates on Manufacturing Surfaces (Constant Radius)
Sections N, P and R (SI Units)

Sect.		N-N		P-P		R-R	
Radius	meters	0.17399		0.19050		0.40640	
c	meters	0.11504		0.11429		0.14184	
γ	radians	-0.281682		-0.110051		0.921257	
Ȳ	meters	0.026929		0.023175		0.003632	
X̄	meters	0.047782		0.053523		0.070836	

STA	X	Y	X	Y	X	Y
1	0.0000	0.0000	0.0000	0.0000	0.0000	0.0000
2	0.0000	-0.000610	0.0000	-0.000569	0.0000	-0.000188
3	0.011504	0.010729	0.011430	0.007447	0.014183	0.000417
4	0.023007	0.019284	0.022857	0.014219	0.028369	0.000975
5	0.034514	0.025684	0.034287	0.019492	0.042553	0.001473
6	0.046017	0.029581	0.045715	0.023277	0.056739	0.001946
7	0.057521	0.030795	0.057145	0.025532	0.070922	0.002433
8	0.069025	0.029271	0.068575	0.025857	0.085105	0.002957
9	0.080528	0.025161	0.080002	0.023790	0.099291	0.003114
10	0.092034	0.018659	0.091432	0.018852	0.113475	0.002611
11	0.103538	0.010144	0.102860	0.010622	0.127660	0.001499
12	0.115042	-0.000264	0.114290	-0.000371	0.141844	-0.000152
13	0.115042	0.000244	0.114290	0.000422	0.141844	0.000142
14	0.103538	0.011471	0.102860	0.012990	0.127660	0.008124
15	0.092034	0.021336	0.091432	0.023150	0.113475	0.005222
16	0.080528	0.029586	0.080002	0.029936	0.099291	0.006421
17	0.069025	0.035616	0.068575	0.033157	0.085105	0.006731
18	0.057521	0.038400	0.057145	0.033315	0.070922	0.006345
19	0.046017	0.037755	0.045715	0.031100	0.056739	0.005740
20	0.034514	0.033853	0.034287	0.026822	0.042553	0.004821
21	0.023007	0.026741	0.022857	0.020462	0.028369	0.003602
22	0.011504	0.015992	0.011430	0.011659	0.014183	0.002042
23	0.0000	0.000665	0.0000	0.000711	0.0000	0.000152
LER	0.000445		0.000518		0.000175	
TER	0.000203		0.000277		0.000170	

TABLE 17
Stator Coordinates on Manufacturing Surfaces (Constant Radius)
Sections A, B, C and D (English Units)

Sect.		A-A		B-B		C-C		D-D	
Radius	inches	9.0		9.25		9.75		10.0	
c	inches	1.8320		1.8260		1.8262		1.8280	
γ	degrees	20° 19' 47"		19° 13' 7"		17° 33' 45"		16° 59' 45"	
Ȳ	inches	0.2090		0.2008		0.1900		0.1885	
X̄	inches	0.9225		0.9180		0.9145		0.9150	

STA	X	Y	X	Y	X	Y	X	Y
1	0.0000	0.0000	0.0000	0.0000	0.0000	0.0000	0.0000	0.0000
2	0.0000	0.0045	0.0000	0.0040	0.0000	0.0045	0.0000	0.0050
3	0.1823	0.0955	0.1826	0.0920	0.1826	0.0890	0.1828	0.0890
4	0.3664	0.1750	0.3652	0.1690	0.3652	0.1633	0.3656	0.1630
5	0.5496	0.2418	0.5478	0.2335	0.5479	0.2250	0.5484	0.2240
6	0.7328	0.2875	0.7304	0.2782	0.7305	0.2682	0.7312	0.2675
7	0.9160	0.3090	0.9130	0.2990	0.9131	0.2858	0.9140	0.2860
8	1.0992	0.3070	1.0956	0.2960	1.0957	0.2822	1.0968	0.2820
9	1.2824	0.2785	1.2782	0.2680	1.2783	0.2555	1.2796	0.2545
10	1.4656	0.2230	1.4608	0.215C	1.4610	0.2025	1.4624	0.2010
11	1.6488	0.1342	1.6434	0.1295	1.6436	0.1205	1.6452	0.1205
12	1.8320	0.0050	1.8260	0.0045	1.8262	0.0050	1.8280	0.0050
13	1.8320	-0.0050	1.8260	-0.0060	1.8262	-0.0045	1.8280	-0.0045
14	1.6488	0.0992	1.6434	0.0925	1.6436	0.0840	1.6452	0.0840
15	1.4656	0.1690	1.4608	0.1600	1.4610	0.1460	1.4624	0.1430
16	1.2824	0.2142	1.2782	0.2025	1.2783	0.1855	1.2796	0.1835
17	1.0992	0.2350	1.0956	0.2235	1.0957	0.2055	1.0968	0.2040
18	0.9160	0.2355	0.9130	0.2245	0.9131	0.2072	0.9140	0.2055
19	0.7328	0.2170	0.7304	0.2050	0.7305	0.1905	0.7312	0.1885
20	0.5496	0.1763	0.5478	0.1658	0.5479	0.1550	0.5484	0.1515
21	0.3664	0.1225	0.3652	0.1150	0.3652	0.1065	0.3656	0.1055
22	0.1823	0.0625	0.1826	0.0575	0.1826	0.0518	0.1828	0.0525
23	0.0000	-0.0050	0.0000	-0.0050	0.0000	-0.0045	0.0000	-0.0040
LER	0.0040		0.0040		0.0040		0.0040	
TER	0.0040		0.0040		0.0040		0.0040	

TABLE 17
Stator Coordinates on Manufacturing Surfaces (Constant Radius)
Sections A, B, C and D (SI Units)

Sect.		A-A		B-B		C-C		D-D	
Radius	meters	0.22860		0.23495		0.24765		0.23400	
c	meters	0.04653		0.04638		0.04639		0.04643	
γ	radians	0.354815		0.335729		0.306519		0.296629	
Ȳ	meters	0.005309		0.005100		0.004826		0.004788	
X̄	meters	0.023431		0.023317		0.023228		0.023241	

STA	X	Y	X	Y	X	Y	X	Y
1	0.0000	0.0000	0.0000	0.0000	0.0000	0.0000	0.0000	0.0000
2	0.0000	0.000114	0.0000	0.000102	0.0000	0.000114	0.0000	0.000127
3	0.004630	0.002426	0.004638	0.002337	0.004638	0.002261	0.004643	0.002261
4	0.009307	0.004445	0.009276	0.004293	0.009276	0.004148	0.009286	0.004140
5	0.013960	0.006142	0.013914	0.005931	0.013917	0.005725	0.013929	0.005690
6	0.018613	0.007303	0.018552	0.007066	0.018555	0.006812	0.018572	0.006795
7	0.023266	0.007849	0.023190	0.007595	0.023193	0.007259	0.023216	0.007264
8	0.027920	0.007798	0.027828	0.007518	0.027831	0.007168	0.027859	0.007163
9	0.032573	0.007074	0.032466	0.006807	0.032469	0.006490	0.032502	0.006464
10	0.037226	0.005664	0.037104	0.005461	0.037109	0.005144	0.037145	0.005105
11	0.041880	0.003409	0.041742	0.003289	0.041747	0.003061	0.041788	0.003061
12	0.046533	0.000127	0.046380	0.000114	0.046385	0.000127	0.046431	0.000127
13	0.046533	-0.000127	0.046380	-0.000152	0.046385	-0.000114	0.046431	-0.000114
14	0.041880	0.002520	0.041742	0.002350	0.041747	0.002134	0.041788	0.002134
15	0.037226	0.004293	0.037104	0.004064	0.037109	0.003708	0.037145	0.003632
16	0.032573	0.005441	0.032466	0.005144	0.032469	0.004712	0.032500	0.004661
17	0.027920	0.005969	0.027828	0.005677	0.027831	0.005220	0.027859	0.005182
18	0.023266	0.005982	0.023190	0.005702	0.023193	0.005263	0.023216	0.005220
19	0.018613	0.005512	0.018552	0.005207	0.018555	0.004839	0.018572	0.004788
20	0.013960	0.004478	0.013914	0.004211	0.013917	0.003937	0.013929	0.003848
21	0.009307	0.003112	0.009278	0.002921	0.009276	0.002705	0.009286	0.002680
22	0.004630	0.001588	0.004638	0.001361	0.004638	0.001341	0.004643	0.001334
23	0.0000	-0.000127	0.0000	-0.000127	0.0000	-0.000114	0.0000	-0.000102
LER	0.000102		0.000102		0.000102		0.000102	
TER	0.000102		0.000102		0.000102		0.000102	

TABLE 18
Stator Coordinates on Manufacturing Surfaces (Constant Radius)
Sections E, F, G and H (English Units)

Sect.		E-E		F-F		G-G		H-H	
Radius	inches	10.55		11.5		12.5		13.5	
c	inches	1.8265		1.8250		1.8230		1.8240	
γ	degrees	16° 13'30"		16°17'36"		15° 37' 35"		13° 47' 36"	
$\bar{Y}$	inches	0.1815		0.1590		0.1485		0.1530	
$\bar{X}$	inches	0.9165		0.9125		0.9130		0.9150	

STA	X	Y	X	Y	X	Y	X	Y
1	0.0000	0.0000	0.0000	0.0000	0.0000	0.0000	0.0000	0.0000
2	0.0000	0.0042	0.0000	0.0045	0.0000	0.0045	0.0000	0.0045
3	0.1827	0.0870	0.1825	0.0795	0.1823	0.0770	0.1824	0.0780
4	0.3653	0.1585	0.3650	0.1440	0.3646	0.1390	0.3648	0.1415
5	0.5480	0.2185	0.5475	0.1975	0.5469	0.1905	0.5472	0.1945
6	0.7306	0.2605	0.7300	0.2360	0.7292	0.2265	0.7296	0.2340
7	0.9133	0.2790	0.9125	0.2530	0.9115	0.2435	0.9120	0.2530
8	1.0959	0.2750	1.0950	0.2495	1.0938	0.2405	1.0944	0.2500
9	1.2786	0.2485	1.2775	0.2260	1.2761	0.2170	1.2768	0.2255
10	1.4612	0.1980	1.4600	0.1765	1.4584	0.1725	1.4592	0.1790
11	1.6439	0.1180	1.6425	0.1055	1.6407	0.1025	1.6416	0.1070
12	1.8265	0.0060	1.8250	0.0060	1.8230	0.0045	1.8240	0.0050
13	1.8265	-0.0035	1.8250	-0.0040	1.8230	-0.0040	1.8240	-0.0040
14	1.6439	0.0795	1.6425	0.0635	1.6407	0.0570	1.6416	0.0580
15	1.4612	0.1360	1.4600	0.1125	1.4584	0.1005	1.4592	0.1030
16	1.2786	0.1740	1.2775	0.1450	1.2761	0.1285	1.2768	0.1315
17	1.0959	0.1925	1.0950	0.1600	1.0938	0.1425	1.0944	0.1455
18	0.9133	0.1935	0.9125	0.1590	0.9115	0.1430	0.9120	0.1445
19	0.7306	0.1170	0.7300	0.1455	0.7292	0.1285	0.7296	0.1280
20	0.5480	0.1425	0.5475	0.1165	0.5469	0.1010	0.5472	0.0995
21	0.3653	0.0975	0.3650	0.0795	0.3646	0.0680	0.3648	0.0655
22	0.1827	0.0482	0.1825	0.0385	0.1823	0.0325	0.1824	0.0310
23	0.0000	-0.0045	0.0000	-0.0042	0.0000	-0.0040	0.0000	-0.0040
LER	0.0041		0.0045		0.0048		0.0052	
TER	0.0040		0.0044		0.0048		0.0052	

TABLE 18
Stator Coordinates on Manufacturing Surfaces (Constant Radius)
Sections E, F, G and H (SI Units)

Sect.		E-E		F-F		G-G		H-H	
Radius	meters	0.26670		0.29210		0.31750		0.34290	
c	meters	0.04639		0.04636		0.04630		0.04633	
γ	radians	0.283176		0.284465		0.272628		0.240736	
$\bar{Y}$	meters	0.004610		0.004039		0.003772		0.003886	
$\bar{X}$	meters	0.023279		0.023178		0.023190		0.023241	

STA	X	Y	X	Y	X	Y	X	Y
1	0.0000	0.0000	0.0000	0.0000	0.0000	0.0000	0.0000	0.0000
2	0.0000	0.00107	0.0000	0.000114	0.0000	0.000114	0.0000	0.000114
3	0.004641	0.002210	0.004636	0.002019	0.004630	0.001956	0.004633	0.001981
4	0.009279	0.004026	0.009271	0.003658	0.009261	0.003531	0.009266	0.003594
5	0.013919	0.005550	0.013907	0.005017	0.013891	0.004839	0.013785	0.004940
6	0.018557	0.006617	0.018542	0.005994	0.018522	0.005753	0.018532	0.005943
7	0.023198	0.007087	0.023178	0.006426	0.023152	0.006185	0.023165	0.006326
8	0.027836	0.006985	0.027813	0.006337	0.027783	0.005109	0.027798	0.006350
9	0.032476	0.006312	0.032449	0.005740	0.032413	0.005512	0.032431	0.005728
10	0.037114	0.005029	0.037084	0.004483	0.037043	0.004382	0.037064	0.004547
11	0.041755	0.002997	0.041720	0.002680	0.041574	0.002604	0.041697	0.002718
12	0.046393	0.000152	0.046355	0.000125	0.045304	0.000114	0.046330	0.000127
13	0.046393	0.000089	0.046355	0.000102	0.463040	0.000102	0.046330	0.000102
14	0.041755	0.002019	0.041720	0.001613	0.041674	0.001448	0.041697	0.001473
15	0.037114	0.003454	0.037084	0.002858	0.037043	0.002553	0.037064	0.002616
16	0.032476	0.004420	0.032449	0.003683	0.032413	0.003264	0.032431	0.003340
17	0.027836	0.004890	0.027813	0.004064	0.027783	0.003620	0.027798	0.003696
18	0.023198	0.004915	0.023178	0.004039	0.023152	0.003632	0.023165	0.003696
19	0.018557	0.004496	0.018542	0.003696	0.018522	0.003264	0.018532	0.003251
20	0.013919	0.003620	0.013907	0.002959	0.013891	0.002565	0.013785	0.002527
21	0.009279	0.002477	0.009271	0.002019	0.009261	0.001727	0.009266	0.001664
22	0.004641	0.001224	0.004636	0.000978	0.004630	0.000826	0.004633	0.000787
23	0.0000	-0.000114	0.0000	-0.000107	0.0000	-0.000102	0.0000	-0.000102
LER	0.000104		0.000114		0.000122		0.000132	
TER	0.000102		0.000112		0.000122		0.000132	

TABLE 19
Stator Coordinates on Manufacturing Surfaces (Constant Radius)
Sections J, K, L and M (English Units)

Sect.		J-J		K-K		L-L		M-M	
Radius	inches	14.0		14.5		15.0		8.55	
c	inches	1.8240		1.8246		1.8246		1.8330	
γ	degrees	13° 3' 42"		12° 34' 56"		12° 27' 4"		22° 14' 41"	
Ȳ	inches	0.1550		0.1560		0.1596		0.2275	
X̄	inches	0.9130		0.9140		0.9180		0.9255	

STA	X	Y	X	Y	X	Y	X	Y
1	0.0000	0.0000	0.0000	0.0000	0.0000	0.0000	0.0000	0.0000
2	0.0000	0.0045	0.0000	0.0050	0.0000	0.0056	0.0000	0.0045
3	0.1824	0.0800	0.1825	0.0808	0.1825	0.0814	0.1833	0.1005
4	0.3648	0.1450	0.3649	0.1450	0.3649	0.1478	0.3666	0.1855
5	0.5472	0.1990	0.5474	0.2010	0.5474	0.2048	0.5499	0.2555
6	0.7296	0.2375	0.7298	0.2428	0.7298	0.2472	0.7332	0.3055
7	0.9120	0.2580	0.9123	0.2628	0.9123	0.2692	0.9165	0.3285
8	1.0944	0.2565	1.0948	0.2598	1.0948	0.2678	1.0998	0.3275
9	1.2768	0.2310	1.2772	0.2352	1.2772	0.2426	1.2831	0.2985
10	1.4592	0.1830	1.4597	0.1868	1.4597	0.1920	1.4664	0.2390
11	1.6416	0.1100	1.6421	0.1120	1.6421	0.1162	1.6497	0.1465
12	1.8240	0.0065	1.8246	0.0055	1.8246	0.0055	1.8330	0.0045
13	1.8240	−0.0050	1.8246	−0.0050	1.8246	−0.0060	1.8330	−0.0030
14	1.6416	0.0590	1.6421	0.0600	1.6421	0.0620	1.6497	0.1115
15	1.4592	0.1040	1.4597	0.1052	1.4597	0.1078	1.4664	0.1875
16	1.2768	0.1330	1.2772	0.1348	1.2772	0.1372	1.2831	0.2360
17	1.0944	0.1475	1.0948	0.1480	1.0948	0.1512	1.0998	0.2595
18	0.9120	0.1450	0.9123	0.1460	0.9123	0.1484	0.9165	0.2590
19	0.7296	0.1275	0.7298	0.1280	0.7298	0.1288	0.7332	0.2370
20	0.5472	0.0990	0.5474	0.0990	0.5474	0.0980	0.5499	0.1935
21	0.3648	0.0670	0.3649	0.0654	0.3649	0.0642	0.3666	0.1350
22	0.1824	0.0310	0.1825	0.0308	0.1825	0.0302	0.1833	0.0695
23	0.0000	−0.0045	0.0000	−0.0055	0.0000	−0.0055	0.0000	−0.0045
LER	0.0052		0.0055		0.0058		0.0040	
TER	0.0052		0.0055		0.0058		0.0040	

TABLE 19
Stator Coordinates on Manufacturing Surfaces (Constant Radius)
Sections J, K, L and M (SI Units)

Sect.		J-J		K-K		L-L		M-M	
Radius	meters	0.35560		0.36830		0.38100		0.21717	
c	meters	0.04633		0.04634		0.04634		0.04656	
γ	radians	0.227966		0.213326		0.217309		0.388238	
Ȳ	meters	0.003937		0.003962		0.004054		0.005779	
X̄	meters	0.023190		0.023216		0.023317		0.023508	

STA	X	Y	X	Y	X	Y	X	Y
1	0.0000	0.0000	0.0000	0.0000	0.0000	0.0000	0.0000	0.0000
2	0.0000	0.000114	0.0000	0.000127	0.0000	0.000142	0.0000	0.000114
3	0.004633	0.002032	0.004636	0.002052	0.004636	0.002068	0.004656	0.002553
4	0.009266	0.003683	0.009268	0.003683	0.009268	0.003754	0.009312	0.004712
5	0.013899	0.005055	0.013904	0.005105	0.013904	0.005202	0.013967	0.006490
6	0.018532	0.006033	0.018537	0.006167	0.018537	0.006279	0.018623	0.007760
7	0.023165	0.006553	0.023172	0.006675	0.023172	0.006838	0.023279	0.008344
8	0.027798	0.006515	0.027808	0.006599	0.027808	0.006802	0.027935	0.008319
9	0.032431	0.005867	0.032441	0.005974	0.082441	0.006162	0.032591	0.007582
10	0.037064	0.004648	0.037076	0.004745	0.037076	0.004877	0.037247	0.006071
11	0.041697	0.002794	0.041709	0.002845	0.041709	0.002951	0.041902	0.003721
12	0.046330	0.000165	0.046345	0.000140	0.046345	0.000140	0.046558	0.000114
13	0.046330	−0.000127	0.046345	−0.000127	0.046345	−0.000152	0.046558	−0.000076
14	0.041697	0.003239	0.041709	0.001524	0.041709	0.001575	0.041902	0.002832
15	0.037064	0.001499	0.037076	0.002672	0.037076	0.002738	0.037247	0.004763
16	0.032431	0.002642	0.032441	0.003424	0.032441	0.003485	0.032591	0.005994
17	0.027798	0.003378	0.027808	0.003759	0.027808	0.003840	0.027935	0.006591
18	0.023165	0.003747	0.023172	0.003708	0.023172	0.003769	0.023279	0.006579
19	0.018532	0.003683	0.018537	0.003251	0.018537	0.003271	0.018623	0.006020
20	0.013899	0.002515	0.013904	0.002515	0.013904	0.002489	0.013967	0.004915
21	0.009266	0.001702	0.009268	0.001661	0.009268	0.001631	0.009312	0.003429
22	0.004633	0.000787	0.004636	0.000782	0.004636	0.000767	0.004656	0.001765
23	0.0000	−0.000114	0.0000	−0.000140	0.0000	−0.000140	0.0000	−0.000114
LER	0.000132		0.000140		0.000147		0.000102	
TER	0.000132		0.000140		0.000147		0.000102	

TABLE 20

Stator Coordinates on Manufacturing Surfaces (Constant Radius)

Sections N and P (English Units)

Sect.		N-N		P-P	
Radius	inches	8.75		15.5	
c	inches	1.8330		1.8246	
γ	degrees	$21°\,15'\,21"$		$13°\,0'\,26"$	
Y	inches	0.2180		0.1640	
X	inches	0.9225		0.9160	

STA	X	Y	X	Y
1	0.0000	0.0000	0.0000	0.0000
2	0.0000	0.0045	0.0000	0.0070
3	0.1833	0.0950	0.1825	0.0850
4	0.3666	0.1780	0.3649	0.1532
5	0.5499	0.2475	0.5474	0.2104
6	0.7332	0.2970	0.7298	0.2532
7	0.9165	0.3195	0.9123	0.2772
8	1.0998	0.3165	1.0948	0.2774
9	1.2831	0.2895	1.2772	0.2528
10	1.4664	0.2325	1.4597	0.2012
11	1.6497	0.1415	1.6421	0.1212
12	1.8330	0.0060	1.8246	0.0062
13	1.8330	−0.0035	1.8246	−0.0070
14	1.6497	0.1065	1.6421	0.0648
15	1.4664	0.1795	1.4597	0.1120
16	1.2831	0.2250	1.2772	0.1430
17	1.0998	0.2480	1.0948	0.1558
18	0.9165	0.2485	0.9123	0.1510
19	0.7332	0.2270	0.7298	0.1304
20	0.5499	0.1835	0.5474	0.0992
21	0.3666	0.1265	0.3649	0.0648
22	0.1833	0.0635	0.1825	0.0300
23	0.0000	−0.0045	0.0000	−0.0054
LER	0.0040		0.0059	
TER	0.0040		0.0059	

TABLE 20

Stator Coordinates on Manufacturing Surfaces (Constant Radius)

Sections N and P (SI Units)

Sect.		N-N		P-P	
Radius	meters	0.22225		0.39370	
c	meters	0.04656		0.04634	
γ	radians	0.370979		0.227015	
Y	meters	0.005536		0.004166	
X	meters	0.023432		0.023266	

STA	X	Y	X	Y
1	0.0000	0.0000	0.0000	0.0000
2	0.0000	0.000114	0.0000	0.000178
3	0.004656	0.002413	0.004636	0.002159
4	0.009312	0.004521	0.009268	0.003891
5	0.013967	0.006287	0.013904	0.005344
6	0.018623	0.007544	0.018537	0.006431
7	0.023279	0.008115	0.023172	0.007041
8	0.027935	0.008039	0.027808	0.007046
9	0.032591	0.007353	0.032441	0.006421
10	0.037247	0.005906	0.037076	0.005110
11	0.041902	0.003594	0.041709	0.003078
12	0.046558	0.000152	0.046345	0.000157
13	0.046558	−0.000089	0.046345	−0.000178
14	0.041902	0.002705	0.041709	0.001646
15	0.037247	0.004559	0.037076	0.002845
16	0.032591	0.005715	0.032441	0.003632
17	0.027935	0.006299	0.027808	0.003957
18	0.023279	0.006312	0.023172	0.003835
19	0.018623	0.005766	0.018537	0.003312
20	0.013967	0.004661	0.013904	0.002520
21	0.009312	0.003213	0.009268	0.001646
22	0.004656	0.001613	0.004636	0.000762
23	0.0000	−0.000114	0.0000	−0.000137
LER	0.000102		0.000150	
TER	0.000102		0.000150	

REFERENCES

1. Tyler, J.M. and T.G. Sofrin, Axial-Flow Compressor Noise Studies, SAE Trans., Vol. 70, pp 309-332, 1962

2. Keenan, M.J. and N.T. Monsarrat, Experimental Evaluation of Transonic Stators, Preliminary Analysis and Design Report, NASA CR-54620, PWA-2749, 1967

3. Keenan, M.J., K.G. Harley and G.A. Bogardus, Experimental Evaluation of Transonic Stators, Data and Performance Report, Multiple-Circular-Arc Stator A, NASA CR-54621, PWA-3260, 1968

4. Robbins, W.H., R.J. Jackson and S. Lieblein, Blade-Element Flow in Annular Cascades, Aerodynamic Design of Axial-Flow Compressors, NASA SP-36, Ch. VII, pp 227-254, 1965

5. Ainley, D.G., Performance of Axial-Flow Turbines, Proc. Inst. Mech. Eng., 1940

6. Peacock, R. E., Flow Control in the Corners of Cascades, A. R. C. 27 291, Oct. 1965

7. Ferri, Kuchemann and Sterne, Progress in Aeronautical Sciences, Vol. II, pp 43-47 and 114-119, Pergamon Press, 1962

8. Keenan, M.J. and J.A. Bartok, Experimental Evaluation of Transonic Stators, Data and Performance Report, Multiple-Circular-Arc Stator B, NASA CR-54622, PWA-3356, 1968

9. Seyler, D.R. and L. H. Smith, Jr., Single-Stage Experimental Evaluation of High-Mach-Number Compressor-Rotor Blading, Part 1 - Design of Rotor Blading, NASA CR-54581, GE R66FPD321, 1967

10. Howell, A.R., Design of Axial Compressors, Proc. Inst. Mech. Engrs., Lond. 153, 1945

11. Seyler, D.R. and J.P. Gostelow, Single-Stage Experimental Evaluation of High-Mach-Number Compressor-Rotor Blading, Part 2 - Performance of Rotor 1B, NASA CR-54582, GER67FPD236, 1967

12. Gostelow, J.P. and K.W. Krabacher, Single-Stage Experimental Evaluation of High-Mach-Number Compressor-Rotor Blading, Part 5-Performance of Rotor 2B, NASA CR-54585, GER67FPD278, 1967

13. Krabacher, K.W. and J.P. Gostelow, Single-Stage Experimental Evaluation of High-Mach-Number Compressor-Rotor Blading, Part 4-Performance of Rotor 2D, NASA CR-54584, GER67FPD276, 1967

14.   Gostelow, J. P. and K. W. Krabacher, Single-Stage Evaluation of High-Mach-Number Compressor-Rotor Blading, Part 3-Performance of Rotor 2E, NASA CR-54583, GER67FPD248, 1967

Distribution List

NASA Headquarters
Washington, D. C. 20546
Attention: N. F. Rekos (RAP) — 1

NASA-Lewis Research Center
21000 Brookpark Road
Cleveland, Ohio 44135
Attention:
Report Control Office, MS 5-5 — 1
Technical Utilization Office, MS 3-19 — 1
Library, MS 60-3 — 2
Fluid Systems Component Div. MS 5-3 — 1
Pump & Compressor Branch, MS 5-9 — 6
A. Ginsburg, MS 5-3 — 1
M. J. Hartmann, MS 5-9 — 1
W. A. Benser, MS 5-9 — 1
D. M. Sandercock, MS 5-9 — 1
L. J. Herrig, MS 7-1 — 1
T. F. Gelder, MS 5-9 — 1
C. L. Ball, MS 5-9 — 1
L. Reid, MS 5-9 — 1
J. H. DeFord, MS 77-3 — 1
S. Lieblein, MS 54-6 — 1
C. L. Meyer, MS 60-4 — 1
J. H. Povolny, MS 60-4 — 1
A. W. Goldstein, MS 7-1 — 1
J. J. Kramer, MS 7-1 — 1
W. L. Beede, MS 5-3 — 1
C. H. Voit, MS 5-3 — 1
J. H. Childs, MS 60-4 — 1
Dr. B. Lubarsky, MS 3-3 — 1
E. Bailey, MS 5-9 — 1

NASA-Langley Research Center
Technical Library
Hampton, Virginia 23365
Attention: M. R. Nichols — 1
J. V. Becker — 1

NASA Scientific & Technical Information Facility
P.O. Box 33, College Park, Maryland 20740
Attention: NASA Representative — 6

U.S. Army Aviation Material Laboratory
Fort Eustis, Virginia
Attention: J. White — 1

Department of Navy
Bureau of Weapons
Washington, D.C. 20525
Attention: R. Brown, RAPP14 — 1

Department of Navy
Bureau of Ships
Washington, D.C. 20360
Attention: G. L. Graves — 1

Wright-Patterson AFB, Ohio 45433
Attention: J. L. Wilkins, SESOS — 1
S. Kobelak, APTP — 1
R. P. Carmichael, SESSP — 1

FAA Headquarters
800 Independence Ave., S.W.
Washington, D.C. 20553
Attention: J. C. Maxwell — 1
F. B. Howard — 1

Air Research Manufacturing Company
402 South 36th Street
Phoenix, Arizona 85034
Attention: R. O. Bullock — 1

Air Research Manufacturing Company
8951 Sepulveda Boulevard
Los Angeles, California 90009
Attention: L. C. Wright — 1

Allison Division, GMC
Department 8894, Plant 8
P.O. Box 894
Indianapolis, Indiana 46206
Attention: J. H. Barney — 1
Library — 1

Avco Corporation
Lycoming Division
550 South Main Street
Stratford, Connecticut
Attention: C. W. Bolton — 1

Chrysler Corporation
Research Office, Dept. 9000
P. O. Box 1118, Detroit, Michigan 48231
Attention: James Furlong — 1

Continental Aviation & Engineering Corp.
12700 Kercheval
Detroit, Michigan 48215
Attention: E. H. Benstein — 1

Curtiss-Wright Corporation
Wright Aeronautical
Woodridge, New Jersey
Attention: S. Lombardo — 1

Douglas Aircraft Company
3855 Lakewood Boulevard
Long Beach, California 90801
Attention: J. E. Merriman — 1

Elliott Company
Jeanette, Pennsylvania
Attention: J. R. Shields — 1

General Electric Company
Aircraft Engine Group
1 Jimson Road, Cincinnati, Ohio   45215
Attention: M. Miller, H-50   1
         L. H. Smith, H-50   1
         Tech. Inf. Center, N-32   1

General Electric Company
1000 Western Avenue
West Lynn, Massachusetts
Attention: L. H. King, Bldg. 2-40   1
         Dr. C. W. Smith Library, Bldg. 2-40M   1

Goodyear Atomic Corporation
P.O. Box 628, Piketon, Ohio
Attention: C. O. Langebrake   1

Hamilton Standard Division
United Aircraft Corporation
Windsor Locks, Connecticut
Attention: Carl Rohrbach   1

Iowa State University of Science & Technology
Ames, Iowa 50010
Attention: Prof. G. K. Serovy   1
         Dept. of Mech. Eng.

Lockheed Missile and Space Company
Building 541, Dept. 80-91
P.O. Box 879, Mountain View, California 94040
Attention: R. S. Poppe   1

Northern Research & Engineering
219 Vassar Street
Cambridge, Massachusetts
Attention: R. A. Novak   1

Pratt & Whitney Aircraft
Florida Research & Development Center
P.O. Box 2691, West Palm Beach, Florida   33402
Attention: R. A. Schmidtke   1
         H. D. Stetson   1
         J. M. Silk   1
         B. A. Jones   1

Solar
San Diego, California 92112
Attention: P. A. Pitt   1

The Boeing Company
P.O. Box 3991
Seattle, Washington 98124
Attention: G. J. Schott MS 80-66   1

The Boeing Company
224 North Wilkinson
Dayton, Ohio 45402
Attention: J. D. Raisbeck   1

Union Carbide Corporation, Nuclear Division
Oak Ridge Gaseous Diffusion Plant
P.O. Box P, Oak Ridge, Tennessee   37830
Attention: R. G. Jordan   1

Westinghouse Electric Corporation
P.O. Box 9175, Philadelphia, Pa. 19113
Attention: S. M. DeCorso   1

Williams Research Corporation
P.O. Box 95, Walled Lake, Michigan
Attention: J. R. Joy   1

California Institute of Technology
Pasadena, California 91109
Attention: Prof. D. Rannie   1

Massachusetts Institute of Technology
Gas Turbine Laboratory
Cambridge, Massachusetts 02139
Attention: Prof. J. Kerrebrock   1